

**Analysis of *in vivo* Purine Nucleotide Catabolism in  
*Arabidopsis thaliana* with Focus on  
Nucleoside Hydrolase 2**

Von der Naturwissenschaftlichen Fakultät der  
Gottfried Wilhelm Leibniz Universität Hannover

zur Erlangung des Grades  
Doktorin der Naturwissenschaften (Dr. rer. nat.)

genehmigte Dissertation  
von  
Chiara Baccolini, Dottore Magistrale (Italien)

[2019]

Referent: Prof. Dr. Claus-Peter Witte

Korreferent: Dr. Sascha Offermann

Tag der Promotion: 20.06.2019

## Abstract

Plants can catabolize purine nucleotides to recycle nutrients, in particular nitrogen. The currently established model of purine nucleotide catabolism consists of a branched pathway that starts from AMP and GMP and proceeds either via the intermediates inosine and hypoxanthine or via guanosine and xanthosine to converge on xanthine. Xanthine is further catabolized in a linear fashion by a fully characterized series of reactions to form glyoxylate, carbon dioxide and ammonia. The ammonia released can be re-assimilated into amino acids. This work focuses on how xanthine is generated, *in vivo*, in Arabidopsis. Metabolite analysis of mutants of a wide set of genes involved in purine catabolism and salvage such as guanosine deaminase, nucleoside hydrolases (NSH), xanthine dehydrogenase, urate oxidase and hypoxanthine guanine phosphoribosyltransferase along with double order and triple order mutants of the same genes showed that xanthine is mainly generated by xanthosine hydrolysis. Inosine and hypoxanthine might enter the pathway from routes other than nucleotide degradation, such as tRNA degradation, DNA repair, and uptake from the soil. Furthermore, xanthosine is not only generated by guanosine deamination as reported in Dahncke and Witte, 2013, but xanthosine monophosphate dephosphorylation is likely to be a source as well. In addition, this work elucidates the function of NSH2. The Arabidopsis genome encodes two nucleoside hydrolases, NSH1 and NSH2. NSH1 is essential for xanthosine and uridine hydrolysis, whereas the function of NSH2 is unclear. Biochemical, genetic and metabolic analyses demonstrate that NSH1 activates NSH2 *in vitro* and *in vivo* forming a heterocomplex that has a higher catalytic efficiency for xanthosine, but not for uridine, in comparison to the NSH1 homomer. The heterocomplex formation is also shown for the NSH enzymes of *Coffea arabica* and *Physcomitrella patens*, suggesting that this interaction is conserved in the plant kingdom. Dynamic NSH heterocomplex formation might regulate the flux through different branches of nucleotide catabolism. By altering the available amount of NSH2, cell metabolism might be able to upregulate or downregulate the flux through purine degradation, which not only enables the cell to control purine and pyrimidine homeostasis, but might also be useful to deal with certain stress conditions. To summarize, this work unravels how xanthine is generated within the purine nucleotide catabolic pathway of Arabidopsis *in vivo*, and proposes a revised model in which xanthosine hydrolysis, catalyzed by a heterocomplex of nucleoside hydrolases, serves as the main source of xanthine.

# Zusammenfassung

Pflanzen können Purinnukleotide abbauen um Nährstoffe, insbesondere Stickstoff, zurück zu gewinnen. Das derzeit etablierte Modell des Nukleotidkatabolismus besteht aus einem verzweigten Stoffwechselweg, der mit AMP und GMP beginnt und über die Intermediate Inosin und Hypoxanthin oder alternativ über Guanosin und Xanthosin in dem Metaboliten Xanthin zusammenläuft. Xanthin wird dann in einem linearen Stoffwechselweg durch mehrere gut charakterisierte Reaktionen zu Glyoxylat, Kohlenstoffdioxid und Ammonium umgesetzt. Der Stickstoff aus dem Ammonium kann dann in der Aminosäuresynthese wiederverwendet werden.

Der Schwerpunkt dieser Arbeit liegt darin, die Bildung von Xanthin *in vivo* in Arabidopsis zu beschreiben. Die Analyse von Metaboliten in Funktionsverlustmutanten von Genen, die wichtig für den Purinkatabolismus und die Wiedergewinnung von Nährstoffen sind, wie Guanosin-Deaminase, Nukleosid-Hydrolase (NSH), Xanthin-Dehydrogenase, Urat-Oxidase, Hypoxanthin/Guanin-Phosphoribosyltransferase sowie den aus diesen Genen abgeleiteten Doppel- und Dreifachmutanten zeigen, dass Xanthin hauptsächlich über den Abbau von Xanthosin gebildet wird. Inosin und Hypoxanthin entstehen vermutlich nicht aufgrund des Nukleotidabbaus sondern entstammen Prozessen wie z.B. dem tRNA Abbau der DNA Reparatur und der Aufnahme aus dem Boden. Weiterhin wird Xanthosin nicht nur durch die Deaminierung von Guanosin, wie zuvor von Dahncke und Witte, 2013 beschrieben generiert, sondern auch die Dephosphorylierung von Xanthosinmonophosphat stellt eine wichtige Quelle für Xanthosin dar.

Außerdem wird in dieser Arbeit die Funktion von NSH2 beschrieben. Im Genom von Arabidopsis gibt es zwei Nukleosid-Hydrolasen, NSH1 und NSH2, und während NSH1 essentiell für die Hydrolyse von Xanthosin und Uridin ist, konnte die Funktion von NSH2 bisher nicht geklärt werden. Biochemische, genetische und metabolische Analysen zeigen, dass NSH2 von NSH1 *in vitro* aktiviert wird und beide Proteine zusammen *in vivo* einen Komplex bilden, der verglichen mit einem Komplex, der nur aus NSH1 besteht, eine höhere katalytische Aktivität für Xanthosin, aber nicht für Uridin aufweist. Die nachgewiesene Bildung eines NSH1/NSH2 Komplexes in *Coffea arabica* und *Physcomitrella patens* deutet auf eine konservierte Funktion im Pflanzenreich hin. Die dynamische Bildung eines NSH1/NSH2 Komplexes könnte den Durchsatz von Metaboliten im Purin- und Pyrimidinkatabolismus regulieren. Durch die Veränderung der verfügbaren Menge von NSH2

könnte ein Hoch- oder Herunterregulieren des Purinabbaus erreicht und damit das Purin-Pyrimidin-Gleichgewicht kontrolliert und z.B. unter Stressbedingungen verändert werden. Zusammenfassend erklärt diese Arbeit wie Xanthin innerhalb des Purinabbaus *in vivo* gebildet wird und entwickelt zusätzlich ein verändertes Modell der Xanthosinhydrolyse durch einen Komplex aus NSH1 und NSH2, dessen Aktivität die Hauptquelle von Xanthin darstellt.

## **Keywords**

Nucleoside hydrolase, purine nucleotide catabolism, *Arabidopsis thaliana*.

# Content

<b>Abstract</b> .....	<b>i</b>
<b>Zusammenfassung</b> .....	<b>ii</b>
<b>Keywords</b> .....	<b>iii</b>
<b>List of Abbreviations</b> .....	<b>viii</b>
<b>List of Figures</b> .....	<b>x</b>
<b>List of Tables</b> .....	<b>xii</b>
<b>1. Introduction</b> .....	<b>1</b>
1.1 Plant and nitrogen .....	1
1.2 Nucleotide metabolism .....	2
1.2.1 Nucleotide function and structure .....	2
1.2.2 Purine nucleotide metabolism .....	4
1.2.2.1 Purine nucleotide biosynthesis .....	4
1.2.2.2 Purine nucleotide catabolism .....	7
1.2.2.3 Purine nucleotide salvage .....	8
1.2.2.4 Biological functions of purine nucleotide catabolism .....	10
1.2.3 Pyrimidine nucleotide metabolism .....	12
1.2.3.1 Pyrimidine nucleotide biosynthesis .....	12
1.2.3.2 Pyrimidine nucleotide catabolism .....	12
1.2.3.3 Pyrimidine nucleotide salvage .....	12
1.3 Nucleoside hydrolase .....	14
1.3.1 Nucleoside hydrolase catalytic mechanism .....	14
1.3.2 Plant nucleoside hydrolases .....	16
1.3.2.1 <i>Arabidopsis thaliana</i> nucleosidases .....	16
1.3.2.2 <i>Physcomitrella patens</i> nucleosidases .....	17
1.3.2.3 <i>Zea mays</i> nucleosidases .....	18
1.4 Aim of this study .....	19
<b>2. Material and Methods</b> .....	<b>20</b>

2.1	Material .....	20
2.1.1	Antibiotics .....	20
2.1.2	Bacterial strains .....	20
2.1.3	Vectors .....	21
2.1.4	Primers .....	23
2.1.5	Plant lines .....	24
2.1.6	Media for bacterial and plant growth .....	26
2.1.7	Buffers and solutions for biochemical studies .....	26
2.1.8	Buffers and solution for metabolite analysis.....	29
2.1.9	Software and databank .....	29
2.2	Methods.....	30
2.2.1	Molecular biology .....	30
2.2.1.1	Cloning and site directed mutagenesis .....	30
2.2.2	Microbiology.....	31
2.2.2.1	Cultures .....	31
2.2.2.2	Transformation .....	31
2.2.3	Plant related methods .....	32
2.2.3.1	Growth of <i>Arabidopsis thaliana</i> .....	32
2.2.3.2	Growth of <i>Nicotiana benthamiana</i> .....	33
2.2.3.3	Stable transformation of <i>Arabidopsis thaliana</i> .....	33
2.2.4	Biochemical methods .....	34
2.2.4.1	Antibody preparation: inclusion body isolation, generation of polyclonal antiserum, and antibody purification.....	34
2.2.4.2	Transient expression in <i>Nicotiana benthamiana</i> .....	34
2.2.4.3	Protein extraction and purification by Strep affinity chromatography .....	35
2.2.4.4	SDS page .....	36
2.2.4.5	Colloidal Coomassie staining and protein quantification .....	36
2.2.4.6	Immunoblot .....	36
2.2.4.7	Sample preparation for protein expression analysis.....	37
2.2.4.8	Activity assay .....	37

2.2.4.9	Immunoprecipitation .....	38
2.2.5	Metabolite analysis by liquid chromatography – mass spectrometry analysis (LC-MS) .....	39
2.2.6	Bioinformatic analyses .....	42
2.2.6.1	Phylogenetic analysis .....	42
2.2.6.2	Protein modelling .....	42
2.2.7	Statistical analysis .....	42
<b>3.</b>	<b>Results.....</b>	<b>43</b>
3.1	Arabidopsis <i>in vivo</i> purine nucleotide catabolism.....	43
3.1.1	Suppression of the <i>UOX</i> mutant phenotype .....	43
3.1.2	Nucleoside and nucleobase content in the mutants of the genes involved in purine nucleotide catabolism .....	47
3.1.3	One more entry point to purine catabolism: XMP dephosphorylation .....	51
3.1.4	Metabolite analysis of purine nucleotide catabolism after dark stress treatment. ....	54
3.1.5	Allopurinol treatment: short-term blockage of purine catabolism.....	56
3.2	Functional analysis of <i>NSH2</i> .....	58
3.2.1	Bioinformatic analysis.....	58
3.2.1.1	Phylogenetic analysis .....	58
3.2.1.2	Modelling of Arabidopsis NSH1 and NSH2.....	60
3.2.2	Biochemical analyses: enzyme purification, activity assessments, and protein-protein interaction studies. ....	62
3.2.2.1	Protein expression and purification.....	62
3.2.2.2	Activity assay and interaction studies .....	63
3.2.3	Analysis of NSH1 and NSH2 expression in Arabidopsis .....	69
3.2.4	Co-immunoprecipitation .....	71
3.2.5	Metabolite analysis of <i>NSH</i> mutants .....	72
3.2.5.1	Metabolite analysis in roots.....	72
3.2.5.2	Metabolite analysis in transgenic lines expressing nucleoside hydrolase variants .....	73



3.2.5.3	Dark stress experiment with NSH mutants .....	76
3.2.6	Interaction of NSH1 and NSH2 in other plant species.....	78
<b>4.</b>	<b>Discussion .....</b>	<b>80</b>
4.1	Arabidopsis <i>in vivo</i> purine nucleotide catabolism.....	80
4.1.1	Functionality of <i>XDH</i> , <i>HGPRT</i> , <i>NSH1</i> , <i>NSH2</i> and <i>GSDA</i> upstream of <i>UOX</i> in purine nucleotide catabolism.....	80
4.1.2	Purine nucleotide catabolism proceeds mainly via guanosine deamination to xanthosine.....	81
4.1.3	XMP dephosphorylation bypassed guanosine deamination in purine nucleotide catabolism.....	83
4.1.4	Inosine, hypoxanthine and guanine are not generated by cytosolic purine nucleotide catabolism.....	84
4.1.5	Updated model of purine nucleotide catabolism.....	86
4.2	Functional analysis of <i>NSH2</i> .....	88
4.2.1	<i>NSH1</i> and <i>NSH2</i> from plants cluster into two clades reflecting a difference in the substrate spectrum .....	88
4.2.2	Arabidopsis <i>NSH1</i> and <i>NSH2</i> interact forming a heterocomplex highly efficient for purine nucleosides hydrolysis.....	89
4.2.3	<i>NSH2</i> exists <i>in vivo</i> in complex with <i>NSH1</i> .....	90
4.2.4	<i>In vivo</i> function of <i>NSH2</i> .....	91
4.2.5	Evolutionary considerations on NSHs activities and interactions in different plant species	94
4.3	Conclusions .....	95
	<b>References .....</b>	<b>97</b>
	<b>Acknowledgment .....</b>	<b>106</b>
	<b>Appendix of Figures .....</b>	<b>107</b>
	<b>Appendix of Tables.....</b>	<b>115</b>
	<b>Curriculum Vitae .....</b>	<b>117</b>

## List of Abbreviations

Amp	Ampicillin
AMP/ADP/ATP	Adenosine monophosphate/diphosphate/triphosphate
APS	Ammonium persulfate
Asp	Aspartate
BCIP	5-bromo-4-chloro-3'-indolyphosphate
BSA	Bovine serum albumin
Carb	Carbenicillin
cmpv	Cowpea mosaic virus
Col-0	<i>Arabidopsis thaliana</i> ecotype Columbia-0
DMF	Dimethylformamide
DMSO	Dimethylsulfoxide
DNA	Deoxyribonucleic acid
DTT	Dithiothreitol
DW	Dried weight
EDTA	Ethylenediaminetetraacetic acid
ESTD	External standard
FW	Fresh weight
Gent	Gentamycin
GMP/GDP/GTP	Guanosine monophosphate/diphosphate/triphosphate
GS/GOGAT	Glutamine synthetase/glutamine oxoglutarate aminotransferase or glutamate synthase
GSDA	Guanosine deaminase
GUS	$\beta$ -glucuronidase
HEPES	4-(2-hydroxyethyl)-1-piperazineethanesulfonic acid
HGPRT	Hypoxanthine guanine phosphoribosyltransferase
HPLC	High performance liquid chromatography
IMP	Inosine monophosphate
IP	Immunoprecipitation
IPTG	isopropyl- $\beta$ -D-thiogalactoside
ISTD	Internal standard

Kan	Kanamycin
KO	Knock out
LB	Lysogeny Broth
LC-MS	Liquid chromatography coupled to mass spectrometry
Lys	Lysine
MES	2-(N-morpholino) ethanesulfonic acid.
mRNA	Messenger RNA
MS	Murashige Skoog
N	Nitrogen
NBT	Nitro-blue tetrazolium chloride
NP	Nonyl phenoxy polyethoxy ethanol
NSH	Nucleoside hydrolase
Page	Polyacrylamide gel electrophoresis
PBS	Phosphate Buffer Saline
PCR	Polymerase chain reaction
PRPP	5-phosphoribosyl-1-pyrophosphate
Rif	Rifampicin
RNA	Ribonucleic acid
rRNA	Ribosomal RNA
SAM	S-adenosylmethionine
SDS	Sodium dodecyl sulfate
TBS (-T)	Tris-buffered saline (with Tween 20)
TEMED	Tetramethylethylenediamine
Tris	Tris(hydroxymethyl)aminomethane
tRNA	Transfer RNA
Tyr	Tyrosine
UOX	Urate oxidase
XDH	Xanthine dehydrogenase
XMP	Xanthosine monophosphate
XMPP	Xanthosine monophosphate phosphatase
YEB	Yeast extract broth

## List of Figures

Figure 1. Nucleotide and nucleobase structure. ....	3
Figure 2. Scheme of Arabidopsis purine nucleotide metabolism.....	5
Figure 3. Caffeine biosynthesis pathway. ....	11
Figure 4. Scheme of Arabidopsis pyrimidine nucleotide metabolism. ....	13
Figure 5. Nucleoside hydrolase reaction. ....	15
Figure 6. Genetic suppression of the <i>uox</i> germination phenotype.....	44
Figure 7. Genetic suppression of the <i>uox</i> seedling establishment phenotype.....	45
Figure 8. Suppression of the <i>uox</i> molecular phenotype. ....	46
Figure 9. Xanthine content in seeds and 10-day-old seedlings of the wild type, the mutants of genes involved in purine nucleotide catabolism and salvage as well as double and triple mutants of the same genes in <i>xdh</i> background. ....	47
Figure 10. Hypoxanthine content of the same samples as in Figure 9.....	48
Figure 11. Guanine and guanosine content of the same samples as in Figure 9.....	49
Figure 12. Xanthosine and inosine content of the same samples as in Figure 9.....	50
Figure 13. Nucleoside content in seeds and seedlings of the wild type, the <i>GSDA NSH1</i> double mutant and the respective single mutants.....	52
Figure 14. Metabolite analysis of rosettes of the wild type, the <i>GSDA NSH1</i> and the <i>GSDA XDH</i> double mutants and the respective single mutants.....	53
Figure 15. Changes in the concentration of purine bases during dark stress. ....	55
Figure 16. Nucleobase concentration changes after conditional short term blockage of purine nucleotide catabolism, dark treatment, and exogenous adenosine application.....	57
Figure 17. Molecular phylogenetic analysis of plant nucleoside hydrolases. ....	59
Figure 18. Homology models of <i>A. thaliana</i> NSH1 and NSH2.....	61
Figure 19. Purification of nucleosidases by Strep affinity chromatography.....	62
Figure 20. Spectrophotometric monitoring of NSH1 and NSH2 nucleoside hydrolase activity. ....	63
Figure 21. Interaction of NSH1 and NSH2 <i>in planta</i> .....	64
Figure 22. Function of the aspartate mutated to alanine in NSH1 and NSH2. ....	66
Figure 23. Purity of affinity (co-) purified nucleoside hydrolases. ....	66
Figure 24. Model of the heterodimer NSH1-NSH2.....	68
Figure 25. Investigation of NSH2 inactivity. ....	69

Figure 26. NSH1 and NSH2 protein expression profiles in different tissues of <i>A. thaliana</i> ...	70
Figure 27. Quantification of NSH1 and NSH2 in roots of <i>A. thaliana</i> .....	71
Figure 28. Interaction of NSH1 and NSH2 in roots of <i>A. thaliana</i> .....	72
Figure 29. Uridine, inosine and xanthosine content in root extracts of Col-0, <i>nsh1</i> and <i>nsh2</i> .	73
Figure 30. Detection of tagged and mutant variants of NSH in Arabidopsis transgenic lines.	74
Figure 31. Concentration of xanthosine, inosine and uridine in extracts of seeds, seedlings and rosettes of the wild type, <i>nsh1</i> , <i>nsh2</i> , <i>nsh1 nsh2</i> , and of the transgenic lines expressing mutant and tagged variants of the NSHs. ....	75
Figure 32. Nucleoside content in rosettes exposed to dark stress. ....	77
Figure 33. Assessment of NSH1 and NSH2 interaction in <i>Physcomitrella patens</i> and <i>Coffea arabica</i> . ....	78
Figure 34. Updated model of purine nucleotide catabolism. ....	87
Figure 35. Dynamic regulation of the NSH1 homomer and NSH-NSH2 heterocomplex. ....	93
Figure A-1. Current model of purine nucleotide catabolism.....	107
Figure A-2. Multiple alignment of the amino acid sequences of plant and algae IU-NSHs..	109
Figure A-3. Expression profile of <i>NSH2</i> in Arabidopsis.....	113
Figure A-4. Expression profile of <i>NSH1</i> and <i>NSH2</i> after hormone and biotic stress treatments.....	114

## List of Tables

Table 2.1-1: Antibiotics.....	20
Table 2.1-2: Bacterial strains. ....	20
Table 2.1-3: Vector list.....	21
Table 2.1-4: Construct list.....	22
Table 2.1-5: Primer list.....	23
Table 2.1-6: <i>Arabidopsis thaliana</i> wild type and knock out lines. ....	24
Table 2.1-7: <i>Arabidopsis thaliana</i> crosses. ....	25
Table 2.1-8: <i>Arabidopsis thaliana</i> transgenic lines generated in the study. ....	25
Table 2.1-9: Media for <i>Agrobacterium tumefaciens</i> (YEB) and <i>Escherichia coli</i> (LB) growth. .....	26
Table 2.1-10: Media for <i>Arabidopsis thaliana</i> growth on plate (half-strength Murashige Skoog) and hydroponic cultures (modified Hoagland solution). ....	26
Table 2.1-11: Buffers for inclusion body isolation. ....	26
Table 2.1-12: Buffer for <i>Nicotiana benthamiana</i> leaf infiltration. ....	26
Table 2.1-13: Buffer for total protein extraction from plant material.....	27
Table 2.1-14: Buffers for extraction and purification of Strep tagged protein. ....	27
Table 2.1-15: Solutions for sodium dodecyl sulfate (SDS) polyacrylamide gel.....	27
Table 2.1-16: Sample loading buffer for SDS polyacrylamide gel electrophoresis.....	27
Table 2.1-17: Running buffer for SDS page. ....	27
Table 2.1-18: Solution for Colloidal Coomassie staining of polyacrylamide gels. ....	28
Table 2.1-19: Solution for immunoblot and detection. ....	28
Table 2.1-20: Buffer for immunoprecipitation (IP). ....	28
Table 2.1-21: Extraction buffer for mass spectrometry sample preparation.....	29
Table 2.1-22: Mass spectrometry running buffer.....	29
Table 2.2-1: PCR program. ....	30
Table 2.2-2: Mass spectrometer source parameter.....	41
Table 2.2-3: MS/MS method parameters .....	41
Table 3-1 Specific activities of different nucleoside hydrolase species.....	65
Table 3-2 Kinetic constants of the NSH1 homomer and the NSH1-NSH2 heteromer. ....	67
Table B-1. Gene locus numbers and accession number.....	115

# 1. Introduction

## 1.1 Plant and nitrogen

Nitrogen (N) is a key element for plant metabolism. In natural ecosystem, it is often a scarce resource limiting growth and reproduction. Plants generate metabolic energy through photosynthesis and are carbon autotrophs, but need to acquire nitrogen from the environment to synthesize N-containing organic molecules. Only a limited group of plants (Leguminosae) is capable of accessing the atmospheric nitrogen pool by nitrogen fixation due to symbiotic association with bacteria in the root nodules. In agriculture, nitrogen is one of the most expensive nutrients supplied as commercial fertilizer. However, most of the administered nitrogen is not imported by the plants, but is lost in the field resulting in soil and water pollution as well as emission of nitrogen oxides, which act as greenhouse gasses. Improvement of plant nitrogen use efficiency in order to lower the fertilizer input without compromising agricultural yield is one of the main goals of plant biotechnology research (Masclaux-Daubresse et al., 2010).

The use of nitrogen by the plant involves three major processes: (i) uptake from the soil, mostly in form of inorganic N (nitrate and ammonium) and reduction of nitrate, (ii) assimilation into glutamate and from there into all other amino acids and N-containing molecules and (iii) remobilization of internally stored nitrogen to synthesized new biomolecules. The molecular mechanisms of nitrogen uptake and assimilation have been studied extensively, and several genes (e.g. nitrate transporters and glutamine synthetase) involved in these processes have been genetically manipulated aiming to improve plant biomass and nitrogen status. Remobilization of N is a key factor for nitrogen use efficiency especially during senescence, when nutrients are recycled from source tissues where they are no longer needed (e.g. old leaves), to sink organs (flowers, seeds, young leaves). Another stage in which remobilization takes place is germination, when seed storage resources are broken down to promote seedlings growth. In cereals, like wheat or rice, 50% to 90% of grain nitrogen content is derived from remobilization (Masclaux-Daubresse et al., 2010). Proteins, especially rubisco, are the main contributors of nitrogen recycling, accounting for 80% of the total leaf N (Masclaux et al., 2000); the remaining 20% is shared between other two endogenous sources of nitrogen, chlorophyll (15%) and nucleotides (5%, Masclaux et al., 2000). The comprehension of nitrogen remobilization from nucleotides is still limited in

plants, and a deeper understanding of this process may contribute to the knowledge base required for the targeted improvement of crops.

## **1.2 Nucleotide metabolism**

### **1.2.1 Nucleotide function and structure**

Nucleotides play an essential role in the metabolism of all organisms. They are building blocks of nucleic acids, and precursors of several essential coenzymes such as nicotinamide adenine dinucleotide (NAD), flavin adenine dinucleotide (FAD), and S-adenosylmethionine (SAM), as well as of the B-class vitamins riboflavin, thiamine and the folates. Additionally, they are fundamental for energy flow, since the trinucleotides, mostly ATP, are the energy donors in most reactions which require energetic coupling. They often participate directly in the synthesis of macromolecules such as proteins and starch, because the activated precursors, AMP-amino acids and ADP-glucose respectively, are generated from ATP. Another important example for a precursor activated by nucleotide binding is UDP-glucose, which acts as a glucosyl donor in several metabolic reactions, for example in the biosynthesis of sucrose, cellulose, and glycoproteins. In addition, nucleotides are required for the production of certain secondary metabolites and hormones such as caffeine and cytokinins (Zrenner et al., 2006).

Nucleotides are composed of three chemical units: a nitrogen-containing heterocycle (the nucleobase), a five-carbon sugar molecule, and phosphate group(s) (Figure 1A). If the phosphate(s) are missing one speaks of nucleosides. The phosphate moiety usually is a mono-, di-, or tri-phosphate, and the respective nucleotide is referred to as nucleoside monophosphate, nucleoside diphosphate or nucleoside triphosphate. The sugar moiety can be ribose in the ribonucleotides, which usually forms a five membered furanose ring, or deoxyribose in the deoxyribonucleotides as well forming a furanose ring but lacking a hydroxy group on carbon 2. Ribonucleotides are present in the ribonucleic acid (RNA) while deoxyribonucleotides are found in deoxyribonucleic acid (DNA). The nucleobases are classified into two groups according to the chemical structure (Figure 1B). Pyrimidine nucleobases are monocyclic and consist of an aromatic ring with four carbon and two nitrogen atoms. Of the pyrimidine bases, uracil is found only in RNA, whereas thymine is present only in DNA. By contrast, cytosine is a constituent of both types of nucleic acids. Purine nucleobases are bicyclic and consist of a



pyrimidine ring fused to an imidazole ring. Adenine, guanine, cytosine, thymine and uracil are called the canonical nucleobases representing the great majority of bases found in nucleic acids. They can be modified by the addition of side chains to generate unusual nucleobases (e.g. N6-methyladenosine and 5-methylcytosine), which are particularly abundant in transfer RNA (tRNA) and ribosomal RNA (rRNA) being necessary for their biogenesis and stability. The unusual nucleobases are present also in messenger RNA (mRNA) where they are involved in post-transcriptional gene regulation (Roundtree et al., 2017).

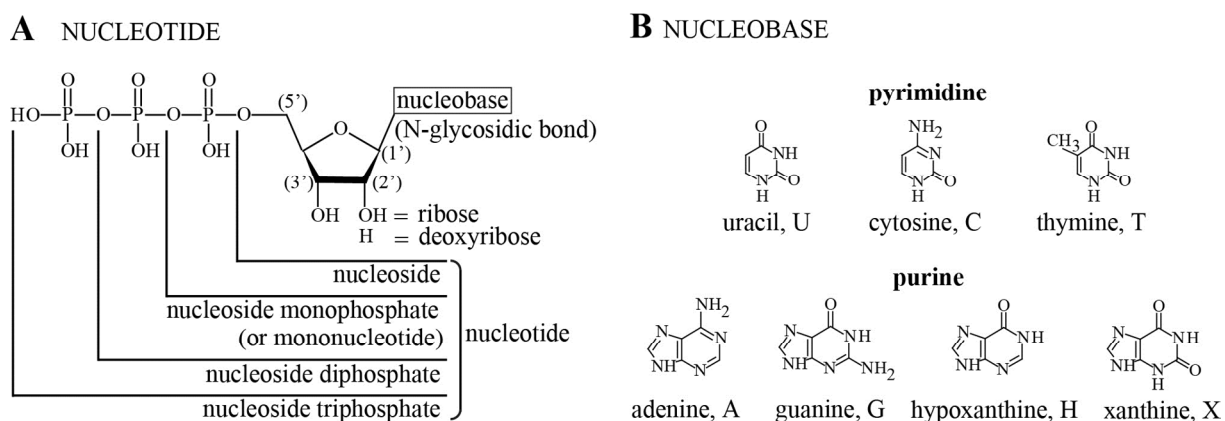


**Figure 1. Nucleotide and nucleobase structure.**

A) Nucleotide structure scheme. B) Chemical structure of the canonical nucleobases uracil, cytosine, thymine, adenine and guanine and two non-canonical ones hypoxanthine and xanthine.

Nucleotide metabolism is broadly divided into three parts: *de novo* synthesis, salvage, and catabolism. While biosynthesis is a high energy consuming process, because the nucleotide ring is built *de novo* starting from small molecules, the salvage reactions require less energy, because they recycle nucleosides and free bases. Catabolism serves to release the nutrient resources (carbon, nitrogen and phosphate) bound in the nucleotide molecules. In addition, nucleotide biosynthesis also involves phosphotransfer reactions to convert mononucleotides derived from *de novo* synthesis or salvage to dinucleotides and finally to the triphosphate form. Reactions to modify nucleotides to produce deoxynucleotides for DNA biosynthesis are part of nucleotide metabolism as well (Zrenner et al., 2006).

## 1.2.2 Purine nucleotide metabolism

### 1.2.2.1 Purine nucleotide biosynthesis

Purine and pyrimidine biosynthesis is evolutionarily conserved in all organisms and common features are shared between prokaryotes and eukaryotes. All living beings are capable of *de novo* synthesis with few exceptions like some parasitic protists (e.g. *Trypanosoma brucei* that cause the sleeping sickness) which lack the biosynthesis machinery and rely completely on importing and recycling nucleotide derivatives from the host (Gopaul et al., 1996; Parkin et al., 1991). Purine *de novo* synthesis consists of 14 reactions (Figure 2) in which the purine ring is gradually formed on a molecule of activated ribose, 5-phosphoribosyl-1-pyrophosphate (PRPP). The process requires the amino acids glutamine, glycine, aspartate, and the C<sub>1</sub> donor N<sup>10</sup>-formyl-tetrahydrofolate. Ten reactions lead to the formation of IMP, then the pathway divides into two branches, one for the synthesis of AMP (two reactions) and the other for the synthesis of GMP (two reactions, Zrenner et al., 2006).

Purine biosynthesis is a highly regulated process to guarantee equilibrium in the nucleotide pool and several steps of the pathway are controlled via feedback regulation mechanisms. For example, the PRPP amidotransferase (ATase) which catalyses the first reaction is inhibited by IMP, AMP and GMP, the adenylosuccinate lyase (ASS) is inhibited by AMP and the IMP dehydrogenase (IMPDH) is inhibited GMP (Stasolla et al., 2003). In animals, *de novo* synthesis enzymes form a multi-enzyme complex called the purinosome (Pedley and Benkovic, 2017), while in plants and prokaryotes they consist of mono functional proteins, with the exceptions of AIR carboxylase (AIRC) and AICAR transformylase/IMP cyclohydrolase (ATIC, Figure 2, Zrenner et al., 2006).

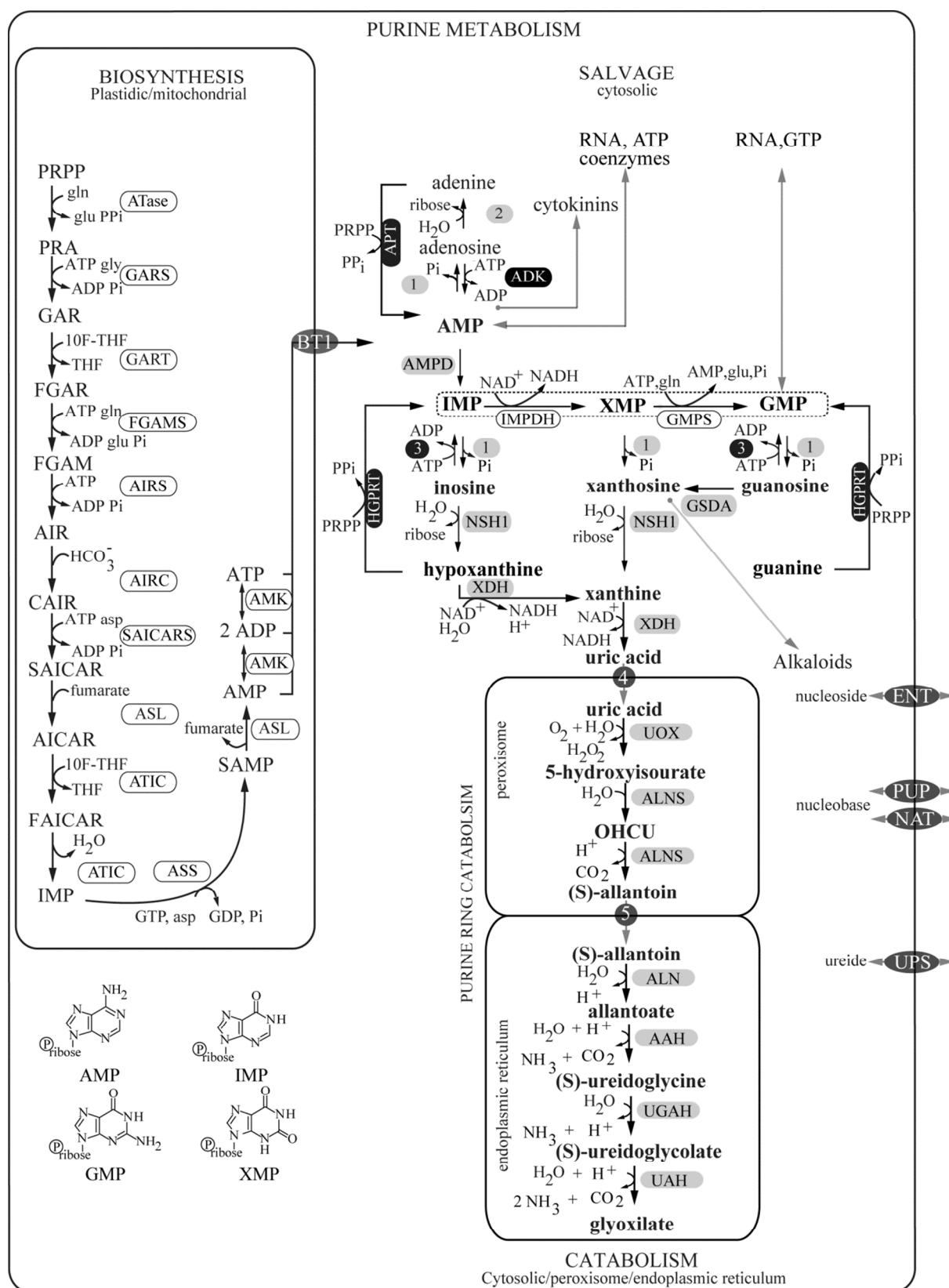


**Figure 2. Scheme of Arabidopsis purine nucleotide metabolism.**

The figure is redrawn from (Zrenner et al., 2006) and updated. Metabolic component

of purine biosynthesis are: 5-phosphoribosyl-1-pyrophosphate (PRPP), glutamine (gln), glutamate (glu), 5-phosphoribosylamine (PRA), pyrophosphate (PPi), glycine (gly), glycinamide ribonucleotide (GAR), 10-formyl tetrahydrofolate (10F-THF), formylglycinamide ribonucleotide (FGAR), formylglycinamide ribonucleotide (FGAM), 5-aminoimidazole ribonucleotide (AIR), 4-carboxy aminoimidazole ribonucleotide (CAIR), aspartate (Asp), N-succinyl-5-aminoimidazole-4-carboxamide ribonucleotide (SAICAR), 5-aminoimidazole-4-carboxamide ribonucleotide (AICAR), 5-formaminoimidazole-4-carboxamide ribonucleotide (FAICAR), inosine monophosphate (IMP), adenylosuccinate (SAMP), adenosine monophosphate (AMP), adenosine diphosphate (ADP), adenosine triphosphate (ATP), xanthosine monophosphate (XMP), guanosine monophosphate (GMP). The cytosolic part of purine *de novo* synthesis (GMP biosynthesis) is in a boxed with dashed border. Enzymes involved in purine biosynthesis are in boxes with white background and are: PRPP amidotransferase (ATase), GAR synthase (GARS), GAR transformylase GART, FGAM synthase (FGAMS), AIR synthase (AIRS), AIR carboxylase (AIRC), SAICAR synthase (SAICARS), adenylosuccinate lyase (ASL), AICAR transformylase/IMP cyclohydrolase (ATIC), adenylosuccinate synthase (ASS), adenylate kinase (AMK), AMP deaminase (AMPD), IMP dehydrogenase (IMPDH), GMP synthetase (GMPS). The last three enzymes belong to both biosynthesis (GMP biosynthesis) and catabolism (AMP/IMP catabolism). Metabolites involved in purine nucleotide catabolism are in bold; OHCU is 2-oxo-4-hydroxy-4-carboxy-5-ureido-imidazoline. Enzymes involved in catabolism are shown with grey background shading and a number is used if the genetic identity of an enzyme is not yet known. These enzymes are: putative nucleotidase(s) for AMP, IMP, XMP and GMP (1), putative adenosine hydrolase (2), guanosine deaminase (GSDA), nucleoside hydrolase 1 (NSH1), xanthine dehydrogenase (XDH), urate oxidase or uricase (UOX), allantoin synthase (ALNS), allantoin amidohydrolase or allantoinase (ALN); allantoate amidohydrolase (AAH), ureidoglycine aminohydrolase (UGAH), ureidoglycolate amidohydrolase (UAH). Enzymes involved in purine salvage are indicated by black background shading and are: putative guanosine inosine kinase (3), hypoxanthine guanine phosphoribosyltransferase (HGPRT), adenosine kinase (ADK), adenine phosphoribosyltransferase (APT). Grey arrows indicate connections with other metabolic pathways. Transporters are indicated in boxes with dark grey background and are: adenine nucleotide transporter (Brittle1, BT1), nucleoside transporters (equilibrative nucleoside transporters, ENT), nucleobase transporters (nucleobase ascorbate transporters, NAT and purine permeases, PUP), ureide transporters (ureide permeases, UPS), putative uric acid transporter (4), putative allantoin transporter (5). Purine metabolism compartmentalization and the formulas of purine nucleotides are shown.

A peculiarity of plant purine nucleotide *de novo* synthesis is the differential localization of AMP and GMP biosynthesis which are predicted to be respectively plastidic and cytosolic (Figure 2). In fact, all the genes encoding enzymes required for IMP and AMP biosynthesis contain sequences that are predicted to encode for N-terminal plastid-transit peptides. However, in *Arabidopsis* the only evidence for chloroplast localization is reported for Atase (Hung et al., 2004). In some plants, IMP biosynthesis might also be localized in both

mitochondria and plastids, as shown for nitrogen-fixing tropical legumes (Atkins et al., 1997). In contrast, the genes responsible for GMP biosynthesis from IMP (IMP dehydrogenase and GMP synthase) do not contain transit peptides; therefore the encoded enzymes might be located in the cytosol (Zrenner and Ashihara, 2011). If AMP and IMP are synthesized in the chloroplast, they later have to be exported to the cytosol. The current hypothesis is that AMP is exported via an adenine nucleotide transporter (Figure 2, and Leroch et al., 2005) from the chloroplast to the cytosol and then converted to IMP by AMP deaminase, to feed the cytosolic branch of GMP biosynthesis.

#### *1.2.2.2 Purine nucleotide catabolism*

In plants, nucleotides derived from the intracellular breakdown of nucleic acids or the general nucleotide pool represent nutrient sources, and they can be degraded completely. The current model of purine nucleotide degradation proposes a branched pathway, in which several routes lead from the nucleotide monophosphates to the oxypurine base xanthine releasing phosphate and (deoxy)ribose on the way. From xanthine, a linear series of reactions results in the complete degradation of the purine ring releasing ammonia, glyoxylate, and carbon dioxide (Figure 2, Figure A1 Appendix).

In detail, IMP, XMP, and GMP are thought to be dephosphorylated to the corresponding nucleosides by phosphatases that are not yet discovered *in vivo* in Arabidopsis. AMP enters the pathway after deamination to IMP by AMP deaminase in the cytosol. The nucleosides xanthosine and inosine are then hydrolysed to release the nucleobase and the ribose. An enzyme required for this step is nucleoside hydrolase 1 (NSH1), which converts in the cytosol inosine to hypoxanthine and xanthosine to xanthine releasing ribose (Jung et al., 2009; Jung et al., 2011; Riegler et al., 2011). NSH1 is involved in pyrimidine degradation as well, hydrolysing the nucleoside uridine to uracil. The function of NSH1 was confirmed *in vivo*: a mutant lacking the functional gene accumulated uridine and xanthosine (Riegler et al., 2011; Jung et al., 2011), and inosine after five days of dark stress (Jung et al., 2011). The ribose released by the hydrolysis of the nucleosides enters plant metabolism after phosphorylation to ribose-5-phosphate catalysed by the enzyme ribokinase, RBSK, in the plastids (Schroeder et al., 2017). The nucleoside guanosine is deaminated to xanthosine by the cytosolic enzyme guanosine deaminase, GSDA (Dahncke and Witte, 2013). High performance liquid chromatography (HPLC) analyses of two independent *GSDA* mutant lines showed

accumulation of guanosine, which was the only nucleoside accumulating in the double mutant *GSDA NSH1*. Therefore, the abrogation of *GSDA* was sufficient to prevent the accumulation of xanthosine in *nsh1* background, which indicates that in Arabidopsis the main source of xanthosine is guanosine deamination and the dephosphorylation of XMP is a negligible source (Dahncke and Witte, 2013).

Of the two nucleobases hypoxanthine and guanine, only the first one is - according to the current model - a source of xanthine, because plants do not possess guanine deaminase (Katahira and Ashihara, 2006; Stasolla et al., 2003; Ashihara et al., 2018), in contrast to bacteria and mammals (Fernández et al., 2009). The nucleobase hypoxanthine is converted by oxidation to xanthine employing the enzyme xanthine dehydrogenase XDH. Xanthine is the first common intermediate of purine nucleotide degradation and it is oxidized by the same enzyme, XDH, to uric acid in the cytosol (Werner and Witte, 2011). Uric acid is imported into the peroxisomes and is oxidized by urate oxidase (UOX) to hydroxyisourate. In Arabidopsis, it is shown that the accumulation of urate in the *UOX* mutant damages the peroxisomes of the cotyledons of the mature embryo and consequently impairs plant development (Hauck et al., 2014). The accumulation of uric acid is not only toxic for plants but also for humans, where high amount of this molecule in the serum is linked to diseases such as hypertension, gout, coronary heart diseases and neurodegenerative disorders. Humans do not possess a functional UOX and the final product of nucleotide degradation is urate, which is excreted in the urine. Unlike humans, plants are capable of full degradation of the purine ring system (Figure 2, Figure A1 Appendix). After uric acid oxidation to hydroxyisourate, two reactions catalysed by allantoin synthase (ALNS) lead to the formation of S-allantoin (Lamberto et al., 2010). Allantoin is then imported in the endoplasmic reticulum and hydrolysed to allantoate by allantoinase (ALN). Three subsequent reactions lead to the full degradation of the purine ring and the release of glyoxylate, carbon dioxide and four molecules of ammonia (Werner et al., 2010). Ammonia is then re-assimilated into amino acids by the coupled activities of glutamine synthetase and glutamate oxoglutarate aminotransferase (GS/GOGAT pathway).

### 1.2.2.3 Purine nucleotide salvage

In addition to *de novo* biosynthesis, nucleotides can be synthesized by recycling nucleosides and free nucleobases by the action of phosphoribosyl-pyrophosphatases and nucleoside kinases. Most of the knowledge about purine salvage in plants has been derived from radio-

tracer experiments in which the fate of exogenously supplied labelled nucleobases and nucleosides was determined by assessing the percentage of radioactivity incorporated into nucleotides and nucleic acids (salvage activity) or into the purine catabolites allantoin, allantoate and carbon dioxide (catabolism, Ashihara et al., 2018). This approach is limited to the supply of nucleobases and nucleosides, because nucleotides are not taken up by plant cells, whereas transporters for nucleosides and nucleobases are present (Figure 2, and Girke et al., 2014).

Of the four nucleobases, adenine is salvaged best and converted to AMP by an adenine phosphoribosyl transferase (APT, Figure 2). In *Arabidopsis* several isoforms of APTs are present, generally they have very low  $K_m$  for adenine and they are assumed to be located in the cytosol, except for one isoform which may be plastidic (Allen et al., 2002; Moffatt and Ashihara, 2002; Ashihara et al., 2018). Guanine and hypoxanthine are recycled by a cytosolic hypoxanthine guanine phosphoribosyl transferase (HGPRT, Figure 2) to GMP and IMP, respectively. However, the activity of this enzyme in plants is much lower than that of the APT activity (Katahira and Ashihara, 2006). Kinetic characterization of the *Arabidopsis* HGPRT showed a lower  $K_M$  for guanine than for hypoxanthine (Liu et al., 2007). The loss of function mutant of the gene coding for HGPRT accumulates guanine (Schroeder et al., 2017), demonstrating that HGPRT is required for guanine salvage *in vivo*. Xanthine is not recycled but is only degraded, as shown by *in situ* tracer experiments with labelled xanthine (Yin et al., 2014).

Of the nucleosides, adenosine is phosphorylated to AMP by an adenosine kinase (ADK, Figure 2). Adenosine enters the degradation pathway or the salvage pathway by being first phosphorylated to AMP, since no adenosine deaminase activity has been found in plants (Stasolla et al., 2003). Two isoforms of ADK were found in *A. thaliana*, and both are located in the cytosol (Moffatt et al., 2000). Inosine and guanosine can be recycled by an inosine guanosine kinase (IGK) to IMP and GMP, as shown by tracer experiments, but the genes encoding the enzyme for this activity are yet to be found in *Arabidopsis*. In contrast to guanosine and inosine, xanthosine is not salvaged but can only enter the catabolic route (Yin et al., 2014).

In plants, the main contribution to purine salvage comes from adenine phosphoribosyl transferase and adenosine kinase. The order of salvage activity is adenine > guanine > hypoxanthine and adenosine > guanosine > inosine (Ashihara et al., 2018). The importance of adenine and adenosine salvage is demonstrated by mutants deficient in APT and ADK

activities. *APT* mutants are characterized by non-fertile pollen (Moffatt and Somerville, 1988); the defects in pollen development are probably due to a deficiency in adenine nucleotides which impairs the energy metabolism (Ashihara et al., 2018). *ADK* mutants show developmental abnormalities caused by the defective adenosine salvage that interferes with the correct SAM (S-adenosylmethionine) utilization and recycling and ultimately inhibits the transmethylation reactions catalysed by the SAM-dependent methyltransferases (Moffatt et al., 2002).

#### 1.2.2.4 *Biological functions of purine nucleotide catabolism*

Nucleotide catabolism allows the release and recycling of the nitrogen stored in the nucleotide. In some nitrogen fixing legumes such as soybean (*Glycine max*) and cowpea (*Vigna unguiculata*) it has been clearly shown that allantoin and allantoate (ureides), products of purine ring catabolism, serve as the nitrogen sources. In these plants, the ureides are the main transport form of the fixed nitrogen from the root to the shoot. N is first assimilated by the GS/GOGAT pathway to form glutamine, which is then incorporated in IMP through the purine biosynthesis pathway. IMP is then degraded via the purine nucleotide degradation pathway to form ureides. Ureides are translocated from the root nodules to the aerial parts of the plant where they are degraded to serve as N source (Christensen and Jochimsen, 1983; Smith and Atkins, 2002).

In non-legume species, such as *Arabidopsis*, a recent study demonstrated the role of the ureides as an endogenous N source in plants grown under limited nitrate conditions (Soltabayeva et al., 2018). However, it has also been shown that defects in the enzymes of purine ring catabolism which prevent nitrogen recycling do not cause marked phenotypes under standard growth conditions (Werner et al., 2008; Werner et al., 2013). This suggests that in non Leguminosae the contribution of purine catabolism in the remobilization processes in non-stressed growth conditions is of minor importance, especially because amino acids, originated from proteins degradation, are the main source from which nitrogen is recycled. It is probable that purine catabolism and its intermediates uric acid, allantoin and allantoate, have different physiological roles. The ureides seem to be involved in protecting plants from abiotic and biotic stress, acting as scavengers of reactive oxygen species (ROS; Smith and Atkins, 2002; Brychkova et al., 2008; Ma et al., 2016). Uric acid seems to interfere with the maintenance of peroxisomes, when it is present at high concentrations (Hauck et al., 2014).



In some species, like coffee (*Coffea arabica*), tea (*Camelia sinensis*), and cacao (*Theobroma cacao*), purine catabolism is related to the production of secondary metabolites, e.g. purine alkaloids. Examples of these metabolites are the methylxanthines caffeine and theobromine that play a role in the defence against insect grub or are released into the soil to inhibit the germination of seeds from other plant species. The biosynthetic pathway of caffeine involves four reactions: three methylation steps and one hydrolysis step (Figure 3). It begins with xanthosine, which is methylated to 7-methylxanthosine by SAM-dependent methyltransferase, 7-methylxanthosine is then hydrolysed to 7-methylxanthine, and then two subsequent methylation steps lead to the formation of theobromine followed by caffeine (Ashihara et al., 2008).

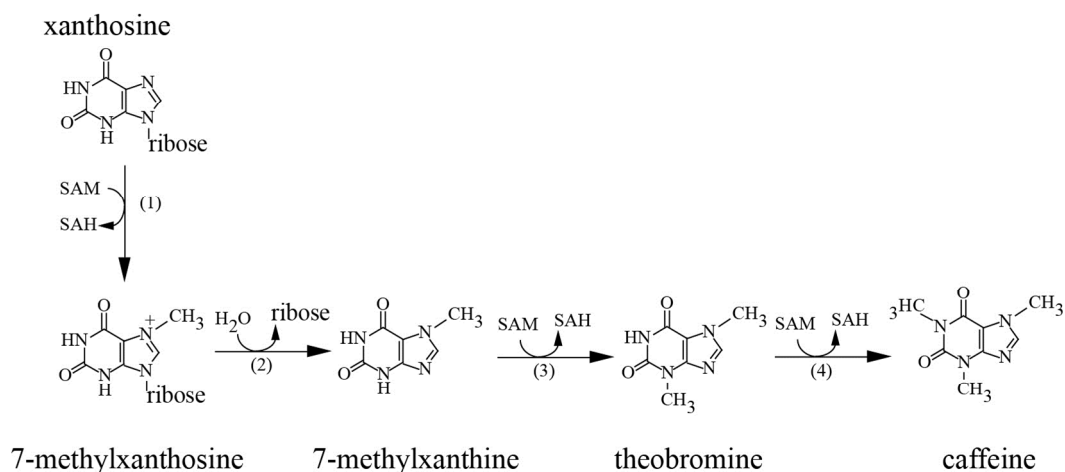


**Figure 3. Caffeine biosynthesis pathway.**

Caffeine biosynthetic pathway from xanthosine. (1) 7-methylxanthosine synthase (xanthosine N-methyltransferase); (2) N-methylnucleosidase; (3) theobromine synthase (monomethylxanthine N-methyltransferase); (4) caffeine synthase (dimethylxanthine N-methyltransferase). SAM, S-adenosylmethionine; SAH, S-adenosinehomocysteine. Figure adapted from Ashihara et al., 2008.

### 1.2.3 Pyrimidine nucleotide metabolism

#### 1.2.3.1 *Pyrimidine nucleotide biosynthesis*

Pyrimidine nucleotide *de novo* synthesis comprises six enzymatic steps (Figure 4) that lead to the formation of uridine monophosphate, UMP, from carbamoylphosphate (CP), aspartate and PRPP (Zrenner et al., 2006). UMP is converted to cytidine triphosphate, CTP, by two phosphorylation steps and one amination reaction. The localization of the pyrimidine biosynthetic pathway is shared between different compartments such as plastids, mitochondria and cytosol (Zrenner and Ashihara, 2011).

#### 1.2.3.2 *Pyrimidine nucleotide catabolism*

UMP and CMP are dephosphorylated by unknown nucleotidases to the nucleosides uridine and cytidine, respectively. Cytidine is deaminated by cytidine deaminase to uridine, and then uridine is hydrolysed by NSH1 to the nucleobase uracil and ribose (Jung et al., 2009). Therefore, NSH1 has a central role in purine and pyrimidine metabolism. Uracil is then catabolized by three subsequent reactions to generate  $\beta$ -alanine,  $\text{CO}_2$  and  $\text{NH}_3$  (Zrenner and Ashihara, 2011).

#### 1.2.3.3 *Pyrimidine nucleotide salvage*

Pyrimidine bases and nucleosides can be salvaged to generate pyrimidine nucleotides. Of the pyrimidine bases, uracil is salvaged by a plastidic PRPP-dependent uracil phosphoribosyltransferase (UPRT), called UPP in Arabidopsis (Mainguet et al., 2009), while no cytosine salvage activity is found in plants as well as animals (Katahira and Ashihara, 2002). The pyrimidine nucleosides uridine and cytidine are salvaged to their respective nucleotides UMP and CMP. A single enzyme, uridine/cytidine kinase which is present in all plants investigated to date is thought to phosphorylate both uridine and cytidine (Chen et al., 2016).

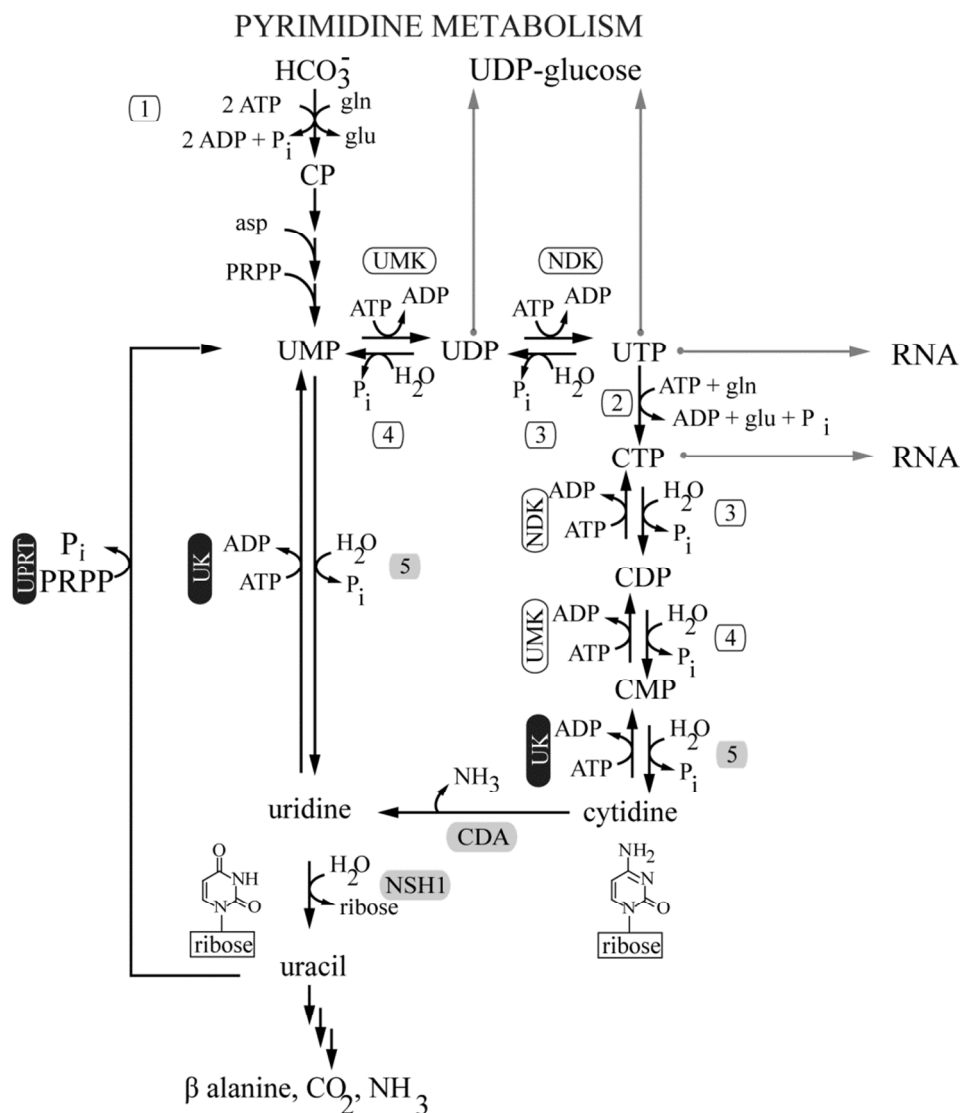


**Figure 4. Scheme of Arabidopsis pyrimidine nucleotide metabolism.**

The figure is redrawn from (Zrenner et al., 2006) and simplified. Metabolites involved in pyrimidine metabolism are: 5-phosphoribosyl-1-pyrophosphate (PRPP), glutamine (gln), glutamate (glu), adenosine triphosphate (ATP), adenosine diphosphate (ADP), inorganic phosphate ( $\text{P}_i$ ), carbamoyl phosphate (CP), uridine monophosphate (UMP), uridine diphosphate (UDP), uridine triphosphate (UTP), uridine diphosphoglucose (UDP-glucose), cytidine monophosphate (CMP), cytidine diphosphate, (CDP), cytidine triphosphate (CTP), pyrophosphate ( $\text{PP}_i$ ), aspartate (asp). Enzymes involved in pyrimidine biosynthesis are in a box with a white background, enzymes whose genetic identity is not known are indicated with a number. The involved enzymes are: carbamoylphosphate synthase (1), uridylylate/cytidylylate kinase (UMK), nucleoside diphosphate kinase (NDK), CTP synthase (2), nucleoside triphosphate phosphatase (3), nucleoside diphosphate phosphatase (4). Enzymes involved in pyrimidine catabolism are indicated by grey background and are: nucleotidase (5), cytidine deaminase (CDA) and nucleoside hydrolase 1 (NSH1). Enzymes involved in pyrimidine salvage are indicated by black shading. These are uridine cytidine kinase (UK) and UPRT (uridine phosphoribosyltransferase). The chemical formulas of uridine and cytidine are shown.

### 1.3 Nucleoside hydrolase

In plants, NSH1 (Section 1.2.2.2, Section 1.2.3.2, Figure 2 and Figure 4) has a pivotal role in pyrimidine and purine nucleoside degradation. Besides NSH1, plant genomes encode a second nucleoside hydrolase, NSH2, which is conserved among plant species but whose function is currently unknown. The next chapter introduces the catalytic mechanism of nucleoside hydrolases (NSHs) and the so far characterized plant NSH enzymes, with focus on *A. thaliana*.

#### 1.3.1 Nucleoside hydrolase catalytic mechanism

Nucleoside hydrolases, or nucleosidases, are glycosidases that catalyze the cleavage of the N-glycosidic bond in nucleosides releasing the ribose and the nucleobase (Figure 5A). These enzymes have been first characterized in protozoa lacking *de novo* biosynthesis (Section 1.2.2.1) such as *Thrypanosoma brucei brucei* (Parkin, 1996a), *Crithidia fasciculata* (Parkin et al., 1991) and *Leishmania major* (Shi et al., 1999). These protozoa are parasites of mammals and insects and cause several diseases e.g. leishmaniasis and sleeping sickness. The NSHs from these organisms were target of pharmaceutical drug design studies, because nucleoside hydrolase homologues do not exist in mammals. Mammals employ nucleoside phosphorylases that catalyze the phosphorolysis of the glycosidic bond and the release of ribose-1-phosphate and the nucleobase. In several organisms, nucleoside hydrolases, nucleoside phosphorylases, and nucleotide biosynthesis co-exist. Often the NSH enzymes of these organisms have lower catalytic efficiency compared to the NSHs of protozoa, and in some cases have developed specific roles, such as prevention of sporulation in *Bacillus anthracis* (Todd et al., 2003), and host anesthesia in the mosquito *Aedes aegypti* (Ribeiro and Valenzuela, 2003).

Nucleosidases are grouped in four different classes based on their substrate specificity: (i) nonspecific hydrolyzing inosine and uridine, IU-NSH (Parkin et al., 1991; Shi et al., 1999), (ii) purine specific inosine-adenosine-guanosine, IAG-NSH (Parkin, 1996a), (iii) 6-oxopurine inosine-guanosine specific, IG-NSH (Estupiñán and Schramm, 1994), (iv) pyrimidine cytidine-uridine specific hydrolase, CU-NSH (Giabbai and Degano, 2004). All NSHs are highly specific for the ribose moiety and differ in the binding of the nucleobase (Kopečná et al., 2013). Crystal structures of several NSHs, empty or in complex with substrates or inhibitors, are available (Shi et al., 1999; Versées et al., 2001; Kopečná et al., 2013).

Nucleoside hydrolases are metalloenzymes characterized by the presence of a conserved N-terminal aspartate motif (DXDXXXDD, DTDPGIDD in plants) which binds to a calcium ion and to the ribose moiety of the substrate. The second aspartate of the cluster acts as a base and abstracts a proton from a catalytic water molecule which performs the nucleophilic attack at the C1 of the ribose moiety of the nucleoside (Figure 5B).

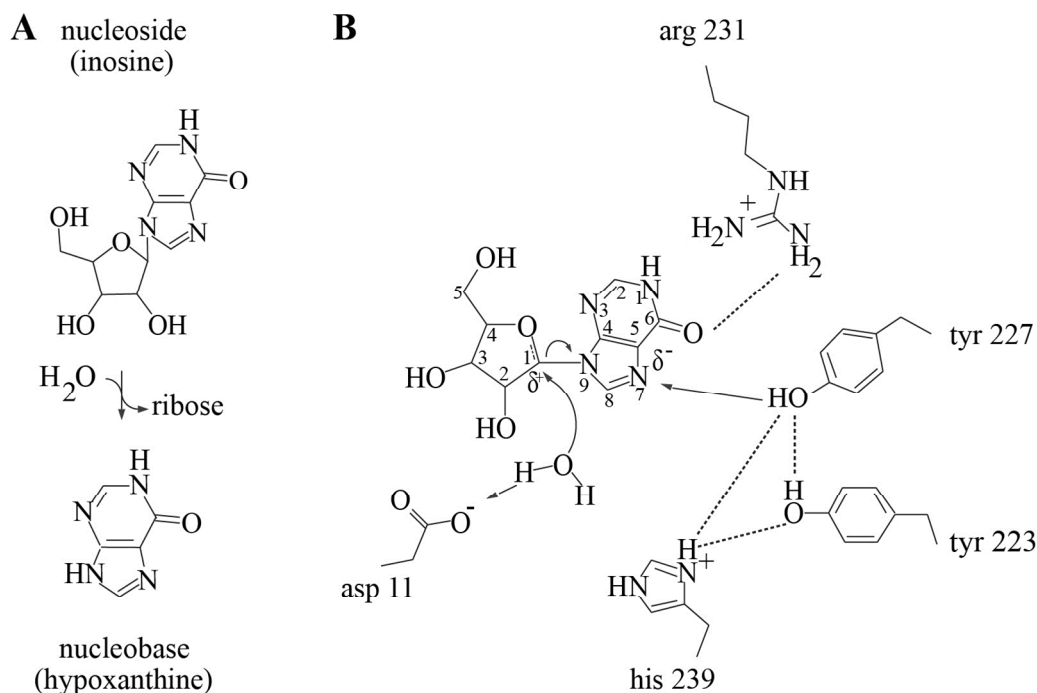


**Figure 5. Nucleoside hydrolase reaction.**

A) Scheme of a generic NSH reaction. B) Reaction mechanism. The catalytic water molecule executes a nucleophilic attack on the C1 of the ribose moiety of the nucleoside. The ribose moiety is distorted toward an oxocarbenium ion-like transition state, bearing a partial positive charge. The developing negative charge in the nucleobase is neutralized by protonation. The figure is from Iovane et al., 2008, and shows the hydrolysis of a purine nucleoside (inosine) in the active site of *Crithidia fasciculata* IU-NSH.

The Ca<sup>2+</sup> is believed to lower the pK<sub>a</sub> of the catalytic water molecule which favors the transfer of a proton to the catalytic base. The hydrolysis of the substrate proceeds via an oxocarbenium ion-like transition state bearing a partial positive charge. The neutralization of the developing negative charge at the nitrogenous base is performed differently according to the type of nucleobase. In case of purines, the N7 atom of the nucleobase is protonated (Figure 5), whereas in case of pyrimidine is the carbonyl O2 atom that is protonated (Iovane et al., 2008). For IU-NSH and CU-NSH, a conserved histidine present in the motif {V, I, L, M} HD located approximately 230 amino acids downstream of the aspartate motif, is the

candidate proton donor. In case of pyrimidine nucleoside hydrolysis, the protonation is performed directly by this histidine, whereas in case of purine nucleoside hydrolysis two other residues act together with the histidine as catalytic triad. In IAG-NSH, the histidine is replaced with an aromatic residue (tyrosine or tryptophan), and in IG-NSH a cysteine in the motif XCDX carries out this function.

### 1.3.2 Plant nucleoside hydrolases

In plants, nucleoside hydrolysis is the only way to degrade nucleosides and thus to release the ammonia stored in the pool of nucleic acids and nucleotides (Jung et al., 2009). Plant nucleoside hydrolase activity has been reported for different plant species such as yellow lupin (*Lupinus luteus*), where a purine specific nucleosidase was purified from seeds (Guranowski, 1982; Szuwart et al., 2006); adenosine specific hydrolase activity was found in coffee (*Coffea arabica*, Campos et al., 2005), barley (*Hordeum vulgare*, Guranowski and Schneider, 1977) and wheat (*Triticum aestivum*, Chen and Kristopeit, 1981) and uridine specific hydrolase activity was found in mung bean (*Phaseolus radiates*, Achar and Vaidyanathan, 1967). Nucleosidase activity was also found in pea (*Pisum sativum*, Christensen and Jochimsen, 1983) and soybean (*Glycine max*, Christensen and Jochimsen, 1983). However, the amino acid sequences of these enzymes have not been reported. The first plant nucleosidases characterized at molecular level are from *A. thaliana* (Jung et al., 2009; Jung et al., 2011; Riegler et al., 2011), *Physcomitrella patens*, and *Zea mays* (Kopečná et al., 2013).

#### 1.3.2.1 *Arabidopsis thaliana* nucleosidases

The *A. thaliana* genome contains five genes that code for putative NSH enzymes, all with the N-terminal aspartate motif typical of nucleoside hydrolases. Of the five genes, NSH1, previously called URH1 (At2g36310) was the first to be characterized. It hydrolyzes uridine, inosine and xanthosine (Section 1.2.2.2). Real time PCR (polymerase chain reaction) data showed that the gene is expressed in leaves, flowers, and stems, but most prominently in roots. GUS ( $\beta$ -glucuronidase) staining of promoter-GUS lines showed gene expression in vascular root tissue, root tips, guard cells and mature pollen (Jung et al., 2009).

NSH2 (At1g05620) is the closest homologue to NSH1, the two proteins contain 322 and 336 amino acid, respectively, and share 49% identical and 67% similar amino acids. Both proteins

are cytosolic (Riegler et al., 2011). Attempts to biochemically characterize NSH2 failed so far because its heterologous expression in *E. coli* leads to the formation of inclusion bodies (Jung et al., 2009; Riegler et al., 2011). Furthermore, mutant plants lacking *NSH2* do not accumulate any of the putative substrates of the enzyme; no increase of inosine, xanthosine or uridine concentration was detected by HPLC analysis in *nsh2* (Riegler et al., 2011). However, there are some reports indicating a role of NSH2 in purine nucleotide degradation: (i) transgenic lines overexpressing NSH2 under the control of the 35S promoter showed slightly increased inosine hydrolysis activity in comparison to wild type plants (Jung et al., 2011); (ii) xanthosine and inosine, but not uridine hydrolytic activity in crude extracts of Arabidopsis leaves and roots of a *NSH2* mutant were reduced (Riegler et al., 2011). It was also shown that the transcript is induced in senescent leaves (Jung et al., 2011), which might indicate an involvement in N-remobilization.

NSH3 (At5g18860) is composed of 891 amino acids and contains two NSH domains. Whereas NSH1 and NSH2 have the conserved His, hallmark of CU- and IU-NSHs, NSH3 contains a tryptophan in the respective position, which is indicative for an IAG-NSH. NSH3 is localized in the apoplast, and it is involved in the removal of extracellular ATP (eATP). eATP has a signaling function in animals and plants, and to act as an efficient signaling molecule it has to be quickly removed from the apoplast after exerting its function. Apyrases, nucleotidases and nucleosidases are involved in this process (Jung et al., 2011).

NSH4 shares 81% identical amino acid composition to the C terminal domain of NSH3, while NSH5 is homologous to the N-terminal part of NSH3, but appears to be truncated. Whether NSH4 and 5 are functional *in vivo* is unclear (Jung et al., 2011).

### 1.3.2.2 *Physcomitrella patens* nucleosidases

The genome of *Physcomitrella patens* encodes three nucleosidases: one homologue to Arabidopsis NSH2 renamed in this work PpNSH2 (formerly called PpNRH1), and two NSH1 paralogues PpNSH1 and PpNSH3 (formerly called PpNRH2 and PpNRH3 respectively). In contrast to Arabidopsis NSH1, PpNSH1 expression and purification in *E. coli* leads to the formation of inclusion bodies and only small quantities of soluble enzyme could be obtained. Attempts to determine the substrate specificity of PpNSH1 revealed that it prefers uridine rather than xanthosine and inosine, and metabolic analysis of a *PpNSH1* mutant showed accumulation of uridine, which is also observed in the *NSH1* mutant of *A. thaliana*. PpNSH2

could be purified and biochemically characterized. The enzyme exhibits xanthosine and inosine hydrolytic activity. The function of PpNSH2 has been confirmed *in vivo*: Physcomitrella mutant lacking *PpNSH2* showed strong accumulation of inosine as well as some accumulation of xanthosine. The crystal structure of PpNSH2 is available and it resembles the structure of *C. fasciculata* NSH (Parkin et al., 1991) and *L. major* NSH (Shi et al., 1999). In the crystal, PpNSH2 is organized in asymmetric units of four similar dimers, and gel filtration chromatography data showed that the active form in solution is a dimer. The main difference between the plant nucleoside hydrolase structure and the ones from protozoa is that a loop region (278-294, PpNSH2 numbering), involved in dimer contact, is longer in plant nucleosidases (Kopečná et al., 2013). *PpNSH3* is thought to play a minor a minor role because evidence for its *in vivo* function is lacking (Kopečná et al., 2013).

### 1.3.2.3 *Zea mays* nucleosidases

The genome of *Zea mays* contains several genes encoding nucleoside hydrolases (Kopečná et al., 2013). Two of these encode enzymes homologues of Arabidopsis NSH2 (renamed in this work ZmNSH2a and ZmNSH2b and formerly called ZmNRH1a and ZmNRH1b), three encode homologues of Arabidopsis NSH1 (ZmNSH1a, ZmNSH1b, ZmNSH1c, formerly called ZmNRH2a, ZmNRH2b and ZmNRH3) and one encode a homologue of Arabidopsis NSH3. As in *A. thaliana*, ZmNSH2a and ZmNSH2b were insoluble when expressed in *E. coli*, only small quantities of soluble enzymes could be obtained to test the activity. The results showed that they are inosine-xanthosine hydrolases. On the other side, ZmNSH1a, ZmNSH1b were mostly active with uridine and xanthosine while ZmNSH1c was mostly active with inosine and xanthosine. Thus, *Zea mays* has two types of NSH1 enzymes, one that hydrolyzes mostly uridine and xanthosine, like the Arabidopsis NSH1, and one that exhibits inosine xanthosine hydrolase activity, like PpNSH2. The reason for this diversification is not known. The structure of ZmNSH1c has been solved; the asymmetric unit contains one dimer. The *in vivo* function of *Zea mays* nucleosidases has not been determined (Kopečná et al., 2013).



## 1.4 Aim of this study

The current model of plant purine nucleotide catabolism consists of multiple pathways that start at the level of nucleotides and converge on xanthine, the first common intermediate of purine nucleotide degradation. From xanthine, a linear series of reactions, fully described *in vivo* and *in vitro*, leads to the complete degradation of the purine ring. The research presented here focuses on the branched part of the pathway upstream of xanthine, and aims to determine the catabolic routes employed *in vivo* by *Arabidopsis*. The current model has been inferred mainly from experiments with radiolabeled nucleosides or nucleobases added to plant extracts or isolated tissues and tracing the metabolic fate of the label. This study reexamines purine nucleotide catabolism by using a different approach, which is phenotypical characterization and metabolic analysis of loss of function mutants of genes involved in purine nucleotide degradation and salvage. Not only single mutants but also combinations of double order and triple order of mutants were used. An additional goal was to elucidate the function of *Arabidopsis* NSH2 which was suspected to play a role in purine nucleotide catabolism but could so far not be placed into the current model of the pathway. For this purpose, biochemical and metabolic analysis were performed to determine the activity and the physiological function of the enzyme.

## 2. Material and Methods

### 2.1 Material

#### 2.1.1 Antibiotics

**Table 2.1-1: Antibiotics.**

Antibiotic	Solvent	Stock concentration (mg mL <sup>-1</sup> )	Working concentration (µg mL <sup>-1</sup> )
Ampicillin (Amp)	H <sub>2</sub> O	100	100
Carbenicillin (Carb)	H <sub>2</sub> O	50	75 in plates, 50 in liquid culture
Gentamycin (Gent)	H <sub>2</sub> O	15	15
Kanamycin (Kan)	H <sub>2</sub> O	50	50
Rifampicin (Rif)	DMSO <sup>1</sup>	50	50

<sup>1</sup>DMSO: dimethyl sulfoxide.

#### 2.1.2 Bacterial strains

**Table 2.1-2: Bacterial strains.**

Species	Strain	Resistance
<i>Escherichia coli</i>	K-12 DH10B (Invitrogen)	-
<i>Escherichia coli</i>	BL21 (DE3) (Novagen)	-
<i>Agrobacterium tumefaciens</i>	GV3101::pMP90RK (Koncz and Schell, 1986)	Rif <sup>R</sup> in the genome, Gent <sup>R</sup> and Kan <sup>R</sup> on the helper plasmid
<i>Agrobacterium tumefaciens</i>	C58C1::pCH322 (Voinnet et al., 2003)	Rif <sup>R</sup>

## 2.1.3 Vectors

Table 2.1-3: Vector list.

Vector Name	Elements	Function
pJET1.2/blunt (Thermo)	Rep (pMB1), Amp <sup>R</sup> , eco47IR, PlacUV5, T7 promoter	Cloning of blunt-ended PCR product.
pXNS2pat-Strep (V42 <sup>1</sup> , Cao et al., 2010)	ori Cole1, ori RK2, p35S, pA35S, BASTA <sup>R</sup> , Amp <sup>R</sup> , Carb <sup>R</sup> , Strep tag	Binary vector for the overexpression of N-terminal Strep-tagged protein <i>in planta</i> .
pET30nco-CTH (V48 <sup>1</sup> , Myrach et al., 2017)	Kan <sup>R</sup> , T7 Promotor, LacI, His tag	Overexpression of N-terminal His-tagged protein in <i>Escherichia coli</i> .
pXS2pat (V51 <sup>1</sup> , Cao et al., 2010)	ori Cole1, ori RK2, p35S, pA35S, BASTA <sup>R</sup> , Amp <sup>R</sup> , Carb <sup>R</sup>	Binary vector for overexpression of untagged protein <i>in planta</i> .
pXNS2pat-myc (V103 <sup>1</sup> , Baccolini and Witte, 2019)	ori Cole1, ori RK2, p35S, pA35S, BASTA <sup>R</sup> , Amp <sup>R</sup> , Carb <sup>R</sup> , myc tag	Binary vector for the overexpression of N-terminal myc- tagged protein <i>in planta</i> . The vector encodes an <i>NcoI</i> recognition sequence in the multiple cloning site.
pXNS1pat-myc (V102 <sup>1</sup> , Baccolini and Witte, 2019)	ori Cole1, ori RK2, p35S, pA35S, BASTA <sup>R</sup> , Amp <sup>R</sup> , Carb <sup>R</sup> , myc tag	Binary vector for the overexpression of N-terminal myc- tagged protein <i>in planta</i> . The vector encodes an <i>NdeI</i> recognition sequence in the multiple cloning site.
pXNS1cpmv-strep (V89 <sup>1</sup> )	ori Cole1, ori RK2, p35S, pA35S, BASTA <sup>R</sup> , Amp <sup>R</sup> , Carb <sup>R</sup> , 5'- and 3'- UTRs of cpmv, Strep tag	Binary vector for the overexpression of N-terminal Strep-tagged protein <i>in planta</i> . The vector contains modified 5'- and 3'- untranslated region (UTR) from Cowpea mosaic virus (CPMV) RNA-2, leading to enhanced protein expression. It encodes an <i>NdeI</i> recognition sequence in the multiple cloning site.
pXNS2cpmv-strep (V90 <sup>1</sup> , Baccolini and Witte, 2019)	ori Cole1, ori RK2, p35S, pA35S, BASTA <sup>R</sup> , Amp <sup>R</sup> , Carb <sup>R</sup> , 5'- and 3'- UTRs of cpmv, Strep tag	Binary vector for the overexpression of N-terminal Strep-tagged protein <i>in planta</i> . The vector contains modified 5' - and 3' - untranslated region (UTR) from Cowpea mosaic virus (CPMV) RNA-2, leading to enhanced protein expression. It encodes an <i>NcoI</i> recognition sequence in the multiple cloning site.
p35S::p19 (Voinnet et al., 2003)	p35S, p19, Kan <sup>R</sup>	Binary vector for the expression of the silencing inhibitor p19.

<sup>1</sup>Laboratory internal reference number.

**Table 2.1-4: Construct list.**

<b>Nr.</b> <sup>1</sup>	<b>Gene</b> <sup>2</sup>	<b>Vector</b>	<b>Cloning</b>	<b>Description</b>
X3	At1g05620	V42	<i>NcoI, BamHI</i>	Expression of N-terminal Strep-tagged NSH2 <i>in planta</i> .
X4	At2g36310	V42	<i>NcoI, BamHI</i>	Expression of N-terminal Strep-tagged NSH1 <i>in planta</i> .
H86 <sup>3</sup>	At1g05620	V103	<i>NcoI, BamHI</i>	Expression of N-terminal myc-tagged NSH2 <i>in planta</i> .
H87 <sup>3</sup>	At2g36310	V103	<i>NcoI, BamHI</i>	Expression of N-terminal myc-tagged NSH1 <i>in planta</i> .
H88 <sup>3</sup>	At1g05620	pJET1.2	Amplification of X3 with primers 1904 and P105 and ligation in pJET1.2	Introduction of <i>SmaI</i> restriction site at the C- terminus of NSH2.
H89 <sup>3</sup>	At2g36310	pJET1.2	Amplification of X4 with primers 1905 and P106 and ligation in pJET1.2	Introduction of <i>SmaI</i> restriction site at the C- terminus of NSH1.
H91 <sup>3</sup>	At1g05620	V48	<i>NcoI, SmaI</i>	Expression of untagged NSH2 in <i>E. coli</i> .
H92 <sup>3</sup>	At2g36310	V48	<i>NcoI, SmaI</i>	Expression of untagged NSH1 in <i>E. coli</i> .
H95 <sup>3</sup>	At1g05620	V90	<i>NcoI, BamHI</i>	Enhanced expression of N-terminal Strep- tagged NSH2 <i>in planta</i> .
H173	At2g36310	V42	Mutagenesis of X4 with primer pairs P468 + P447 and P446 + P469	Expression of N-terminal Strep-tagged $\Delta$ NSH1 <i>in planta</i> (Doering, 2018, MSc thesis).
H181	At2g36310	V42	Mutagenesis of X4 with primer pairs P468 + P453 and P452 + P469	Expression of N-terminal Strep-tagged (K300A) NSH1 <i>in planta</i> . Construct provided by Lennart Doering.
H182 <sup>3</sup>	At2g36310	V103	<i>NcoI, BamHI</i>	Expression of N-terminal myc-tagged $\Delta$ NSH1, <i>in planta</i> .
H192	At1g05620	V103	Mutagenesis of H95 with primer pairs 0001 + P514 and P513 + 0002	Expression of N-terminally myc-tagged $\Delta$ NSH2, <i>in planta</i> . Construct provided by Lennart Doering.
H193	At1g05620	V90	<i>NcoI, BamHI</i>	Expression of N-terminally Strep-tagged $\Delta$ NSH2, <i>in planta</i> . Construct provided by Lennart Doering.
H196 <sup>3</sup>	At2g36310	V103	<i>NcoI, BamHI</i>	Expression of N-terminal myc-tagged (K300A) NSH1, <i>in planta</i> .

H42	V89	<i>NdeI, BamHI</i>	Expression of N-terminal Strep-tagged NSH1 of <i>Coffea arabica</i> , <i>in planta</i> (Lohani, 2016, MSc thesis).
H43	V89	<i>NdeI, XmaI</i>	Expression of N-terminal Strep-tagged NSH2 of <i>Coffea arabica</i> , <i>in planta</i> (Lohani, 2016, MSc thesis).
H197 <sup>3</sup>	V102	<i>NdeI, BamHI</i>	Expression of N-terminal myc-tagged NSH1 of <i>Coffea arabica</i> , <i>in planta</i> .
H198 <sup>3</sup>	V102	<i>NdeI, XmaI</i>	Expression of N-terminal myc-tagged NSH2 of <i>Coffea Arabica</i> , <i>in planta</i> .

<sup>1</sup> Laboratory internal construct number.

<sup>2</sup> The cDNA of the gene is cloned in the corresponding construct.

<sup>3</sup> Construct made in this study.

#### 2.1.4 Primers

**Table 2.1-5: Primer list.**

Nr. <sup>1</sup>	Sequence	Description
1903	TTCCATGGCGATAGGAGACCG	Forward primer to clone NSH2 cDNA.
1904	TTGGATCCTTAAGACTCCATAAGC CTATCCATTA	Reverse primer to clone NSH2 cDNA.
1905	TTCCATGGATTGTGGTATGGAGAA TTG	Forward primer to clone NSH1 cDNA.
1906	TTGGATCCTTATGGCTTCATCAGCT TTG	Reverse primer to clone NSH1 cDNA.
P105	TTCCCGGGTTAAGACTCCATAAGC CTATCCATTA	Reverse primer to insert a <i>SmaI</i> recognition site at the 3' end of NSH2 cDNA.
P106	TTCCCGGGTTATGGCTTCATCAGCT TTG	Reverse primer to insert a <i>SmaI</i> recognition site at the 3' end of NSH1 cDNA.
P446	AAGCTCATTATCGATACAGCCCCA GGAATTGATGATAGC	Site directed mutagenesis of NSH1 to prepare $\Delta$ NSH1.
P447	GCTATCATCAATTCCTGGGGCTGT ATCGATAATGAGCTT	Site directed mutagenesis of NSH1 to prepare $\Delta$ NSH1.
P468	TTGAAAAAGGCGCCTCCATGGATT GTGGTATGGAG	Site directed mutagenesis of NSH1 to prepare $\Delta$ NSH1.
P469	GAAGTAGTGGATCCTTATGGCTTC ATCAGCTTTGCTTTGAC	Site directed mutagenesis of NSH1 to prepare $\Delta$ NSH1.

P452	CTCATGGATCAAGGCCTCGCGAGA TGGAACGGAAGCAA	Site directed mutagenesis of NSH1 to prepare K300A NSH1.
P453	TTGCTTCCGTTCCATCTCGCGAGGC CTTGATCCATGAG	Site directed mutagenesis of NSH1 to prepare K300A NSH1.
P513	GAAGATTATCATCGATACTGCTCC TGGAATCGATGATGCAA	Site directed mutagenesis of NSH2.
P514	TTGCATCATCGATTCCAGGAGCAG TATCGATGATAATCTTC	Site directed mutagenesis of NSH2.
0001	AAGGAAGTTCATTTTCATTTG	Site directed mutagenesis of NSH1 and NSH2.
0002	AGCGAAACCCTATAAGAA	Site directed mutagenesis of NSH1 and NSH2.

<sup>1</sup> Laboratory internal primer number.

### 2.1.5 Plant lines

**Table 2.1-6: *Arabidopsis thaliana* wild type and knock out lines.**

Nr. <sup>1</sup>	Name	Ecotype	Lines	Collection	Reference <sup>2</sup>
WT	Col-0	Col-0	-	-	-
KO 10 <sup>3</sup>	<i>uox-1</i>	Col-0	SALK131438	SALK (Alonso et al., 2003)	(Hauck et al., 2014)
KO 25 <sup>3</sup>	<i>xdh1-2</i>	Col-0	GK049D04	GABI-Kat (Kleinboelting et al., 2012)	(Hauck et al., 2014); allele assignment by Ma et al. (2016)
KO 27 <sup>3</sup>	<i>gsda-1</i>	Col-0	SAIL305B08	SAIL (Sessions et al., 2002)	(Dahncke and Witte, 2013)
KO 28 <sup>3</sup>	<i>gsda-2</i>	Col-0	GK432D08	GABI-Kat (Kleinboelting et al., 2012)	(Dahncke and Witte, 2013)
KO 29 <sup>3</sup>	<i>hgprt-2</i>	Col-0	GK015E03	GABI-Kat (Kleinboelting et al., 2012)	(Schroeder et al., 2017)
KO 32 <sup>3</sup>	<i>nsh2-1</i>	Col-0	SALK128723	SALK (Alonso et al., 2003)	(Riegler et al., 2011)
KO 34 <sup>3</sup>	<i>nsh1-1</i>	Col-0	SALK083120	SALK (Alonso et al., 2003)	(Jung et al., 2011)

<sup>1</sup> Laboratory internal knock out number.

<sup>2</sup> Citation of the first mentioning and allele assignment.

<sup>3</sup> Line obtained by T-DNA insertion mutagenesis from the European Arabidopsis Stock Center (NASC). The line has been previously genotyped and lack functional allele of the corresponding gene.

**Table 2.1-7: *Arabidopsis thaliana* crosses.**

Number <sup>1</sup>	Name	Pollen recipient	Pollen donor
C11 <sup>2</sup>	<i>uox-1 xdh1-2</i>	<i>uox-1</i>	<i>xdh1-2</i>
C13 <sup>2</sup>	<i>uox-1 hgprt-2</i>	<i>hgprt-2</i>	<i>uox-1</i>
C17 <sup>2</sup>	<i>uox-1 gsda-1</i>	<i>gsda-1</i>	<i>uox-1</i>
C18 <sup>2</sup>	<i>uox-1 gsda-2</i>	<i>gsda-2</i>	<i>uox-1</i>
C40 <sup>2</sup>	<i>uox-1 nsh2-1</i>	<i>nsh2-1</i>	<i>uox-1</i>
C39 <sup>2</sup>	<i>uox-1 nsh1-1</i>	<i>nsh1-1</i>	<i>uox-1</i>
C30 <sup>2</sup>	<i>xdh1-2 hgprt-2</i>	<i>hgprt-2</i>	<i>xdh1-2</i>
C60 <sup>2</sup>	<i>xdh1-2 gsda-2</i>	<i>xdh1-2</i>	<i>gsda-2</i>
C50 <sup>2</sup>	<i>xdh1-2 nsh1-1</i>	<i>xdh1-2</i>	<i>nsh2-1</i>
C51 <sup>2</sup>	<i>xdh1-2 nsh2</i>	<i>xdh1-2</i>	<i>nsh1-1</i>
C47 <sup>2</sup>	<i>gsda-2 nsh1-1</i>	<i>gsda-2</i>	<i>nsh1-1</i>
C49 <sup>2</sup>	<i>nsh1-1 nsh2-1</i>	<i>nsh1-1</i>	<i>nsh2-1</i>
C70 <sup>t2</sup>	<i>uox-1 nsh1-1 nsh2-1</i>	<i>uox-1 nsh1-1</i>	<i>uox-1 nsh2-1</i>
C69 <sup>t2</sup>	<i>xdh1-2 nsh1-1 nsh2-1</i>	<i>xdh1-2 nsh2-1</i>	<i>xdh1-2 nsh1-1</i>

<sup>1</sup> Laboratory internal reference number.

<sup>2</sup> The preparation and the genotyping of the cross were performed previously and were not part of this work.

**Table 2.1-8: *Arabidopsis thaliana* transgenic lines generated in the study.**

Nr. <sup>1</sup>	Name	Recipient	Promoter	Gene	Tag	resistance
H173	<i>nsh1::ΔNSH1-s</i>	<i>nsh1-1</i>	35S	At2g36310	Strep	BASTA <sup>R</sup>
X4	<i>nsh1::NSH1-s</i>	<i>nsh1-1</i>	35S	At2g36310	Strep	BASTA <sup>R</sup>
H87	<i>nsh1::NSH1-m</i>	<i>nsh1-1</i>	35S	At2g36310	myc	BASTA <sup>R</sup>
H95	<i>nsh2::NSH2-s</i>	<i>nsh2-1</i>	35S	At1g05620	Strep	BASTA <sup>R</sup>
H86	<i>nsh2::NSH2-m</i>	<i>nsh2-1</i>	35S	At1g05620	myc	BASTA <sup>R</sup>

<sup>1</sup> Laboratory internal reference number.

### 2.1.6 Media for bacterial and plant growth

**Table 2.1-9: Media for *Agrobacterium tumefaciens* (YEB) and *Escherichia coli* (LB) growth.**

Medium	Composition
Lysogeny Broth (LB)	1% (w/v) tryptone; 0.5% (w/v) yeast extract; 1% (w/v) NaCl, pH 7.0 (adjusted with NaOH); to prepare solid media 1.5% (w/v) agar.
Yeast extract broth (YEB)	0.5% (w/v) meat extract; 0.1% (w/v) yeast extract; 0.5% (w/v) pepton; 0.5% (w/v) sucrose; 2mM MgSO <sub>4</sub> , pH 7.2 (adjusted with NaOH); to prepare solid media 1.5% (w/v) agar.

**Table 2.1-10: Media for *Arabidopsis thaliana* growth on plate (half-strength Murashige Skoog) and hydroponic cultures (modified Hoagland solution).**

Medium	Composition
Half-strength Murashige Skoog (half-strength MS)	2.45 gL <sup>-1</sup> MS salt including vitamins and MES <sup>1</sup> buffer (Duchefa); pH 5.7 (adjusted with KOH), 0.8% (w/v) phytoagar (Duchefa).
Modified Hoagland solution (Myrach et al., 2017)	1.5 mM KNO <sub>3</sub> ; 0.75 mM Ca(NO <sub>3</sub> ) <sub>2</sub> ; 0.75 mM MgSO <sub>4</sub> ; 0.5 mM (NH <sub>4</sub> ) <sub>2</sub> SO <sub>4</sub> ; 0.5 mM K <sub>2</sub> HPO <sub>4</sub> ; 0.5 mM KCl; 0.1 mM Fe-EDTA <sup>2</sup> ; 50 μM H <sub>3</sub> BO <sub>3</sub> ; 20 μM ZnSO <sub>4</sub> ; 10 μM MnSO <sub>4</sub> ; 1 μM CuSO <sub>4</sub> ; 1 μM Na <sub>2</sub> O <sub>3</sub> Si; 0.1 μM Na <sub>2</sub> MoO <sub>4</sub> ; pH 5.7, adjusted with HCl.

<sup>1</sup> 2-(N-morpholino) ethanesulfonic acid.

<sup>2</sup> Ethylenediaminetetraacetic acid.

### 2.1.7 Buffers and solutions for biochemical studies

**Table 2.1-11: Buffers for inclusion body isolation.**

Buffer	Composition
Lysis	50 mM Tris <sup>1</sup> -HCl pH 8; 0.25% (w/v) sucrose; 1 mM EDTA.
Detergent	20 mM Tris-HCl pH 7.5; 2 mM EDTA (pH 8.0); 200 mM NaCl, 1% (w/v) deoxycholic acid; 1% (v/v) Nonidet P-40.
Washing	0.5% Triton X-100; 1 mM EDTA (pH 8.0).
Phosphate Buffer Saline (PBS)	137 mM NaCl; 2.7 mM KCl; 10 mM Na <sub>2</sub> HPO <sub>4</sub> ; 1.8 mM KH <sub>2</sub> PO <sub>4</sub> .

<sup>1</sup> tris(hydroxymethyl)aminomethane.

**Table 2.1-12: Buffer for *Nicotiana benthamiana* leaf infiltration.**

Buffer	Composition
Infiltration Buffer	10 mM MES (pH 5.6, adjusted with KOH), 10 mM MgCl <sub>2</sub> , 150 μM acetosyringone.



**Table 2.1-13: Buffer for total protein extraction from plant material.**

Buffer	Composition
Extraction Buffer	100 mM HEPES <sup>1</sup> buffer pH 8; 100 mM NaCl; 5 mM EDTA; 0.005% (w/v) TritonX 100; 15 mM DTT <sup>2</sup> .

<sup>1</sup> 4-(2-hydroxyethyl)-1-piperazineethanesulfonic acid.

<sup>2</sup> Dithiothreitol.

**Table 2.1-14: Buffers for extraction and purification of Strep tagged protein.**

Buffer	Composition
Extraction	100 mM HEPES buffer pH 8; 100 mM NaCl; 5 mM EDTA; 0.005% (w/v) TritonX 100; 15 mM DTT; 100 µg mL <sup>-1</sup> avidin.
Washing	100 mM HEPES buffer pH 8; NaCl 100 mM, 0.5 mM EDTA; 0.005% (w/v) TritonX 100; 2 mM DTT.
Elution	100 mM HEPES buffer pH 8; NaCl 100 mM, 0.5 mM EDTA; 0.005% (w/v) TritonX 100; 2 mM DTT; 10 mM biotin.

**Table 2.1-15: Solutions for sodium dodecyl sulfate (SDS) polyacrylamide gel.**

Buffer	Composition
Stacking gel	125 mM Tris-HCl (pH 6.8); 4% (w/v) Acrylamide : Bis-acrylamide (37.5 : 1); 0.1% (w/v) SDS; 0.1% (w/v) APS <sup>1</sup> ; 0.1% (w/v) TEMED <sup>2</sup> .
Resolving gel	375 mM Tris-HCl (pH 8.8); 10% (w/v) Acrylamide : Bis-acrylamide (37.5 : 1); 0.1% (w/v) SDS; 0.075% (w/v) APS; 0.05% (w/v) TEMED.

<sup>1</sup> Ammonium persulfate.

<sup>2</sup> Tetramethylethylenediamine.

**Table 2.1-16: Sample loading buffer for SDS polyacrylamide gel electrophoresis (SDS-page).**

Buffer	Composition
SDS loading buffer (five-fold)	500 mM DTT; 300 mM Tris-HCl (pH 6.8); 50% (v/v) glycerol; 10% (w/v) SDS; 0.2% bromophenol blue.

**Table 2.1-17: Running buffer for SDS page.**

Buffer	Composition
Running buffer	25 mM Tris-HCl; 192 mM Glycine; 0.1% (w/v) SDS.

**Table 2.1-18: Solution for Colloidal Coomassie staining of polyacrylamide gels.**

<b>Buffer</b>	<b>Composition</b>
Fixation	40% (v/v) ethanol; 10% (v/v) acetic acid.
Colloidal Coomassie dye stock	0.1% (w/v) Coomassie Brilliant Blue G-250; 10% (w/v) ammonium sulfate; 1% (v/v) phosphoric acid.
Staining solution	80% (v/v) Colloidal Coomassie dye stock; 20% (v/v) methanol.

**Table 2.1-19: Solution for immunoblot and detection.**

<b>Buffer</b>	<b>Composition</b>
Blotting buffer	48 mM Tris-HCl (pH 9.2); 0.5 mM SDS; 40 mM glycine; 20% (v/v) methanol.
TBS <sup>1</sup>	20 mM Tris-HCl (pH 7.6); 150 mM NaCl.
TBS-T	20 mM Tris-HCl (pH 7.6); 150 mM NaCl; 0.1% (v/v) Tween 20.
Blocking solution	5% (w/v) milk powder in TBS-T.
Alkaline phosphatase buffer (AP buffer)	100 mM Tris-HCl (pH 9.5); 100 mM NaCl; 5 mM MgCl <sub>2</sub> .
BCIP <sup>2</sup>	50 mg mL <sup>-1</sup> in DMF <sup>3</sup> .
NBT <sup>4</sup>	50 mg mL <sup>-1</sup> in 70% (v/v) DMF.

<sup>1</sup>Tris-buffered saline

<sup>2</sup>5-bromo-4-chloro-3'-indolyphosphate

<sup>3</sup>Dimethylformamide

<sup>4</sup>Nitro-blue tetrazolium chloride

**Table 2.1-20: Buffer for immunoprecipitation (IP).**

<b>Buffer</b>	<b>Composition</b>
IP Lysis/Wash buffer	0.025 M Tris, 0.15 M NaCl, 0.001 M EDTA, 1% NP <sup>1</sup> -40, 5% glycerol, pH 7.4, Pierce Classic IP Kit (Thermo Fisher Scientific).

<sup>1</sup> nonyl phenoxy polyethoxy ethanol

### 2.1.8 Buffers and solution for metabolite analysis

**Table 2.1-21: Extraction buffer for mass spectrometry sample preparation.**

Buffer	Compounds to detect	Composition <sup>1</sup>
Extraction buffer -1	Uric acid	10 mM Ammonium acetate pH 9.5 adjusted with ammonium hydroxide solution (Fluka)
Extraction buffer -2	Purine nucleosides, nucleobases and uridine	10 mM Ammonium acetate pH 9.5 adjusted with ammonium hydroxide solution (Fluka)

<sup>1</sup>All solvents and chemicals are LC-MS grade.

**Table 2.1-22: Mass spectrometry running buffer.**

Buffer	Compounds to detect	Composition <sup>1</sup>
Mobile phase A-1	Uric acid	10 mM Ammonium acetate pH 9.5 adjusted with ammonium hydroxide solution (Fluka)
Mobile phase A-2	Purine nucleosides, nucleobases and uridine	10 mM Ammonium acetate pH 9.5 adjusted with ammonium hydroxide solution (Fluka)
Mobile phase B	Purine nucleosides and nucleobases, uridine and uric acid	Methanol

<sup>1</sup>All solvents and chemicals are LC-MS grade.

### 2.1.9 Software and databank

Software and databank used for bioinformatic analysis:

BLASTP: <https://blast.ncbi.nlm.nih.gov/Blast.cgi>

Phytozome: <https://phytozome.jgi.doe.gov/pz/portal.html>

Clustal Omega: <https://www.ebi.ac.uk/Tools/msa/clustalo/>

BoxShade: [https://embnet.vital-it.ch/software/BOX\\_form.html](https://embnet.vital-it.ch/software/BOX_form.html)

MEGA6: <https://www.megasoftware.net/>

Phyre<sup>2</sup>: <http://www.sbg.bio.ic.ac.uk/phyre2/html/page.cgi?id=index>

Chimera 1.10: <https://www.cgl.ucsf.edu/chimera/>

Databank used for gene expression analysis:

Arabidopsis eFP browser: <http://bar.utoronto.ca/efp/cgi-bin/efpWeb.cgi>

## 2.2 Methods

### 2.2.1 Molecular biology

#### 2.2.1.1 Cloning and site directed mutagenesis

The plasmids X3 and X4 (Table 2.1-4), carrying the cDNA of *NSH1* and *NSH2* of *Arabidopsis thaliana*, were provided. Starting from X3 and X4, the other constructs were prepared by traditional cloning. The plasmid containing the DNA fragment to be cloned and the destination vector were digested with the restriction enzymes listed in Table 2.1-4. The destination vector was dephosphorylated to prevent self-ligation. The digestion products were resolved on a 1% agarose gel, run at 100 V, for 20 minutes. The fragment of interest was cut out from the gel and purified by the PCR Clean-up kit according to manufacturer's instruction (Macherey-Nagel), and ligated in the final vector. Restriction enzymes, enzyme for dephosphorilation (Shrimp alkaline phosphatase, rSAP) and ligation (T4 DNA ligase) were from New England Biolabs (NEB) and the supplier's protocols were followed. The isolation of plasmid DNA from *Escherichia coli* was carried out with the GenJet Plasmid Miniprep Kit (Thermo Fisher Scientific).

PCR was performed prior to cloning to introduce new restriction sites. The Phusion High-Fidelity (HF) DNA polymerase from NEB was used. A typical PCR reaction was set up in a total volume of 20  $\mu$ L as follows: 4  $\mu$ L of five-fold HF buffer, 0.2 mM dNTP, 0.2  $\mu$ M of each primer, 0.5  $\mu$ L of polymerase, and 1 - 2 ng of plasmid DNA as template. The PCR program is shown in Table 2.2-1.

**Table 2.2-1: PCR program.**

Step	Temperature	Time
Initial denaturation	98 °C	30s
Denaturation <sup>C</sup>	98°C	10s
Annealing <sup>C</sup>	X <sup>1</sup> °C	30s
Elongation <sup>C</sup>	72 °C	30s per kilobase
Final extention	72 °C	10 min
Hold	4-10 °C	

<sup>C</sup> cycle (n = 25-30)

<sup>1</sup> primer annealing temperature determined with the web-tool  
<http://www.thermoscientificbio.com/webtools/multipleprimer/>.

The amplified DNA was run on an agarose gel, purified, ligated into pJET1.2/blunt (Table 2.1-3), sequenced (GATC Biotech), and then cloned in the destination vector.

Site-directed mutagenesis of *NSH1* was described in Lennart Doering's master thesis and is only briefly summarized here. The *NSH1* cDNA cloned in V42 was amplified with the primer pairs P468 + P447 and P446 + P469 (Table 2.1-5). The two fragments were assembled with the NEBuilder HiFi DNA Assembly Cloning Kit (NEB); the resulting fragment was further amplified with P468 + P469 and cloned into V42 and V103. The same procedure was followed to prepare a second point mutant of *NSH1* (K300A) using the primer pairs 0001 + P514 and P513 + 0002 (Table 2.1-5), and to mutate *NSH2* with the primer pairs 0001 + P514 and P513 + 0002 (Table 2.1-5).

## 2.2.2 Microbiology

### 2.2.2.1 Cultures

*Escherichia coli* cultures were grown on LB media (Table 2.1-9) with the appropriate antibiotics (Table 2.1-1, Table 2.1-4). Liquid cultures were placed in an incubator at 37°C, at 200 rpm, for 12 to 16 hours. When grown on solid media, bacteria were plated and incubated at 37 °C overnight.

*Agrobacterium tumefaciens* GV3101::pMP90RK was grown on YEB media (Table 2.1-9) at 28°C. Four antibiotics (Table 2.1-1) were added to the media, because the strain GV3101::pMP90RK is resistant to rifampicin, kanamycin and gentamicin and acquires resistance to carbenicillin when transformed with the binary vectors (Table 2.1-1). *Agrobacteria* were grown on solid media for two to three days and then densely inoculated into liquid media supplemented with the antibiotics to achieve a sufficient optical density (OD) after 12 to 16 hours (Witte et al., 2004). Liquid cultures were incubated at 28°C, 180 rpm. The *Agrobacterium* strain (C58C1::pCH322, Table 2.1-2) transformed with the vector expressing the inhibitor of the plant silencing machinery p19 (Table 2.1-3), was grown at 28°C on YEB plate, with rifampicin and kanamycin for 12-16 hours. Glycerol stocks were prepared with a ratio 1 : 1 of liquid culture : 50% (v/v) glycerol.

### 2.2.2.2 Transformation

To amplify the vectors and the ligation products of the cloning procedure, *E. coli* DH10B chemo competent cells (internal laboratory production) were transformed via heat shock. An

aliquot of competent cells was thawed on ice, 50 ng of vector or 2-4  $\mu\text{L}$  of ligation reaction were added to the cells and incubated on ice for 10 min. The heat shock was performed at 42°C for 45 s in a water bath. After adding 0.5 mL of LB media, cells were incubated in a shaker (200 rpm), at 37°C, for one hour and centrifuged at 3,000g for 5 min. The supernatant was discarded, the pellet was re-suspended in 100  $\mu\text{L}$  of LB media and plated on LB solid media containing the appropriate antibiotics and grown overnight at 37°C.

To introduce exogenous DNA in *A. tumefaciens*, electro competent cells (internal laboratory production) were used. 150-250 ng of plasmid DNA were added to an aliquot of competent cells, gently mixed and transferred to a pre-cooled electroporation cuvette. After an incubation step of 10 minutes on ice, the cuvette was placed in the electroporator (Micro Pulser electroporator, Bio-Rad) and transformed. After electroporation, 0.5 mL of YEB medium was added and cells were incubated for one hour, shaking at 180 rpm, at 28 °C. 10  $\mu\text{L}$  were then plated on YEB solid media with the appropriate antibiotics.

### 2.2.3 Plant related methods

#### 2.2.3.1 Growth of *Arabidopsis thaliana*

*Arabidopsis* seed sterilization was performed with 70% ethanol, for 10 minutes. Seeds were dried under the clean bench and sown on half-strength MS plates (Table 2.1-10) or on soil (Type 0 Nullerde). Seeds were vernalized for two days, at 4°C, to obtain uniform germination. The pots or the plates were then transferred in the growth chambers with long day conditions: 16 h light period, at 22°C, and 8 h dark period, at 20°C, under controlled humidity (70%). Plants were fertilized twice a week with Fertyl 3 Mega 0.07% solution.

*uox-1* and the double and triple mutants in *uox-1* background were first germinated on plates supplemented with 1% (w/v) sucrose and, after seedling establishment, transferred to soil (Hauck et al., 2014).

For the allopurinol treatment, plates with 7-day-old seedlings (approximately 100 seedlings per plate) were sprayed with 500  $\mu\text{L}$  of a 200  $\mu\text{M}$  allopurinol solution (Ma et al., 2016). Allopurinol has low solubility in water; therefore, a 20 mM stock solution was prepared by dissolving it in DMSO and then diluting it prior to use.

For the dark stress treatment, plants were grown as described by Schroeder et al. (2017).

To harvest root material for the IP experiment, plants were grown hydroponically using an Araponics system (Araponics). Seeds were sown in half-strength MS media with 0.65%

phytoagar and placed in the Araponic box filled with deionized water. One week after planting, the water was substituted with nutrient solution (Table 2.1-10) and renewed every two weeks. Plants were grown for six weeks in a growth chamber, under short day condition (8 h light, 20°C day, 18°C night, and 60% relative humidity).

#### 2.2.3.2 *Growth of Nicotiana benthamiana*

*N. benthamiana* plants were grown under long day condition (16 hours of light) on soil (92% peat, 0.15% salinity, pH 5-6) in the greenhouse. After approximately five weeks, they were used for protein expression.

#### 2.2.3.3 *Stable transformation of Arabidopsis thaliana*

Six-week-old *Arabidopsis* plants were transformed by floral dipping method (Clough and Bent, 1998). The stable transgenic lines that were generated are listed in table Table 2.1-8. After revitalization of the *Agrobacterium* glycerol stock carrying the construct of interest on a YEB plate with appropriate antibiotics, a liquid culture (100 mL per plant) was inoculated with bacteria and grown for 12 to 16 hours at 28 °C with shaking at 180 rpm. Cells were centrifuged at 3,000g for 20 minutes at room temperature, the supernatant was discarded, and the pellet was re-suspended in 100 mL of a 5% (w/v) sucrose solution with 0,05% Silwet L-77. Cells were diluted to an OD of 0.6 - 0.8 with the same solution. Plants were transformed by dipping the flowers in the bacterial solution. Then they were incubated overnight without light in a plastic bag to preserve high humidity, and transferred into a growth chamber with 16 h light/8 h dark cycle. The seeds were collected and screened for the transformed ones. The binary vector used for transformation carried a gene coding for the phosphinotricin-N-acetyltransferase which confers resistant to the herbicide glufosinate (phosphinotricin, BASTA). Seeds were sown on soil, grown for one week, and sprayed with BASTA. The surviving plants expressing the protein of interest were selected. Protein expression was assessed by immunoblot (Section 2.2.4). The seeds derived from the selected plants (T0 generation) were collected, sown on soil and screened by BASTA, for single insertion lines. A survival rate of 75% indicated that the T1 seedlings only had a single transgene insertion in the genome. Twelve T1 plants were selected, seeds harvested, and screened by BASTA for homozygosity. 100% of survival of the T2 seedlings after BASTA treatment indicated that the single-copy transgene was homozygous in these plants.

## 2.2.4 Biochemical methods

### 2.2.4.1 *Antibody preparation: inclusion body isolation, generation of polyclonal antiserum, and antibody purification*

To isolate inclusion bodies for rabbit immunization and antibody production for NSH1 and NSH2, the constructs H91 and H92 (Table 2.1-4), were transformed in *E. coli* BL21 (Table 2.1-2). One colony was inoculated in a starting culture and incubated overnight at 37°C with shaking at 200 rpm. This culture was transferred to 1.5 L of LB medium, and when an OD of 0.5 was reached, protein expression was induced by adding 500  $\mu$ M isopropyl- $\beta$ -D-thiogalactoside (IPTG). After 3 hours, the cells were harvested, re-suspended in 80 mL of lysis buffer (Table 2.1-11), and vortexed. 200 mg of lysozyme were added in 20 mL of lysis buffer and the slurry was incubated on ice for 30 minutes. Cells were disrupted by sonication on ice and 200 mL of detergent buffer (Table 2.1-11) were added. The lysate was centrifuged at 5,000g for 10 minutes, the supernatant was removed, and the pellet was re-suspended in 250 mL of washing buffer (Table 2.1-11). Centrifugation and resuspension were repeated until a tight pellet was obtained. The pellet was washed in 250 mL 70% ethanol, suspended in a small volume of freshly prepared PBS (Table 2.1-11) and used for commercial rabbit antisera production and antibody purification (immunoGlobe).

The first batch of antibodies against NSH1 and NSH2 showed cross reactivity: the anti-NSH2 antibody recognized NSH2 but also NSH1 as well as the anti-NSH1 antibody recognized NSH1 but also NSH2. To obtain a specific polyclonal antibody for NSH1, the anti-NSH1 antiserum was run for eight times over a column with immobilized NSH2 to deplete the majority of the antibody cross reacting to NSH2. The flow through was then passed over a column with immobilized NSH1 and the eluted fraction represented the specific anti-NSH1 antibody. It was not possible to follow the same procedure for the anti-NSH2 antiserum due to a high loss of antibodies in the depletion steps. Therefore, the anti-NSH2 antiserum was run one time over a column with immobilized NSH2, and the elution fraction was used as dual specific anti-NSH1/2 antibody.

### 2.2.4.2 *Transient expression in Nicotiana benthamiana*

The *Agrobacterium* glycerol stocks were revitalized on YEB plates with appropriate antibiotics and inoculated in liquid cultures (Section 2.2.2.1). The *Agrobacterium* strain carrying the gene of interest was co-infiltrated in *Nicotiana benthamiana* with the bacterial



strain carrying the coding sequence for the p19 protein of tomato bushy stunt virus (Table 2.1-2, Table 2.1-3, Section 2.2.2.1). p19 suppresses gene silencing in *N. benthamiana* (Voinnet et al., 2003). Bacterial cells were harvested in a 15 mL Falcon tube by a centrifugation at 3,000g, the supernatant was removed, the cells were re-suspended in infiltration buffer (Table 2.1-12), and the OD determined. The OD of the Agrobacteria was adjusted to 0.4 for those containing the construct of interest, and to 0.1 for those expressing p19. In co-purification experiments, where Strep- and myc-tagged variants of nucleosidases were co-expressed, the ODs of the respective Agrobacteria were adjusted to 0.2 each. These bacterial suspensions were mixed together and, after 1 to 4 hours of incubation at room temperature, infiltrated in *N. benthamiana* young just fully expanded leaves with a 1 mL syringe without needle. Protein extraction was performed after three days.

#### 2.2.4.3 Protein extraction and purification by Strep affinity chromatography

Strep tagged proteins transiently expressed in *N. benthamiana* leaves were purified by affinity chromatography as described by (Werner et al., 2008), with some minor changes.

In detail, 0.75 g of leaf material was collected and ground in 1.5 mL of extraction buffer (Table 2.1-14) using a mortar and a pestle pre-cooled in an ice bath. All the steps were performed at 4°C. The extract was centrifuged at 20,000g, for 10 min, at 4°C. The supernatant was transferred to a new vial, 40 µL were taken as sample CL (clarified lysate) and 10 µL of five-fold SDS sample loading buffer were added (Table 2.1-16). 40 µL of Strep-Tactin Macroprep (50% slurry, IBA Lifesciences) were added to the supernatant and incubated on a rotating wheel for 10 min at 4°C to facilitate the binding of the recombinant protein. The sample was centrifuged at 700g for 30 s. 40 µL of the supernatant were taken to trace the purification process (sample NB, not bound to the Strep-Tactin Macroprep beads); the remaining part of supernatant was discarded. The beads were washed five times with 500 µL of washing buffer (Table 2.1-14). From the last washing step a 40 µL sample was taken (sample W, protein in the last washing step). To elute the protein, 75 µL of elution buffer containing an excess of biotin (Table 2.1-14) were added and incubated in a shaker, at 1,000 rpm, at room temperature, for 5 minutes. The sample was centrifuged at 700g for 30 s and a second elution step was performed. The eluted fractions were pooled together (sample E, elution fraction). To determine the amount of protein that did not elute from the beads (sample B), 1.5 mL of washing buffer was added to the beads and resuspended. 40 µL were

taken and 10  $\mu\text{L}$  of five-fold SDS sample loading buffer were added and incubated at 95 °C for 10 min.

#### 2.2.4.4 SDS page

After adding the SDS loading buffer, samples were incubated at 95 °C for 5 minutes before loading on the gel. The SDS polyacrylamide gel (10% resolving gel, 4% stacking gel, Table 2.1-15) was placed in a Bio-rad electrophoresis chamber and assembled according to manufacturer's instructions. The running buffer (Table 2.1-17) was added. 12.5  $\mu\text{L}$  of samples were loaded. The gel was run at 80 V until the front lane of reached the resolving gel, and then at 120 V for approximately one hour.

#### 2.2.4.5 Colloidal Coomassie staining and protein quantification

After electrophoresis, the gel was incubated in fixing solution (Table 2.1-18) for 30 minutes, rinsed twice with distilled water, and incubated in staining solution (Table 2.1-18) for a minimum of 4 hours to overnight. The gel was then destained by washing it in distilled water.

#### 2.2.4.6 Immunoblot

After SDS page, the gel was first equilibrated in blotting buffer for 10 minutes (Table 2.1-19). A semi-dry blotting method was used to transfer the proteins from the gel onto a nitrocellulose membrane. A sandwich that consisted of three pieces of filter paper, the membrane, the gel and again three pieces of filter paper, was soaked in blotting buffer (Table 2.1-19) and then placed in the cassette of a Trans-Blot Turbo™ Instrument (Bio-rad). The blotting program was set up at 25 V for 7 minutes. After blotting, the membrane was incubated in blocking solution (Table 2.1-19) for 30 minutes with shaking at room temperature. To detect Strep-tagged protein, the membrane was rinsed quickly in TBS-T (Table 2.1-19) to remove the biotin present in the milk powder and then incubated for 10 min in 10 mL of TBS-T with 2  $\mu\text{g mL}^{-1}$  avidin at room temperature with shaking. 2.5  $\mu\text{L}$  of StrepTactin alkaline phosphatase conjugate (StrepTactin-AP, IBA Lifesciences) was added to the membrane. After one hour of incubation at room temperature, the membrane was washed three times for 5 minutes with 25 mL of TBS-T to remove the unbound StrepTactin-AP. The membrane was incubated with 10 mL of AP buffer (Table 2.1-19) containing BCIP and NBT (Table 2.1-19), which are chromogenic substrates of the alkaline phosphatase. After

developing of the color, the staining solution was removed. To detect myc-tagged proteins, and the native NSH1 and NSH2 of *A. thaliana*, the membrane was incubated with primary antibody for one hour at room temperature, washed three times with 25 mL of TBS-T for 5 minutes, and incubated one hour with the secondary antibody conjugated to AP. The membrane was washed again three times with TBS-T for 5 minutes and detected as for StrepTactin-AP detection. Myc-tagged proteins were detected using a mouse anti-c-myc antibody (Roche 11667149001, dilution 1:400) and a goat anti-mouse IgG alkaline phosphatase conjugated secondary antibody (Sigma A3562, dilution 1:10,000). The native NSH1 and NSH2 from *A. thaliana* were detected with rabbit anti-NSH1 antibody ( $0.2 \mu\text{g mL}^{-1}$ ) and anti-NSH1/2 dual specific antibody ( $1 \mu\text{g mL}^{-1}$ ). As secondary antibody, a goat anti-rabbit IgG alkaline phosphatase conjugate (Sigma A3687, dilution 1:30,000) was used.

#### 2.2.4.7 Sample preparation for protein expression analysis

Cell lysates from different tissues were prepared to determine the expression level of NSH1 and NSH2 expression. The tissues selected were: 10-day-old seedlings grown on half-strength MS plates (Table 2.1-10), roots and rosettes of 4-week-old plants grown on soil before bolting, young leaves (leaves up to position 14), middle leaves (13 to 7), old leaves (6 to 1), cauline leaves, flowers, and siliques of a 6-week-old plant grown on soil, and dried seeds. The tissues were ground on ice with two volumes of protein extraction buffer (Table 2.1-13), and centrifuged at  $4^{\circ}\text{C}$  with 20,000g for 10 minutes. To prepare seed lysates, four volumes (w/v) of buffer were used. Samples ( $12 \mu\text{L}$ ) were loaded on a 10% SDS polyacrylamide gel.

#### 2.2.4.8 Activity assay

The nucleosidases were expressed in *N. benthamiana* and purified by Strep affinity chromatography. For activity assays, the heterocomplex NSH1-NSH2 was always purified via the Strep-tagged NSH2 enzyme to avoid excess of NSH1 that, being active, would have interfered with the evaluation of the activity of the heterocomplex.

The NSH activity was assessed spectrophotometrically using a UV/VIS Spectrophotometer (UV-2700, Shimadzu), according to Kopečná et al., 2013 and Parkin, 1996b. The assay was set up at room temperature, in a 0.5 cm quartz cuvette, in a total volume of 1 mL. The reaction buffer was 100 mM HEPES, pH 8, mixed with substrates at specific concentrations. The reaction was initiated by adding 5 to  $10 \mu\text{L}$  of purified NSH1 or NSH2 and 10 to  $30 \mu\text{L}$  of purified NSH1-NSH2 complex. The activity was determined by monitoring the absorption

decrease due to the consumption of xanthosine ( $\Delta\epsilon_{248} = -3.7 \text{ mM}^{-1} \text{ cm}^{-1}$ , Kopečná et al., 2013), uridine ( $\Delta\epsilon_{280} = -1.8 \text{ mM}^{-1} \text{ cm}^{-1}$ , Kopečná et al., 2013) and inosine ( $\Delta\epsilon_{280} = -0.92 \text{ mM}^{-1} \text{ cm}^{-1}$ , Parkin, 1996b). The activity per volume of enzyme was calculated according to the following formula:

$$\text{Volume activity} = \frac{(\text{assay volume} \times \frac{\Delta A}{\Delta t})}{\text{enzyme volume} \times \text{path length} \times \Delta \epsilon}$$

$\Delta\epsilon$ : differential extinction coefficient; A: absorption.

The volume activity was normalized by the concentration of protein used in the assay to determine the activity per milligram of enzyme. The protein concentration was determined by SDS page gel electrophoresis: 12.5  $\mu\text{L}$  of elution fraction were loaded on a polyacrylamide gel together with a BSA (bovine serum albumin) standard curve containing 2  $\mu\text{g}$ , 1  $\mu\text{g}$ , 0.5  $\mu\text{g}$ , 0.25  $\mu\text{g}$ , 0.125  $\mu\text{g}$  of protein per lane. Since NSH1 and NSH2 have different molecular weight, they can be resolved on a gel and the concentration of each NSH in the heterocomplex can be determined. Band intensities were quantified with an Odyssey Fc Imager from Li-Cor Biosciences. The heterocomplex NSH1-NSH2 was always purified via the Strep-tagged NSH2 enzyme. The specific activity was calculated normalizing the activity per mg of NSH dimer. To calculate the amount of dimer, the quantified amount of co-purified NSH1, which was only purified because it was in a complex with NSH2, was multiplied by factor 2. Excess NSH2 was not considered. This is possible, because NSH2 has no activity on its own. The kinetic constants were determined using the following concentrations: 0.1, 0.2, 0.4, 0.6, 1.0, 1.6 mM for uridine; 0.03, 0.06, 0.12, 0.24, 0.30, 0.45 mM for xanthosine and 0.25, 0.5, 0.75, 1.0, 1.5, 2.0 mM for inosine. The choice of concentrations for each substrate was limited by the detector linearity of the spectrophotometer, which became non-linear at absorbance value above 3. The curves were recorded three times and the kinetic parameters were determined using the Michaelis Menten equation to fit the data with the Graph Pad Prism V4 software.

#### 2.2.4.9 Immunoprecipitation

The immunoprecipitation (IP) was performed using the Pierce Classic IP Kit (Thermo Fisher Scientific) which is designed for mammalian tissue extracts and adapted in this work for plant tissues. Roots (300 mg) from six-week-old *Arabidopsis* plants grown hydroponically in short day conditions were ground on ice with a pre-cooled mortar and pestle in 540  $\mu\text{L}$  of IP Lysis/Wash Buffer (Pierce Classic IP Kit, Table 2.1-20) and 60  $\mu\text{L}$  of protease inhibitor

(cOmplete, EDTA-free, protease inhibitor cocktail, Roche). The cell lysate was centrifuged at 20,000g for 10 min at 4 °C. The supernatant was pre-cleared with a Control Agarose Resin Slurry (Pierce Classic IP Kit) to prevent unspecific binding to the agarose resin used for the immunoprecipitation. 2 µg of anti-NSH1 antibody were added to the clarified supernatant and incubated for 1 hour and 45 minutes, at 4 °C, in a rotating wheel, to form the anti-NSH1/NSH1 immune complex. After the incubation with the antibody, the sample was added to the Protein A/G Plus Agarose (Pierce Classic IP Kit) packed in the spin column. A screw cap and a bottom plug were attached and the column was incubated on a rotating wheel at 4 degree for 1 hour. The bottom plug was then removed, the screw cap was loosened, and the column was placed in a collection tube and centrifuged at 1,000 g for 1 minute. The column was then placed in a new collection tube and washed three times with TBS (Pierce Classic IP Kit) and one time with one-fold conditioning buffer (Pierce Classic IP Kit). To elute the immune complex, the SDS loading buffer provided by the kit was directly added to the column and incubated at 100 °C for 5-10 minutes. The column was centrifuged to collect the eluate.

### **2.2.5 Metabolite analysis by liquid chromatography – mass spectrometry analysis (LC-MS)**

Metabolite analysis was performed using an Agilent HPLC 1200 system with binary pumps (LC) coupled to an Agilent 6460 series triple quadrupole mass spectrometer (MS). Nucleosides, nucleobases and uric acid were separated by a Polaris 5 C18A column (50 x 4.6 mm, particle size 5 µm; Agilent). Solvent A and solvent B are indicated in Table 2.1-22. The flow rate was 0.8 mL min<sup>-1</sup>. The gradient applied was 0 min, 5% B; 1.5 min 5% B; 3.5 min, 15% B; 6 min, 100% B; 7 min, 100% B; 7.1 min, 5% B; 13 min, 5% B. The injection volume was 20 µL. Two separate methods were used to measure (i) uric acid, which was detected in negative mode, and (ii) xanthine, guanine, hypoxanthine, inosine, xanthosine, guanosine and uridine, which were detected in positive mode. Xanthine and uric acid have a low solubility in water at room temperature, 69 and 60 mg L<sup>-1</sup> respectively. In some samples, such as *uox* and *xdh*, they were expected to accumulate to high concentrations (Hauck et al., 2014). To guarantee an adequate extraction, the method used was the one from Hauck et al., 2014, which is described in detail in Hauck and Witte, 2015. This extraction method was characterized by a water based extraction and a boiling step at 95°C. Yanes et al., 2011

showed the higher efficiency of this method in extracting nucleobases in comparison to extraction with organic solvent.

The extraction protocol was different according to the type of tissues analyzed. For an efficient disruption of seed tissues, 10 mg of material was weighted in a 2 mL Eppendorf tube and one 7 mm steel bead and four 5 mm steel beads were added. Samples were frozen in liquid nitrogen and ground with a mixer mill (Retsch MM400) at a frequency of 19 Hz for 4 min and 30 sec. The sample holders were precooled in liquid nitrogen. Ground material was extracted with 500  $\mu$ L of extraction buffer containing internal standards (ISTDs  $^{15}$ N5-guanosine,  $^{15}$ N2-uridine,  $^{15}$ N4-inosine from Cambridge Isotope Laboratories). The extraction buffer was the same as the mobile phase A (Table 2.1-21 and Table 2.1-22) and differed in pH according to compounds of interest. The basic pH allowed an incremented extraction of uric acid (Hauck and Witte, 2015), while pH 7.5 allowed a proper separation of purine nucleosides and nucleobase in the elution profile of the liquid chromatography. Samples were incubated at 95 °C for 10 minutes at 1,000 rpm in a thermoshaker and then centrifuged at 50,000g for 20 min. To remove particles, samples were passed through a micro spin filter (Thermo scientific, PVDF, 0.2  $\mu$ m). Before loading, samples were generally diluted with extraction buffer without ISTDs. The dilution factor was 100 if uric acid was detected and 10 if nucleoside, nucleobase and uridine were detected. In case of seedlings, roots, and rosettes, the procedure was the same with only minor changes in the extraction. 50 mg of fresh material was harvested and ground with four 5 mm steel beads, at a frequency of 30 Hz. 500  $\mu$ L of extraction buffer was added, and samples were diluted five times to measure seedlings and two times to measure roots. In case of metabolite analysis after dark stress treatment, 4-week-old rosettes were harvested in a falcon tube and frozen at – 80 °C. Leaf material was freeze dried for 18 hours and 10 mg were weighted at room temperature, ground as for the other material and 1 mL of extraction buffer was added. Samples were diluted 10 times.

Guanosine, uridine and inosine were quantified by the respective ISTD and all other compounds by external standard (ESTDs, calibration curve). For ESTDs, standard solutions of xanthosine (0; 0,03; 0,06; 0,1; 0,5; 1; 5  $\mu$ g mL<sup>-1</sup>), xanthine (0; 0,03; 0,06; 0,1; 0,5; 1; 5  $\mu$ g mL<sup>-1</sup>), hypoxanthine (0; 0,01; 0,03; 0,06; 0,1; 0,5; 1  $\mu$ g mL<sup>-1</sup>), guanine (0; 0,01; 0,03; 0,06; 0,1; 0,5; 1  $\mu$ g mL<sup>-1</sup>) and uric acid (0; 0.01; 0.05; 0.075; 0.1; 0.25  $\mu$ g mL<sup>-1</sup>) were added into the matrix (Col-0 extracts). Uric acid and xanthine stock solutions were prepared according to Hauck and Witte, 2015. Guanosine, uridine, xanthosine, xanthine, and guanine were analyzed using the method parameters described by Schroeder et al., 2017. Method parameters for

inosine, hypoxanthine, and uric acid are listed in Table 2.2-3. A signal-to-noise ratio < 10 was considered as not detected.

**Table 2.2-2: Mass spectrometer source parameter**

Ion source	AJS ESI
Gas temperature	300°C
Gas flow	12 mL min <sup>-1</sup>
Nebulizer	30 psi
Sheath gas heater	300°C
Sheath gas flow	11 L min <sup>-1</sup>
Capillary	4000 V

**Table 2.2-3: MS/MS method parameters**

Metabolite	Formula	Theoretical mass (g mol <sup>-1</sup> )	Precursor ion (m/z)	F <sup>1</sup> (V)	Product ion (m/z)	CE <sup>2</sup> (V)	RT <sup>3</sup> (min)
Uric acid	C <sub>5</sub> H <sub>4</sub> N <sub>4</sub> O <sub>3</sub>	168.112	167	91	124 69.2	14 20	0.83
Inosine	C <sub>10</sub> H <sub>12</sub> N <sub>4</sub> O <sub>5</sub>	268.229	269.1	55	136.9 118.9	14 40	2,87
<sup>15</sup> N <sub>4</sub> inosine	C <sub>10</sub> H <sub>12</sub> *N <sub>4</sub> O <sub>5</sub>	272.20	273,1	55	140.9	14	2,87
Hypoxanthine	C <sub>5</sub> H <sub>4</sub> N <sub>4</sub> O	136.114	137,1	11 7	118.1 110 55.2	22 22 34	1,35

<sup>1</sup> Fragmentor.

<sup>2</sup> Collision energy.

<sup>3</sup> Retention time.

\* Isotopically labeled atom.

## **2.2.6 Bioinformatic analyses**

### *2.2.6.1 Phylogenetic analysis*

Protein sequences were retrieved using Basic Local Alignment Search Tool (BLAST) from the database Phytozome and from the National Center for Biotechnology Information (NCBI). *Arabidopsis thaliana* NSH2 and NSH1 were used as queries. The sequences were first aligned by Clustal Omega. The tree was generated by the Molecular Evolutionary Genetics Analysis (MEGA6) software.

### *2.2.6.2 Protein modelling*

*Arabidopsis* nucleosidase protein models were generated by homology modelling using Phyre<sup>2</sup>. The structure of *Physcomitrella* NSH2 was used as template (PDB accession 4KPN). Models were visualized and analyzed by CHIMERA.

## **2.2.7 Statistical analysis**

One way ANOVA with Tukey's post-test was performed to determine significant differences ( $P < 0.05$ ) within a set of data.



## 3. Results

The Results chapter is divided into two sections. First the investigation of the *in vivo* purine nucleotide catabolism is reported and then the elucidation of the function of NSH2 is covered.

### 3.1 Arabidopsis *in vivo* purine nucleotide catabolism

#### 3.1.1 Suppression of the *UOX* mutant phenotype

The urate oxidase, UOX, is the enzyme responsible for the oxidation of uric acid to hydroxyisourate (Figure 6A, Figure A1 Appendix). The *UOX* mutant has an elevated uric acid concentration in all tissues (Hauck et al., 2014), which leads to a severe phenotype especially in developing embryos: seed germination is impaired and those seeds which do germinate cannot establish a seedling. The addition of sucrose to the plate growth media partially restores seedling establishment (Hauck et al., 2014).

Taking advantage of the strong *uox* phenotype, the mutant was used to study whether a gene was involved in purine nucleotide catabolism by crossing a mutant allele of any gene of interest into the *uox* background, and assessing the potential suppression of the *uox* phenotype and of the uric acid accumulation in the double mutant. Mutant alleles of the following genes were tested: *XDH*, *HGPRT*, *NSH1*, *NSH2* and *GSDA* (Figure 6A). The mutant lines used in this study were described in the literature (Table 2.1-6) and in all of them the corresponding gene has completely lost its function. The wild type, the mutants for *XDH*, *HGPRT*, *NSH1*, *NSH2*, and *GSDA*, in parallel with the double mutants *UOX XDH*, *UOX HGPRT*, *UOX NSH1*, *UOX NSH2*, *UOX GSDA-1*, *UOX GSDA-2* and the triple mutant *UOX NSH1 NSH2* were sown side by side on one half-strength MS plate (in several repeats) without sucrose and were phenotypically and metabolically characterized. The phenotypes of the different genotypes were assessed by evaluating the germination rate and the seedling establishment rate. The number of germinating seeds was recorded at day 3, 4, 5 and 10 after imbibition. The plate used for the germination phenotype assessment was evaluated for the seedling establishment phenotype 15 days after imbibition. As far as the germination phenotype was concerned, all the double mutants presented a delay at day 3 in comparison to wild type plants (Figure 6B and C). The delay was stronger for the lines *uox hgpert* and *uox nsh2* that showed no germination, as the *uox* line. The germination phenotype of lines *uox gsdA-1* and *uox gsdA-2*

correlated with the germination delay of *gsda-1* and *gsda-2*, which was caused by guanosine accumulation (Schroeder et al., 2017).

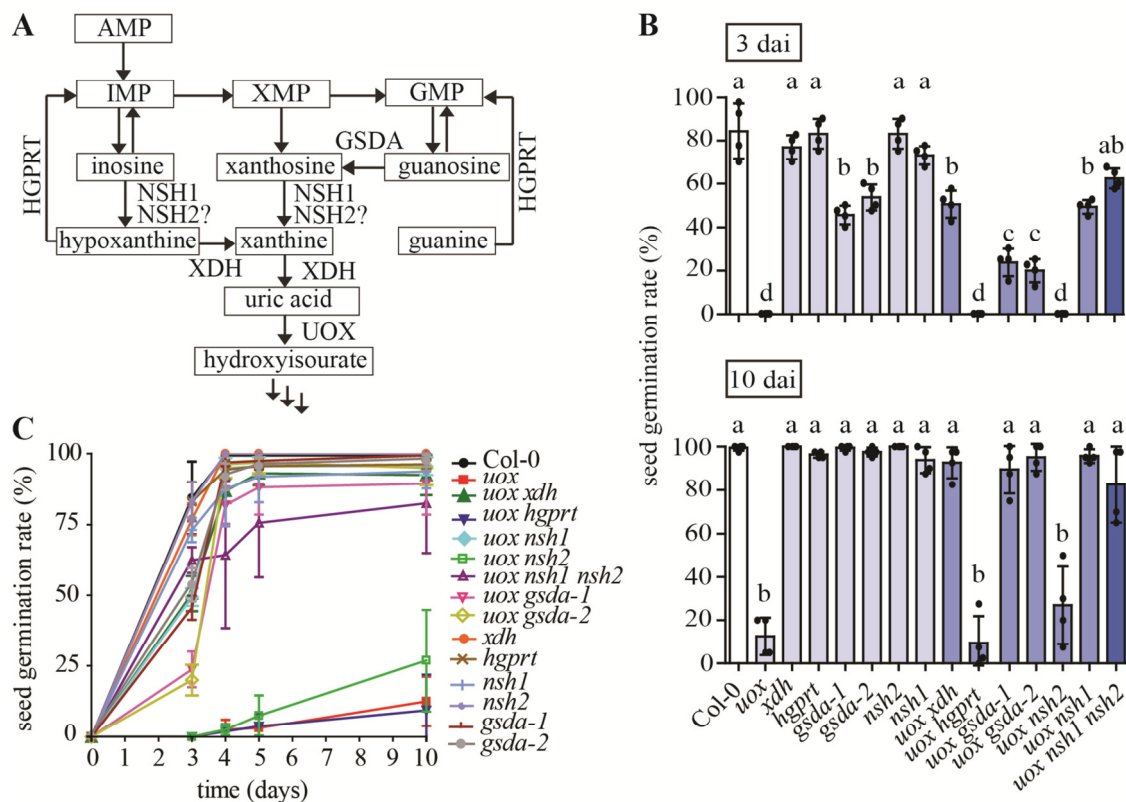


**Figure 6. Genetic suppression of the *uox* germination phenotype**

A) Simplified scheme of the current model of purine nucleotide catabolism showing the enzymes guanosine deaminase (GSDA), nucleoside hydrolase 1 and 2 (NSH1, NSH2), xanthine dehydrogenase (XDH) and urate oxidase (UOX). The function of NSH2 is not yet clarified. From hydroxyisourate a series of linear reactions leads to the release of ammonia, glyoxylate and carbon dioxide. B) Seed germination rate at 3 and 10 days after imbibition of the wild type (Col-0, white bars) and single mutants (light blue bars) of *UOX*, *XDH*, *HGPRT*, *GSDA-1*, *GSDA-2*, *NSH2*, *NSH1* as well as double mutants (blue bars) and a triple mutant (dark blue bar) of the same genes in *uox* background. The genotypes were grown on half-strength MS plates in absence of sucrose. Four plates with 40 seeds of each genotype were analyzed in parallel (n = four biological replicates). Individual data points (dots) are shown as the mean (bar)  $\pm$  SD (error bars). One way ANOVA with Tukey's post-test was used for statistical analysis. Different letters indicate significant differences (p < 0.05). C) Time course of the experiment in B. The data at 3, 4, 5 and 10 days after imbibition are shown. The error bars are SD.

The data presented in the current Section (Section 3.1.1) are from Baccolini and Witte, 2019.

The two lines *uox xdh* and *uox nsh1* presented the same phenotype at day 3 after imbibition: the germination rate was approximately 35% reduced in comparison to the wild type. The triple mutant performed, in tendency, better than the other lines tested. At day 10, the mutant phenotype was completely suppressed in all the double mutant lines except for *uox hgprt* and

*uox nsh2*. In *uox hgpert* and *uox* the germination rate was 10%, while in *uox nsh2* it was slightly higher (approximately 25%) but the statistical analyses did not indicate significance at  $p < 0.05$ . This suggested that *HGPRT* and maybe also *NSH2* were not functional upstream of *UOX* in purine nucleotide catabolism.

As far as the seedling establishment phenotype was concerned, the wild type phenotype (Figure 7A) was restored in *uox xdh*, *uox gsda-1*, *uox gsda-2*, *uox nsh1* and *uox nsh1 nsh2*, but not in *uox hgpert* and *uox nsh2*.

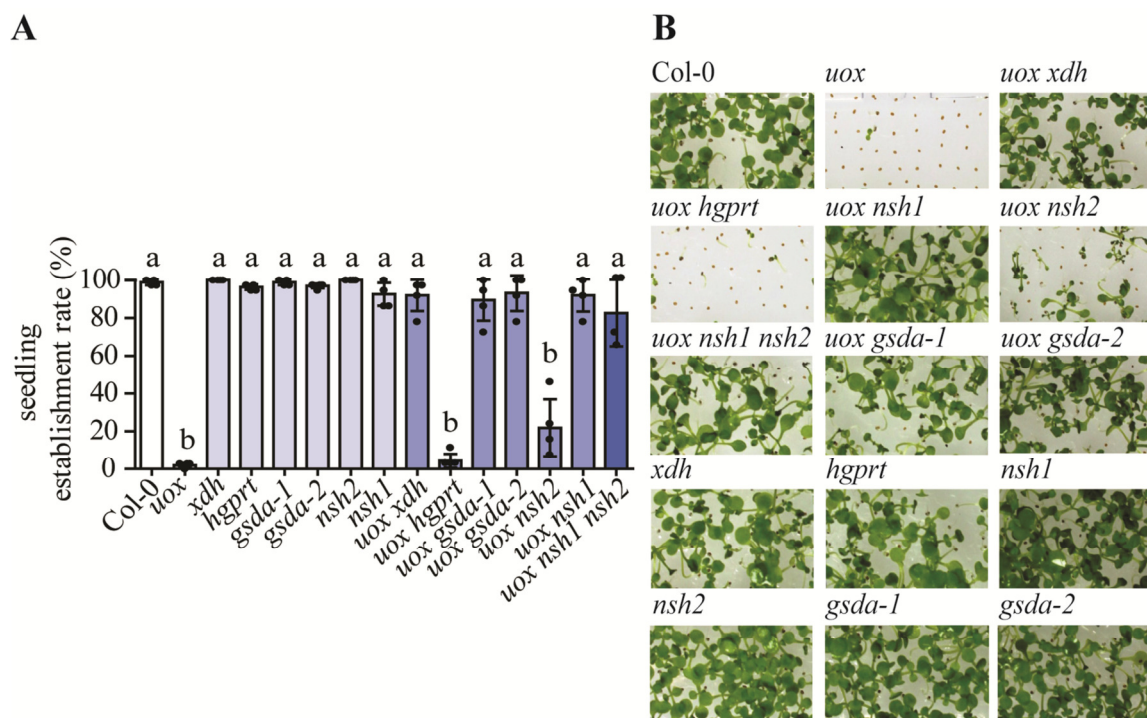


**Figure 7. Genetic suppression of the *uox* seedling establishment phenotype.**

A) Percentage of seedlings established 15 days after sowing. The genotypes analyzed were the wild type (Col-0, white bars) and the single mutants (light blue bars) of *UOX*, *XDH*, *HGPRT*, *GSDA-1*, *GSDA-2*, *NSH2*, *NSH1* as well as the double mutants (blue bars) and the triple mutant (dark blue bar) in *uox* background. The genotypes were grown on half-strength MS plates, in absence of sucrose. Four plates were analyzed in parallel ( $n =$  four biological replicates) and 40 seeds of each genotype were sown side by side. Individual data points (dots) are shown as the mean (bar)  $\pm$  SD (error bars). One way ANOVA with Tukey's post-test was used for statistical analysis. Different letters indicate significant differences ( $p < 0.05$ ). B) A representative plate of the experiment in A and in Figure 6.

The suppression pattern was the same as observed for the germination phenotype. However, by qualitatively comparing the seedling establishment phenotype of *uox nsh2* with *uox* (Figure 7B), the mutation of *NSH2* in *uox* background seemed to suppress slightly the mutant phenotype, although the statistical tests were indicating no significance at  $p < 0.05$ .

The qualitative difference between *uox*, *uox hgpert* and *uox nsh2* could be due to different uric acid content in these mutants. The uric acid concentration in the seeds was measured by LC-MS (Figure 8). The uric acid concentration in seeds of *uox* and in *uox hgpert* was the same (approximately 32  $\mu\text{mol g}^{-1}$  FW), but it was slightly though significantly reduced in *uox nsh2* (to about 26  $\mu\text{mol g}^{-1}$  FW) suggesting a role of NSH2 in purine nucleotide degradation. This reduction was apparently sufficient to enable the establishment of a higher number of seedlings in *uox nsh2* than in *uox* and *uox hgpert*. Uric acid accumulated in *uox gsda-1* and *uox gsda-2* only up to 20% of the concentration found in *uox*. This might explain why these two genotypes showed a lower germination rate at day 3 in comparison to *gsda-1* and *gsda-2*, because the suppressive effect of guanosine on germination was added to the negative effect of uric acid. The uric acid content in *uox nsh1* and *uox nsh1 nsh2* was suppressed up to 95% in comparison to *uox*, while in *uox xdh* there was no uric acid accumulation at all – the concentration was as low as in the wild type.

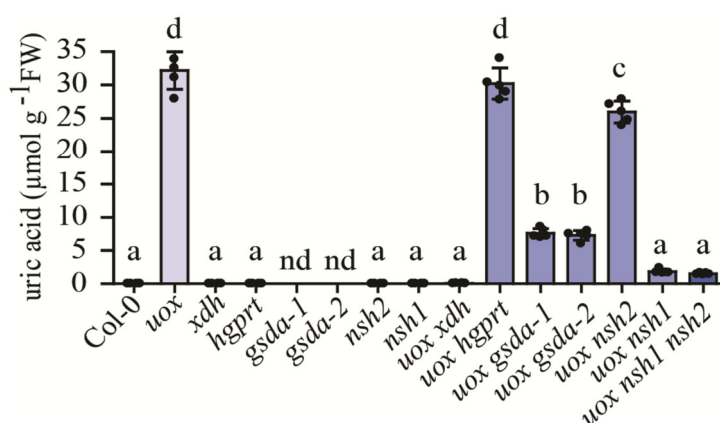


**Figure 8. Suppression of the *uox* molecular phenotype.**

Uric acid content in seeds of wild type (Col-0, white bar) and single mutants (light blue bars) of *UOX*, *XDH*, *HGPRT*, *GSDA-1*, *GSDA-2*, *NSH2*, *NSH1* as well as double mutants (blue bars) and a triple mutant (dark blue bar) in *uox* background. Five biological replicates were analyzed for each genotype. Single data points (dots), the mean (bars)  $\pm$  SD (error bars) are shown. ANOVA with Tukey's post-test was used for statistical analysis. Different letters indicate significant difference ( $p < 0.05$ ). nd, not detectable. FW, fresh weight.

The experiment showed that (i) *XDH*, *NSH1* and *GSDA* are functional in purine nucleotide catabolism and, when mutated in the *uox* background, prevented the accumulation of 100%, 95%, and 80%, respectively, of the uric acid in *uox*; (ii) *NSH2* might have a minor role; (iii) *HGPRT* seemed not to influence the flux of metabolites of the pathway.

### 3.1.2 Nucleoside and nucleobase content in the mutants of the genes involved in purine nucleotide catabolism

To validate the results concerning the genetic suppression of the *UOX* mutant (Section 3.1.1), a similar experiment was set up where *XDH* was used as a reporter gene instead of *UOX*.

It was investigated if the high accumulation of xanthine observed in the *xdh* background is altered when other potential suppressor genes are additionally mutated. In contrast to uric acid, the accumulation of xanthine is not toxic for the plants, and the *xdh* mutant does not show any severe phenotype under standard growth conditions. Seeds and 10-day-old seedlings of the following genotypes were analyzed by mass spectrometry: *xdh hgpert*, *xdh gsda-2*, *xdh nsh2*, *xdh nsh1*, *xdh nsh1 nsh2* and the respective single mutants. The xanthine level in the double mutant *XDH NSH1* and the triple mutant *XDH NSH1 NSH2* was suppressed up to 90% in seeds and totally suppressed in seedlings in comparison to *xdh*, with no significant difference between *xdh nsh1* and *xdh nsh1 nsh2*. In seeds of *xdh nsh2*, the xanthine content was partially suppressed in comparison to *xdh* and in seedlings this was confirmed in tendency. In *xdh gsda-2*, xanthine was reduced up to 80%, whereas in *xdh hgpert* it was not altered.

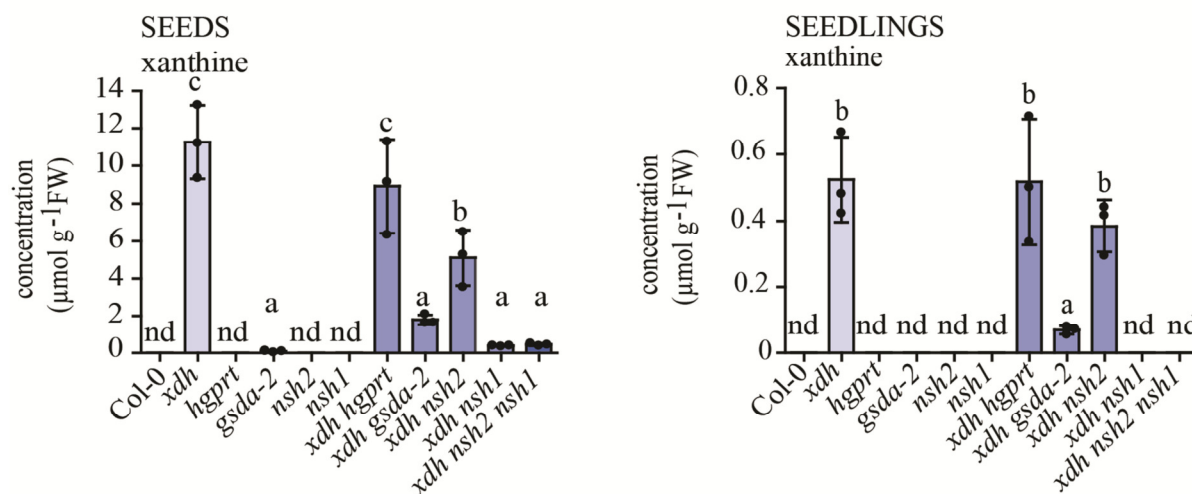


**Figure 9. Xanthine content in seeds and 10-day-old seedlings of the wild type, the mutants of genes involved in purine nucleotide catabolism and salvage as well as double and triple mutants of the same genes in *xdh* background.**

The genotypes analyzed are the wild type (Col-0, white bar), single mutants (light blue bars) of *XDH*, *HGPRT*, *GSDA-2*, *NSH2*, *NSH1* as well as double mutants (blue bars) and a triple mutant (dark blue bars) in *xdh* background. Three biological replicates were analyzed for each genotype. Single data points (dots), the mean (bars)  $\pm$  SD (error bars) are shown. ANOVA with Tukey's post-test was used for statistical analysis. Different letters indicate significant difference ( $p < 0.05$ ). nd, not detectable. FW, fresh weight.

The data presented in the current Section (Section 3.1.2) are from Baccolini and Witte, 2019.

These results are consistent with the data about the accumulation of uric acid in the *uox* background (Figure 8, Section 3.1.1), showing that (i) *NSH1* and *GSDA* are functional in purine nucleotide catabolism and when mutated in the *xdh* background prevent the accumulation of respectively 90% and 80% of the xanthine; (ii) *HGPRT* is not functional in purine nucleotide catabolism; (ii) *NSH2* has a role.

In parallel with xanthine, the concentrations of hypoxanthine, guanine, xanthosine, inosine and guanosine were determined as well. These data provided further insight into purine nucleotide degradation and salvage. According to the current model of purine nucleotide catabolism, XDH is responsible of two reactions: the oxidation of (i) hypoxanthine to xanthine and of (ii) xanthine to uric acid (Figure A1 Appendix). However, in *xdh*, only xanthine accumulated in both seedlings and seeds (Figure 9) and no hypoxanthine was detected (Figure 10). Considering that HGPRT can recycle hypoxanthine and guanine to IMP and GMP, it might be that hypoxanthine did not accumulate in *xdh*, because it was constantly recycled to IMP. Indeed, when recycling and degradation of hypoxanthine were blocked in the double mutant *xdh hgprt*, hypoxanthine accumulated (Figure 10). However, the hypoxanthine concentration in *xdh hgprt* was one order of magnitude lower than that of xanthine (Figure 9 and Figure 10), suggesting that xanthine originated mainly from xanthosine hydrolysis rather than hypoxanthine oxidation.

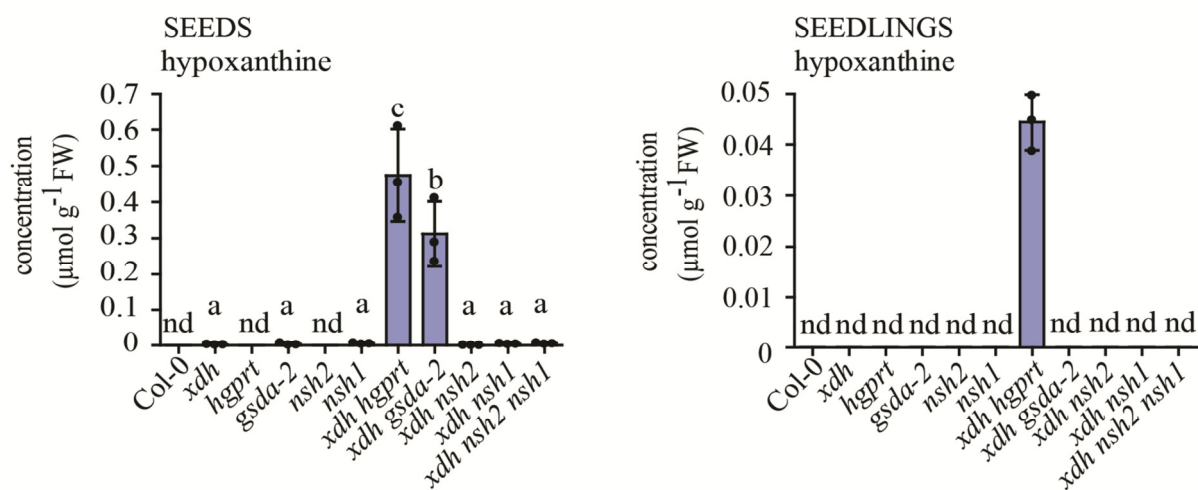


**Figure 10. Hypoxanthine content of the same samples as in Figure 9.**

In seeds, hypoxanthine also accumulated in the double mutant *xdh gsda*. This mutant contained high amount of guanine (Figure 11) derived from degradation of guanosine (Schroeder et al., 2017). Hypoxanthine and guanine are both substrates of HGPRT, but the

enzyme has a lower  $K_M$  for guanine (Liu et al., 2007). The guanine in *xdh gsd* probably saturates HGPRT, preventing it from recycling hypoxanthine and thus causing hypoxanthine accumulation.

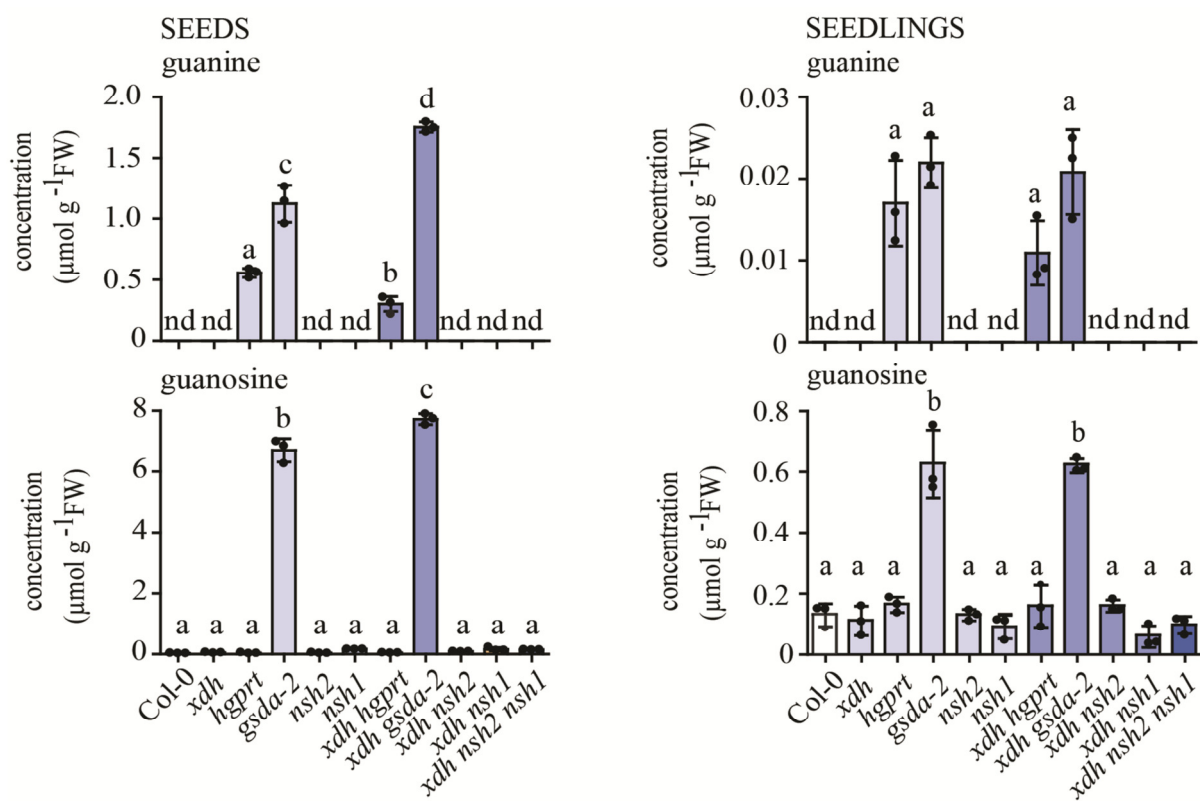


**Figure 11. Guanine and guanosine content of the same samples as in Figure 9.**

The concentrations of xanthosine and inosine were measured as well. Xanthosine and inosine accumulated in *nsh1* and *xdh nsh1* in both seeds and seedlings (Figure 12). However, in both mutants the concentration of xanthosine was two to three orders of magnitude higher than the one of inosine. This indicated that the amount of metabolites degraded via xanthosine-xanthine was higher than the one degraded via inosine-hypoxanthine-xanthine, supporting the hypothesis that xanthosine hydrolysis is the main source of xanthine. Guanine was not a source of xanthine either, because Arabidopsis does not possess guanine deaminase but degrade G (guanylates, guanosine, and guanine) via guanosine deamination by GSDA (Dahncke and Witte, 2013). The oxidation of inosine to xanthosine was not relevant as well because an inosine dehydrogenase has so far not been observed in any species (Dahncke and Witte, 2013). Since all purine nucleotide catabolic routes lead to xanthine (Figure 6A, Figure A1 Appendix) the route which is the main source of xanthine must be the main route for purine nucleotide degradation. The data presented here demonstrate that this is the xanthosine-xanthine route.

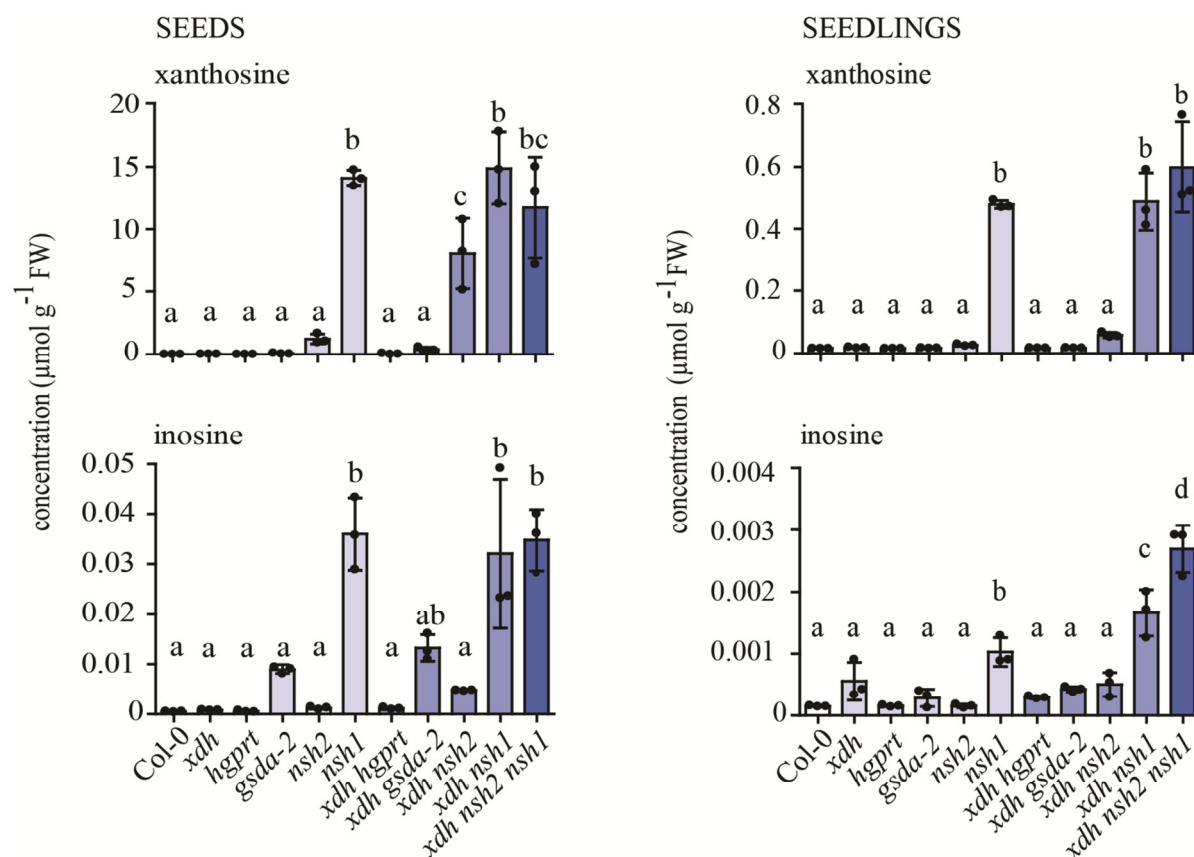


**Figure 12. Xanthosine and inosine content of the same samples as in Figure 9.**

It is interesting to note that xanthosine accumulated in *nsh2* in both seedlings and seeds, though not statistically significant at  $p < 0.05$  in these data sets. It also accumulated at a higher extent in *xdh nsh2*. This was the first time that an accumulation of a potential substrate of *NSH2* could be measured in the *NSH2* mutant. The analysis was performed by LC-MS which was a more sensitive method in comparison to HPLC coupled to UV detection used before by others (Riegler et al., 2011). The apparent reduction of the uric acid content in *uox nsh2*, and of the xanthine content in *xdh nsh2*, as well as the accumulation of xanthosine in the *NSH2* mutant and in particular in the *XDH NSH2* double mutant, indicated that *NSH2* plays a role in purine nucleotide catabolism *in vivo*.

The results shown so far can be summarized as follows:

- I. *HGPRT* is not involved in purine nucleotide catabolism because there were no changes in the xanthine content of *xdh hgpert* in comparison to *xdh*.
- II. Hypoxanthine oxidation is not a significant source of xanthine because hypoxanthine did not accumulate in *xdh*. It accumulated in *hgpert xdh*, where recycling is also blocked, but to a by far lower extent than xanthine.



- III. The accumulation of inosine in *nsh1* and *xdh nsh1* was orders of magnitude lower than the xanthosine accumulation, indicating that xanthosine hydrolysis is the main route for purine nucleotides degradation.
- IV. NSH2 has a function in purine nucleotide catabolism.

### 3.1.3 One more entry point to purine catabolism: XMP dephosphorylation

In *uox gsda-1* and *uox gsda-2* as well as in *xdh gsda-2*, the abrogation of *GSDA* suppressed 80% of the uric acid and the xanthine accumulation normally observed in *uox* and *xdh* backgrounds, respectively (Figure 8 and Figure 9). It appears that most of the flux of metabolites of purine nucleotide catabolism runs via *GSDA*. Additionally, it was demonstrated that xanthine originates mainly from xanthosine and by far less from inosine/hypoxanthine (Section 3.1.2). The pathway from guanosine via xanthosine to xanthine accounted for 80% of purine nucleotide degradation. The remaining 20% is probably derived from the dephosphorylation of XMP to xanthosine catalyzed by an XMP phosphatase, named XMPP. This reaction was previously considered a negligible source of xanthosine (Dahncke and Witte, 2013). These authors showed by HPLC analysis that a *NSH1 GSDA* double mutant did not accumulate xanthosine, indicating that the mutation of *GSDA* was sufficient to prevent the accumulation of this nucleoside in the *nsh1* background. In Dahncke and Witte, 2013, the tissues analysed were rosettes, siliques and roots of *gsda-2 nsh1*, and the seeds of a *GSDA NSH1* double mutant containing another mutant allele of *NSH1*.

Here the genotypes *nsh1*, *gsda-2*, and *nsh1 gsda-2* were analyzed by LC-MS in parallel with the wild type. In contrast to Dahncke and Witte, 2013, it was observed that xanthosine accumulated in *nsh1 gsda-2*, both in seeds and seedlings (Figure 13). In seedlings, it was 20% of the xanthosine detected in the *nsh1* background, which correlated with the 20% of xanthine left in *xdh gsda-2* seedlings in comparison to *xdh*. Inosine, guanosine and uridine concentration were measured as well (Figure 13). In seeds, inosine accumulated more in *nsh1 gsda-2* than in *nsh1*. This might be explained by compromised inosine salvage due to the high concentration of guanosine in *nsh1 gsda-2*, because both might be salvaged by a not yet identified dual-specific inosine guanosine kinase, IGK (Figure A1 Appendix). It is known that guanosine is more efficiently recycled than inosine (Ashihara et al., 2018). If the guanosine concentration is high, IGK might be saturated with it, and inosine salvage might be partially compromised. However, inosine accumulation was never massive even in a condition where

its salvage was potentially compromised, as in *nsh1 gsd-2*. This is an additional indication for a comparatively small flux of purine nucleotide catabolism via the inosine branch.

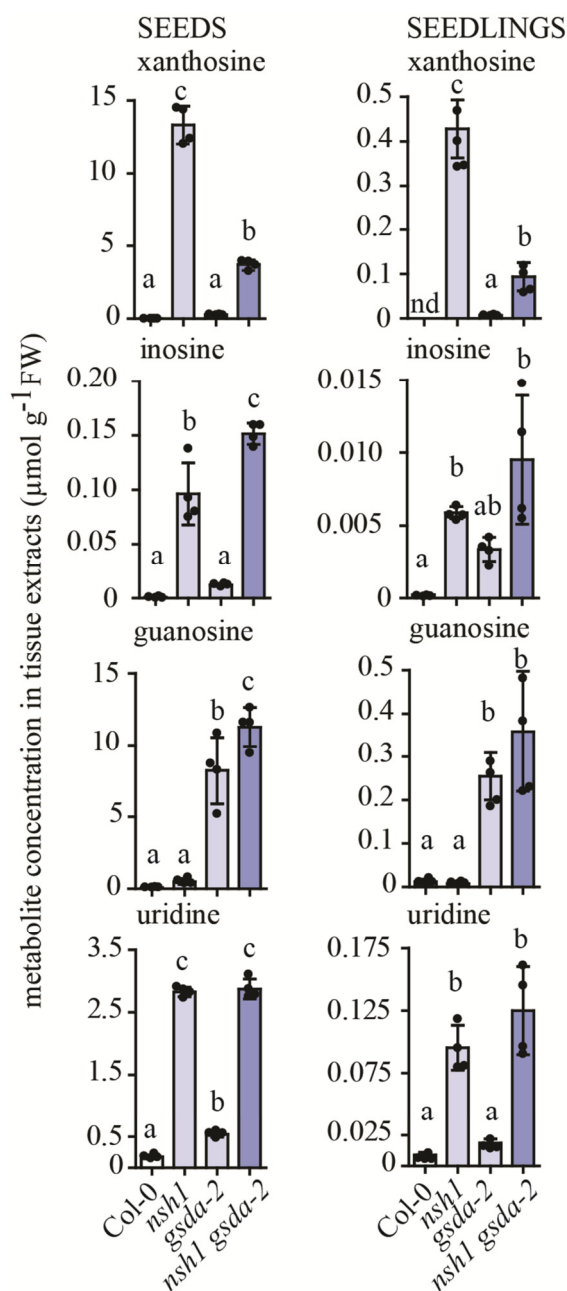


**Figure 13. Nucleoside content in seeds and seedlings of the wild type, the *GSDA NSH1* double mutant and the respective single mutants.**

Xanthosine, inosine, guanosine and uridine content in seeds and in 7-day-old seedlings of the wild type (Col-0, white bars), the single mutants (light blue bars) of *NSH1* and *GSDA*, as well as the double mutant *NSH1 GSDA* (blue bars). Four replicates were analyzed per genotype and tissue. Single data points (dots) and the mean (bars)  $\pm$  SD (error bars) are shown. ANOVA with Tukey's post-test was used for statistical analysis. Different letters indicate significant difference ( $p < 0.05$ ). nd, not detectable. FW, fresh weight.

The data presented in the current Section (Section 3.1.3) are from Baccolini and Witte, 2019.

Some accumulation of xanthosine was observed in *nsh1 gsd-2* seeds and seedlings in contrast to what was reported by Dahncke and Witte, 2013. To confirm this in a further tissue, the nucleoside content in rosettes of 4-week-old plants of the same set of genotypes was measured (Figure 14). Rosettes displayed a lower total nucleoside content in comparison to seeds and seedlings, which was already noted by Riegler et al., 2011. The accumulation of xanthosine in *nsh1* was almost completely suppressed in *nsh1 gsd-2*. Thus, the rosette appears to be a tissue in which the purine nucleotide degradation pathway is more linear and operates almost exclusively from GMP to guanosine, then via xanthosine to xanthine.

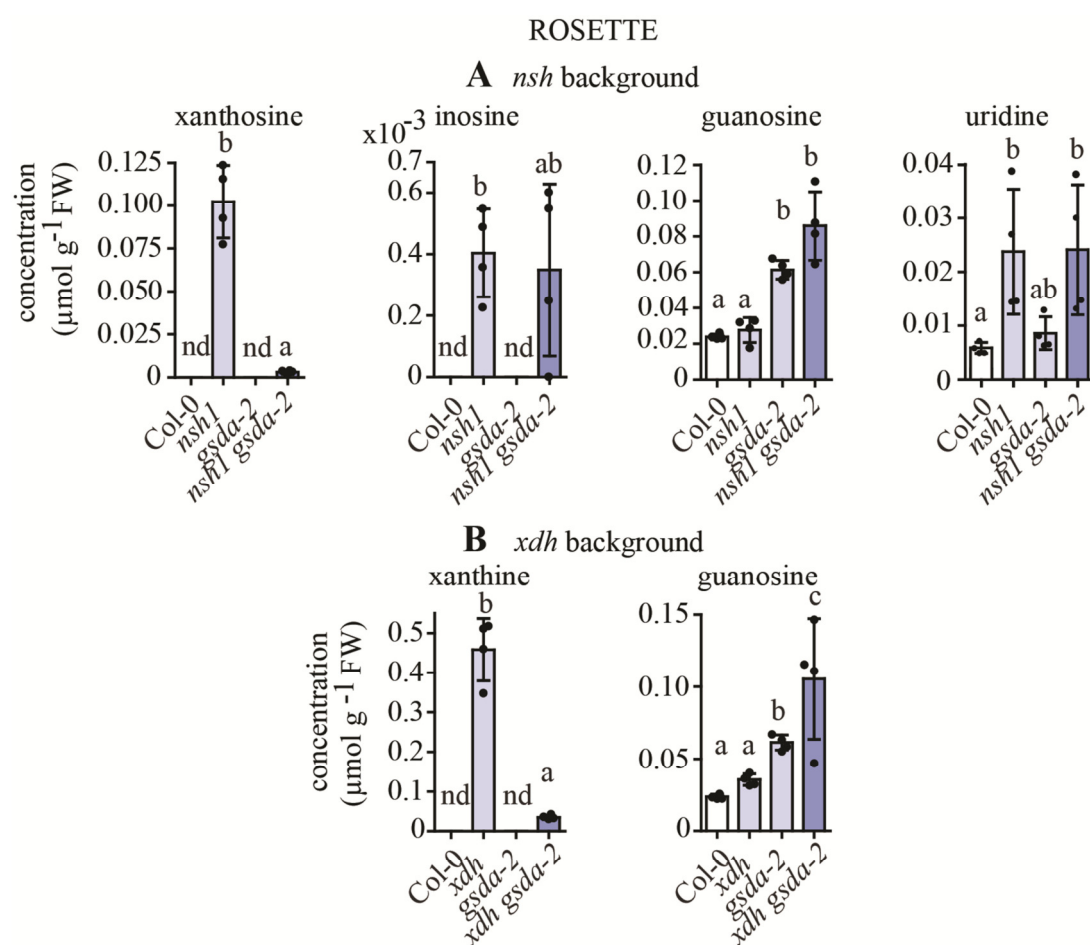


**Figure 14. Metabolite analysis of rosettes of the wild type, the *GSDA NSH1* and the *GSDA XDH* double mutants and the respective single mutants.**

Nucleoside content in rosettes of the wild type and mutant of *GSDA* in *nsh1* (A) and *xdh* (B) background, and the corresponding single mutant. Four biological replicates were analyzed. Plants were grown side by side. Single data points (dots) and the mean (bars)  $\pm$  SD (error bars) are shown. ANOVA with Tukey's post-test was used for statistical analysis. Different letters indicate significant difference ( $p < 0.05$ ). nd, not detectable. FW, fresh weight.

Therefore, the xanthine content in rosettes should be almost fully suppressed in *xdh gsdA* background. To test this hypothesis, *xdh gsdA-2* was included in the study. It was observed that the amount of xanthine left in *xdh gsdA-2* was only 10% of what accumulated in *xdh* (Figure 14), confirming that in rosettes the purine nucleotide catabolism pathway is mostly linear and proceeds via GSDA.

### 3.1.4 Metabolite analysis of purine nucleotide catabolism after dark stress treatment

Dark treatment can be employed to induce metabolite remobilization (Brychkova et al., 2008a). Under stress conditions, plants shift from nutrient assimilation to metabolite turnover, in order to facilitate adaptation to the changed environment. Purine nucleotide catabolism is particularly induced by dark stress, probably because the ureides, which are downstream intermediates of xanthine degradation, have a protective role in senescence (Jung et al., 2011; Schroeder et al., 2017, 2017; Brychkova et al., 2008a).

Purine nucleotide catabolism was enhanced by dark treatment to assess whether hypoxanthine accumulated in a condition of increased flux through the pathway, thereby proving or disproving the relevance of hypoxanthine as intermediate. The genotypes Col-0, *xdh*, *hgprt* and *xdh hgprt* were exposed to dark stress treatment. Plants were grown in the growth chamber for three weeks, and then the dark treatment was applied by covering the plants with a lid and a black towel for three days. Samples were taken immediately before the beginning of the dark stress and after two and three days of treatment. Whereas the xanthine concentration in *xdh* and *xdh hgprt* increased up to day two and three of darkness (Figure 15), indicating enhanced purine nucleotide degradation, hypoxanthine concentration in *xdh hgprt* did not. If purine nucleotide catabolism had run via hypoxanthine, an increase of this nucleobase in *xdh hgprt* would have been expected. However, hypoxanthine did not accumulate indicating that the increased xanthine is derived from xanthosine hydrolysis which is thus confirmed to be the main route of purine nucleotide catabolism.

An open point was the dark-induced accumulation of guanine in *xdh hgprt* in the experiment shown in Figure 15. This is difficult to reconcile with a model in which guanine is not an intermediate of the purine nucleotide catabolism. The experiment was repeated and no accumulation of guanine was observed the second time. Arabidopsis has no guanine deaminase (Dahncke and Witte, 2013), and GSDA suppresses most of the uric acid, xanthine and xanthosine build-up when mutated in the *uox*, *xdh* and *nsh1* backgrounds, respectively, (Figure 8, Figure 9, Figure 13, Figure 14) clearly showing that GSDA and guanosine are

central for purine nucleotide catabolism. By contrast, a role of guanine is not consistently supported by the data.

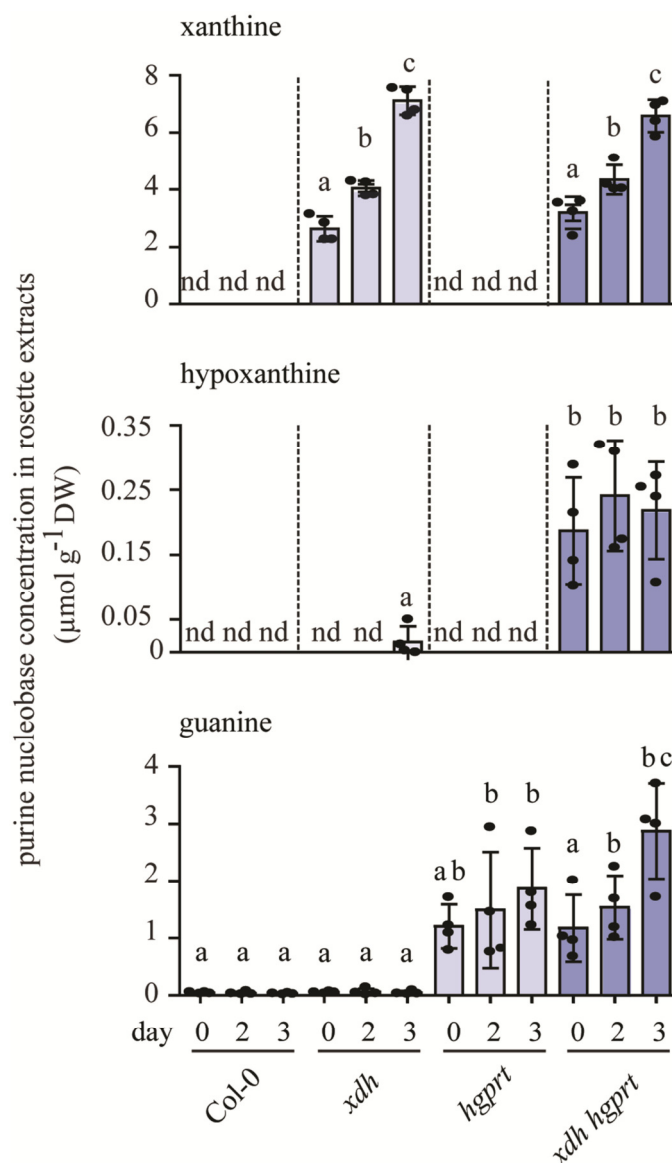


**Figure 15. Changes in the concentration of purine bases during dark stress.**

Quantification of xanthine, hypoxanthine and guanine in the wild type, *XDH* and *HGPRT* single mutants (light blue bars) and the *XDH HGPRT* double mutant (blue bars) in rosettes of three-week-old plants before dark treatment (day 0) and after two and three days of darkness. Single data points (dots) and the mean (bars)  $\pm$  SD (error bars) of four biological replicates are shown. ANOVA with Tukey's post-test was used for statistical analysis. Different letters indicate significant difference ( $p < 0.05$ ). nd, not detectable. DW, dried weight.

### 3.1.5 Allopurinol treatment: short-term blockage of purine catabolism

The concept of purine nucleotide catabolism operating mostly via guanosine and xanthosine to generate xanthine (and not via inosine and hypoxanthine) was to some extent deduced from data of mutants that accumulated high amounts of xanthine because of *xdh* background (Figure 9). One could speculate that the high level of xanthine in *xdh* background might potentially interfere with the enzymatic activities upstream of XDH, possibly creating artefacts. The *xdh* background was used because it allowed studying the metabolic profiles of purine nucleotide catabolism blocked in a bottleneck reaction. To avoid the high xanthine background, a short-term experiment with the XDH inhibitor allopurinol was set up. Allopurinol [4-hydroxypyrazolo-(3,4-d)pyrimidine], is an isomer of hypoxanthine, and is a substrate and inhibitor of XDH. It is oxidized by XDH to the corresponding xanthine analogue, oxipurinol, which irreversibly inhibits the enzyme resulting in xanthine accumulation in plant tissues (Montalbini and Della Torre, 1995). It has been extensively used in the medical field to relieve hyperuricemia (Rundles and Wyngaarden, 1969), because a high concentration of xanthine (xanthinuria) is - in contrast to uric acid - not toxic.

The wild type Col-0 and *hgprt* were grown side by side on a half-strength MS plate in the growth chamber. One week after sowing, at the beginning of the light period, plates were separated in different treatments. Some were sprayed with allopurinol, some with water as control and some with allopurinol together with adenosine to enhance purine nucleotide catabolism by external delivery of a nucleoside. Adenosine can be taken up by nucleoside transporters, be phosphorylated to AMP (Figure 2), be converted to IMP, and enter purine nucleotide degradation. Additionally, dark stress was applied to some plates to enhance purine nucleotide catabolism. Some plates were sprayed with allopurinol and then covered. Seedlings were harvested after 8 hours of treatment to apply a short-term blockage of purine catabolism.

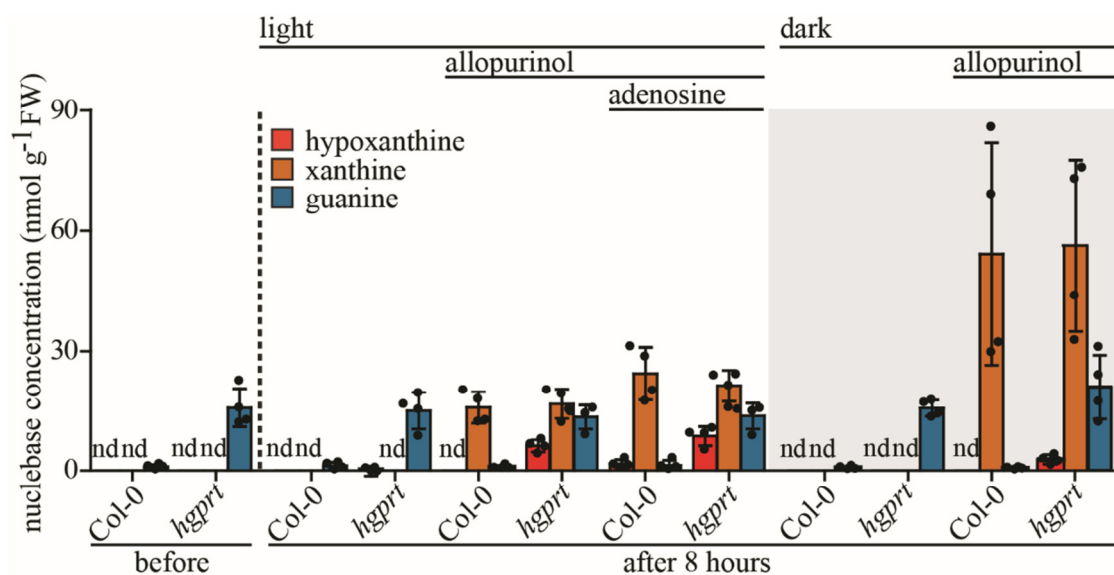


**Figure 16. Nucleobase concentration changes after conditional short term blockage of purine nucleotide catabolism, dark treatment, and exogenous adenosine application.**

Hypoxanthine, xanthine and guanine concentrations in one-week-old Col-0 and *hgprt* seedlings grown side by side on half-strength MS plates before and after treatment with (i) water and normal light cycle (control) (ii) allopurinol and normal light cycle, (iii) allopurinol and adenosine in normal light cycle, (iv) water and dark stress and (v) allopurinol and dark stressed. Four plates (biological replicates) were measured per each treatment. Individual data points (dots), and the mean (bars)  $\pm$  SD (error bars) are shown. FW, fresh weight.

The allopurinol treatment successfully blocked XDH because xanthine accumulated in both Col-0 and *hgprt* in allopurinol sprayed samples (Figure 16). Xanthine accumulated especially in dark treated samples, (approximately 55 nmol g<sup>-1</sup> in the dark against 17 nmol g<sup>-1</sup> in the light), whereas hypoxanthine accumulated more in light (approximately 1.5 nmol g<sup>-1</sup> in the dark against 5 nmol g<sup>-1</sup> in the light). In the samples treated with adenosine and allopurinol, some hypoxanthine accumulated in Col-0 samples, showing that the inosine-hypoxanthine branch was more relevant when the pathway was perturbed by an exogenous input.

The minor accumulation of hypoxanthine when purine catabolism was shortly blocked in comparison to the higher accumulation of xanthine confirmed that hypoxanthine is not an intermediate of purine nucleotide catabolism.

## 3.2 Functional analysis of *NSH2*

The role of *NSH2* in nucleotide catabolism is unclear. A main obstacle in assessing its biochemical function was the formation of inclusion bodies after protein expression in *Escherichia coli* (Jung et al., 2011; Riegler et al., 2011). A good functional lead was also not obtained by the analysis of the corresponding mutant line because none of assumed substrates were altered in concentration (Riegler et al., 2011). However, the partial suppression of the *uox* phenotype in *uox nsh2* (Figure 7 and Figure 8), of the xanthine content in *xdh nsh2* (Figure 9), and the accumulation of xanthosine in *nsh2* and in particular in *xdh nsh2* (Figure 12) were indications of the involvement of NSH2 in purine nucleotide catabolism *in vivo*. Despite these indications, several questions were still open. First, biochemical data concerning the enzymatic activity of NSH2 were lacking. Second, NSH1 was alone apparently sufficient for xanthosine degradation (Jung et al., 2011; Riegler et al., 2011) and the triple mutants *uox nsh1 nsh2* and *xdh nsh1 nsh2* were metabolically behaving as the double mutants *uox nsh1* and *xdh nsh1*, respectively (Figure 8 and Figure 9), arguing against a prominent role of NSH2 in purine nucleotide catabolism. Therefore, detailed bioinformatic, biochemical, and metabolic analyses of *NSH2* were conducted with the aim to elucidate its function.

### 3.2.1 Bioinformatic analysis

#### 3.2.1.1 Phylogenetic analysis

Molecular phylogenetic analysis was performed to investigate whether NSH1 and NSH2 are conserved in the plant kingdom. The Basic Local Alignment Search Tool (BLAST) from the databases Phytozome and NCBI (National Center for Biotechnology Information) was used to retrieve the sequences of NSH1 and NSH2 enzymes from algae to vascular plants. The multiple sequence alignment was generated by Clustal Omega (Figure A2 Appendix) and then processed by the Molecular Evolutionary Genetics Analysis (MEGA6) software to prepare a phylogenetic tree (Figure 17).

All the species analyzed, from the bryophyte to the vascular plants, possess at least one gene coding for NSH1 and one encoding NSH2. The nucleosidases cluster into the NSH1 and the NSH2 clades, which suggests a distinct function for each of the two enzymes types.



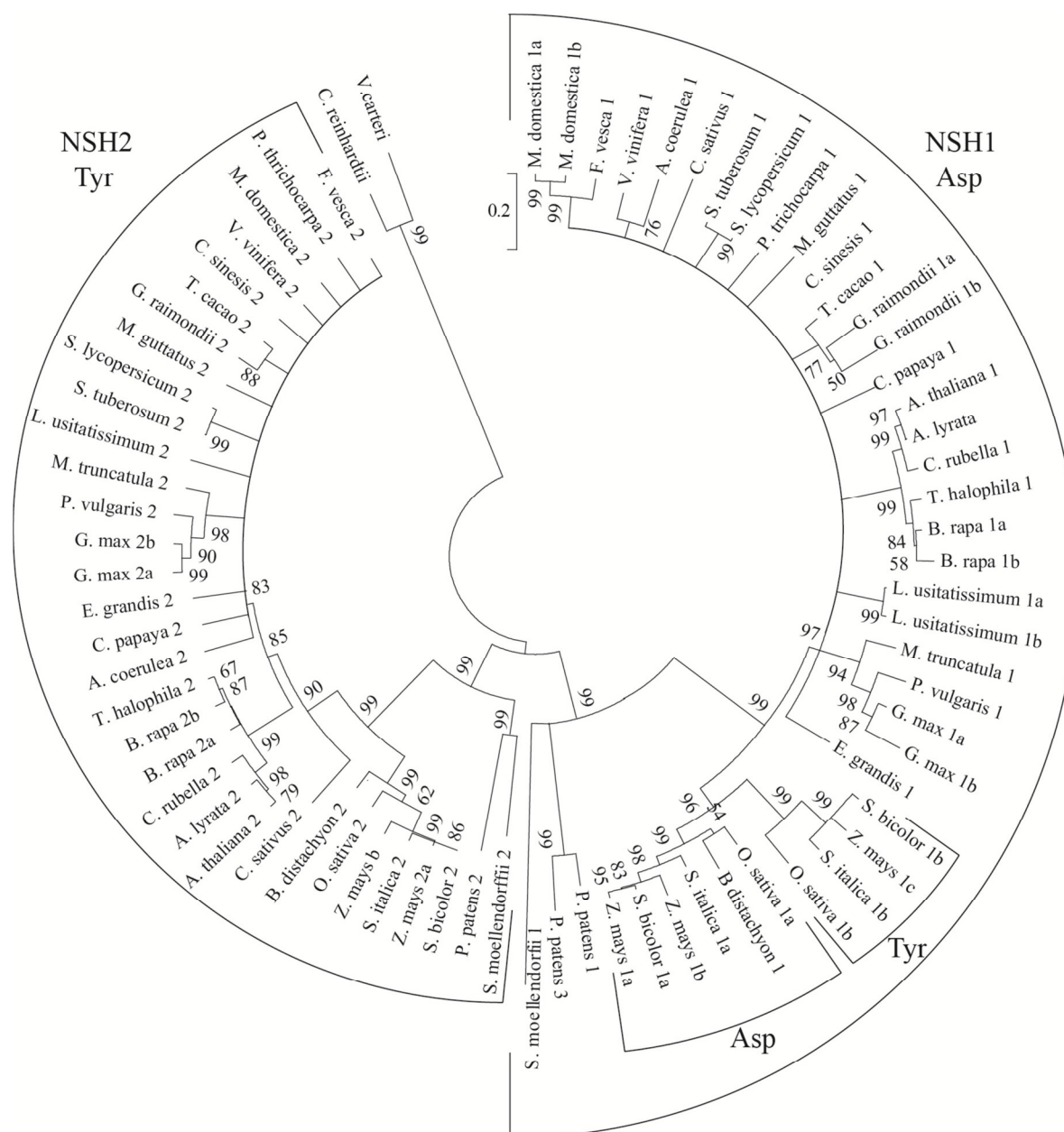


**Figure 17. Molecular phylogenetic analysis of plant nucleoside hydrolases.**

The evolutionary history was inferred by using the neighbor-joining method with the aid of the MEGA6 software. The bootstrap consensus tree (1000 replicates) was made using the model of Jones-Taylor-Thornton. The tree is drawn to scale, with branch lengths that measured the number of substitutions per site. NSH1 and NSH2 clades are shown. Tyr (tyrosine) and Asp (aspartate) indicate the residue corresponding to position 249 in *Physcomitrella* NSH2 that potentially confer specificity for xanthosine and inosine (Tyr) or uridine (Asp). The two subclades of Gramineae NSH1 are shown. Accession and gene locus numbers are shown in Table B-1 (Appendix).

In the genome of the two species of green algae analyzed (*Chlamydomonas reinhardtii* and *Volvox carteri*), only one nucleosidase gene is found, thus the functional distinction between

NSH1 and NSH2 is specific for plants. The Graminaceae (Figure 17; *Oryza sativa*, *Setaria italica*, *Zea mays*, *Sorghum bicolor*, *Brachiopodium distachion*), with the exception of *Brachiopodium distachion*, have two isoforms of NSH1 which cluster into two subclades.

The sequences of the NSH2 were compared with the NSH1. The differences that could be found were already highlighted by Kopečná et al., 2013. In particular, the authors suggested that two residues, 244 and 249 (*P. patens* NSH2 numbering), involved in substrate binding are important in determining substrate specificity. The presence of a tyrosine (Tyr) in both positions makes the enzyme specific for inosine and xanthosine, whereas the presence of a tryptophan in position 244 and an aspartate in position 249 confers higher affinity for uridine. *A. thaliana* NSH2, as well as all the enzymes belonging to the NSH2 clade, have a Tyr in both positions (Tyr-238 and Tyr-233 in Arabidopsis NSH2), suggesting that these have an activity similar to *P. patens* NSH2, for which inosine and xanthosine are the best substrates. *A. thaliana* NSH1, as well as all other enzymes of the clade, have an aspartate and a tryptophan at the respective positions. The only exceptions are the enzymes from one of the NSH1 subclades of the Graminaceae, which have a Tyr in position 249, suggesting that enzymes from this NSH1 subclade might have substrate spectrum similar to NSH2.

### 3.2.1.2 Modelling of Arabidopsis NSH1 and NSH2

Arabidopsis NSH1 and NSH2 were modelled to further investigate differences that could give an indication about the biochemical function of NSH2. The models were generated with Phyre<sup>2</sup> using the structure of Physcomitrella NSH2 as template. The modelled Arabidopsis NSH1 and NSH2 have the typical NSH fold containing 12  $\beta$ -strand and 13  $\alpha$ -helices (Figure 18A and Kopečná et al., 2013). The molecular surfaces of the models were colored by amino acid hydrophobicity using the software CHIMERA (Figure 18B). One region was found to be particularly different. It corresponded to lysine 217 in Arabidopsis NSH1, isoleucine 203 in Arabidopsis NSH2, and tyrosine 214 in Physcomitrella NSH2 (Figure 18C). Interestingly this residue was always a valine or isoleucine in all NSH2s, except for Physcomitrella NSH2 (Figure A2 Appendix). Both isoforms of NSH2 in *Zea mays* contain valine and they were insoluble in *E. coli* (Section 1.3.2 and Kopečná et al., 2013). Isoleucine is found in Physcomitrella NSH1 at this position, and this enzyme was as well insoluble in *E. coli* (Section 1.3.2 and Kopečná et al., 2013). In all other NSH1 homologs as well as in Physcomitrella NSH2, this position is filled by a polar amino acid or by cysteine in some cases. Isoleucine and valine are the most hydrophobic amino acids according to the Kyte and

Doolittle hydrophobicity scale. Maybe these hydrophobic residues form the hydrophobic determinant that impairs the expression of soluble protein in *E. coli*.

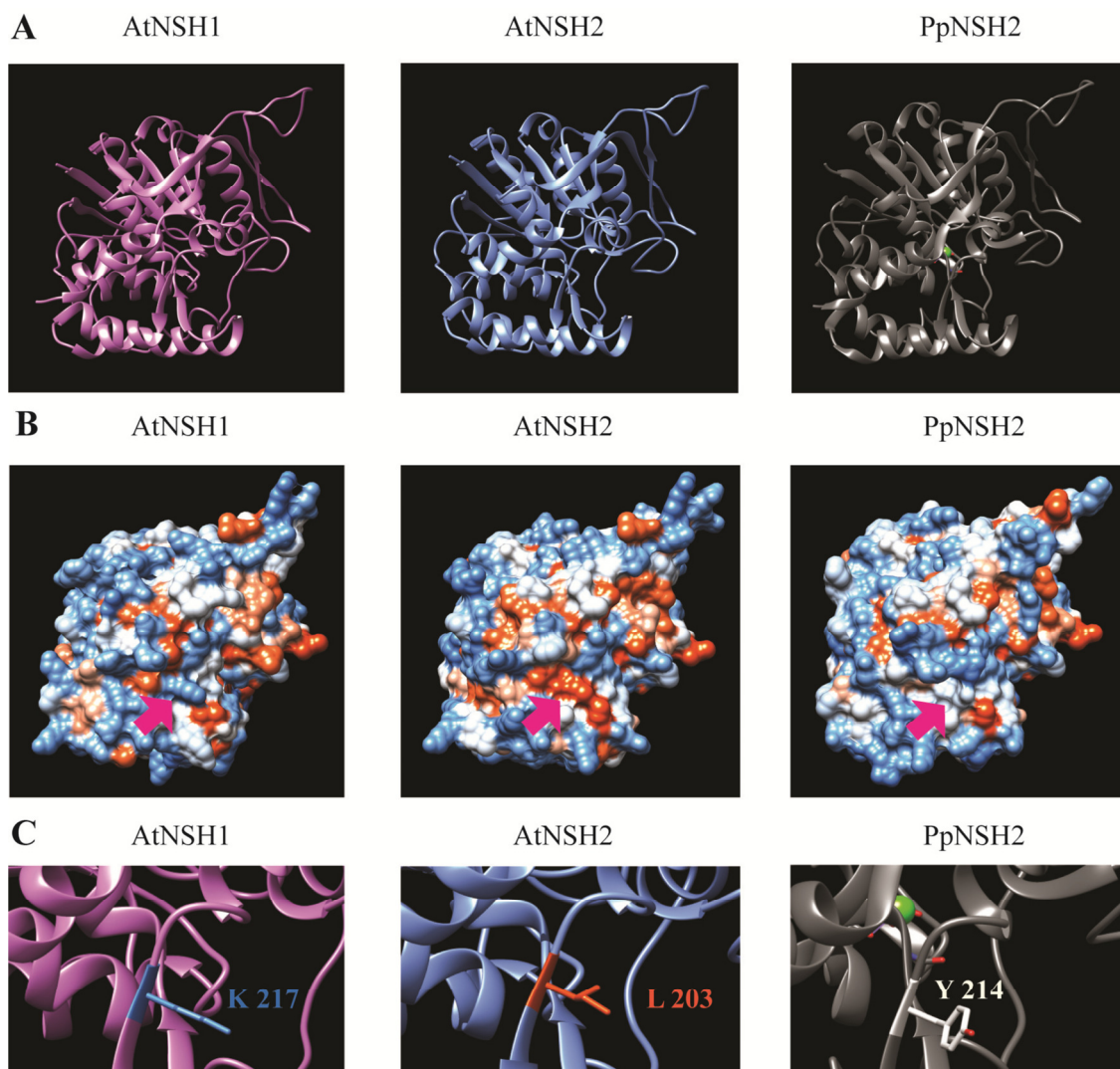


**Figure 18. Homology models of *A. thaliana* NSH1 and NSH2.**

*A. thaliana* NSH1 and NSH2 were modelled by homology modelling using the structure of *P. patens* NSH2 as template (PDB accession 4KPN). The structure prediction service was provided by Phyre<sup>2</sup>. Models were visualized and analyzed by CHIMERA.

(A) Models of *A. thaliana* NSH1 (AtNSH1), NSH2 (AtNSH2) and *P. patens* NSH2 (PpNSH2). (B) Hydrophobicity of the surface of the proteins according to the Kyte and Doolittle hydrophobicity scale. Hydrophobicity is colored from blue for the most hydrophilic residues over white for intermediate to red for highest hydrophobicity. The arrows indicate a region highlighted in C. (C) Focus on a surface region different between the distinct nucleosidases. The calcium in the active site of PpNSH2 is indicated in green.

### 3.2.2 Biochemical analyses: enzyme purification, activity assessments, and protein-protein interaction studies.

#### 3.2.2.1 Protein expression and purification

*Arabidopsis thaliana* NSH1 and NSH2 were transiently expressed as N-terminally Strep-tagged variants in leaves of *Nicotiana benthamiana*. The plant expression system enabled the purification of NSH2, though the expression level and consequently the purification yield were lower in comparison to NSH1 (Figure 19A).

To confirm the solubility of the proteins in *N. benthamiana* leaves, a solubility test was performed. Clarified cell lysates of leaves which had expressed either NSH1 or NSH2 were centrifuged at 100,000g, for one hour. After the centrifugation, the supernatant (soluble fraction) and the pellet (insoluble fraction) were tested on an immunoblot to detect the presence of the nucleosidases. Both enzymes were mainly found in the supernatant, confirming the solubility of the proteins expressed *in planta* (Figure 19B).

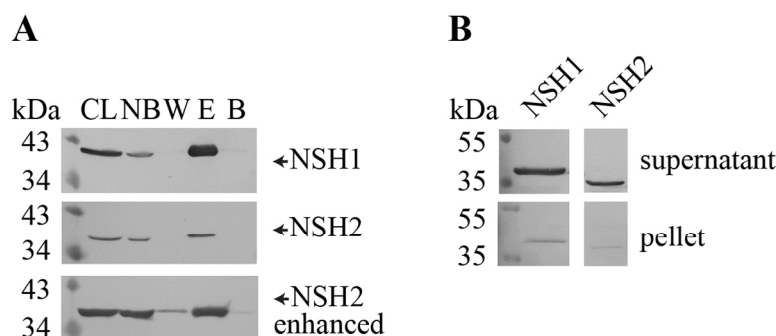


**Figure 19. Purification of nucleosidases by Strep affinity chromatography.**

(A) Purification of N-terminally Strep-tagged NSH1 and NSH2 after transient expression in leaves of *N. benthamiana* (upper and middle panels). The lower panel (NSH2 enhanced) shows the purification of NSH2 expressed from a construct, in which *NSH2* was flanked by viral enhancer sequences boosting expression (Table 2.1-4). Proteins were detected by immunoblot with StrepTactin-alkaline phosphatase (AP) conjugate. 12.5  $\mu$ L were loaded per lane. CL, clarified cell lysate; NB, protein not bound to the affinity matrix; W, protein in the last washing step; E, elution fraction; B, protein remaining bound to the affinity matrix after elution. (B) Solubility of NSH1 and NSH2 expressed in *N. benthamiana* leaves. Immunoblot of the supernatant and the pellet fractions derived from a 1 hour centrifugation step at 100,000g of the clarified cell lysate of *N. benthamiana* leaves. The immunoblot was developed with StrepTactin-AP. The data are from Baccolini and Witte, 2019.

### 3.2.2.2 Activity assay and interaction studies

The NSH activity could be assessed spectrophotometrically because the substrates (xanthosine, inosine, and uridine) and the respective products (xanthine, hypoxanthine, and uracil) had different absorption spectra (Parkin, 1996a; Kopečná et al., 2013). NSH1 was active (Figure 20) with all the substrates, confirming what had been reported in the literature (Jung et al., 2009; Jung et al., 2011; Riegler et al., 2011). By contrast, NSH2 did not hydrolyze any of the nucleosides provided. To exclude the possibility that NSH2 was not active due its lower amount, *NSH2* cDNA was cloned in a vector containing viral enhancer sequences to improve its expression. Both expression and purification were enhanced (Figure 19A, lower panel). The activity of NSH2 was tested again, but the enzyme was still inactive (Figure 20).

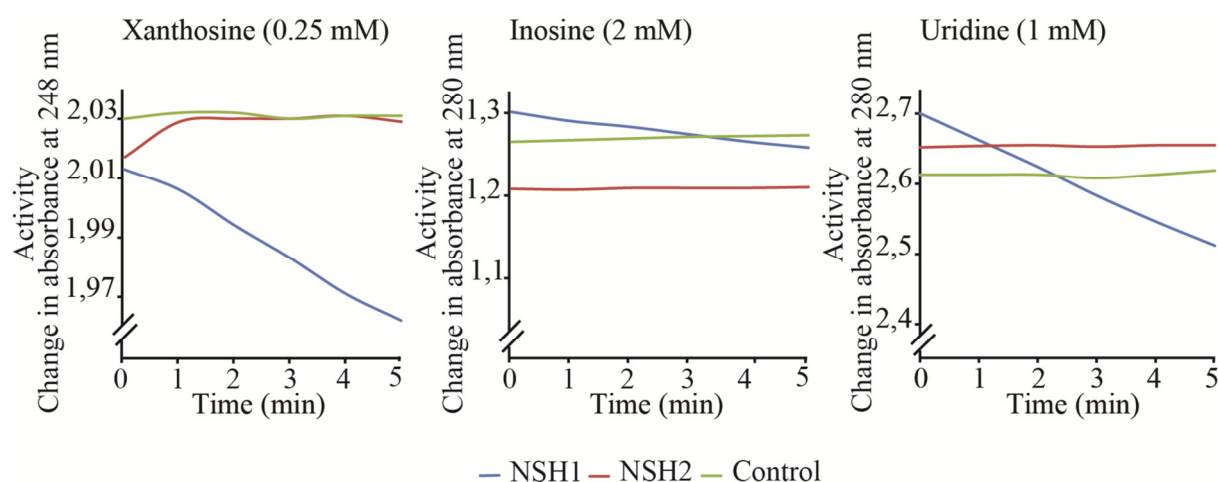


**Figure 20. Spectrophotometric monitoring of NSH1 and NSH2 nucleoside hydrolase activity.**

Preliminary assessment of Arabidopsis NSHs activity. The decrease in the absorbance is an indication of the conversion of the substrate to the product. The nucleosides tested were xanthosine, inosine and uridine applied at different concentrations. 5  $\mu$ L of purified enzyme were added to the reactions. NSH2 from the enhanced expression system was used. Control, reaction with no enzyme added.

As shown in section 3.1.1 and 3.1.2, there is evidence for an *in vivo* function of NSH2 in purine nucleotide catabolism (Figure 7, Figure 8, Figure 9, Figure 12), but this function might not be enzymatic because NSH2 showed no activity (Figure 20). NSH2 of *P. patens* was demonstrated to be an active xanthosine inosine hydrolase. Maybe NSH2 of higher plants has lost its catalytic function during evolution in favor of a regulatory function modulating the activity of NSH1. A regulatory role of NSH2 appears possible judging from the results of the

*NSH2 XDH* double mutant analysis, which showed that the double mutant accumulated significantly more xanthosine than *nsh2* (Figure 12). The reason for this might have been that NSH1 activity was reduced by the lack of NSH2 potentially acting as positive regulator of NSH1 as well as by the high amounts of xanthine in *xdh nsh2* acting as product inhibitor of NSH1 (Figure 9). If NSH2 was a positive regulator of NSH1, the two proteins might physically interact. To assess this hypothesis, the nucleosidases were transiently co-expressed *in planta* as N-terminally myc- and Strep- tagged variants in different combinations (Figure 21, input). The enzymes were purified by Strep affinity chromatography and the purified fractions (Figure 21, output) were loaded on immunoblots to detect whether the respective myc-tagged proteins were co-purified. Indeed, NSH1 and NSH2 interacted in this experiment (Figure 21, last two lanes). Interestingly, NSH1 interacted also with itself (third lane), whereas NSH2 did not (sixth lane). Thus, NSH2 could only form a complex with NSH1 but not with itself. The inability to form a homomer distinguishes Arabidopsis NSH2 from its homolog in *Physcomitrella*, which is a homodimer as shown by structural and size exclusion chromatography data (Kopečná et al., 2013).

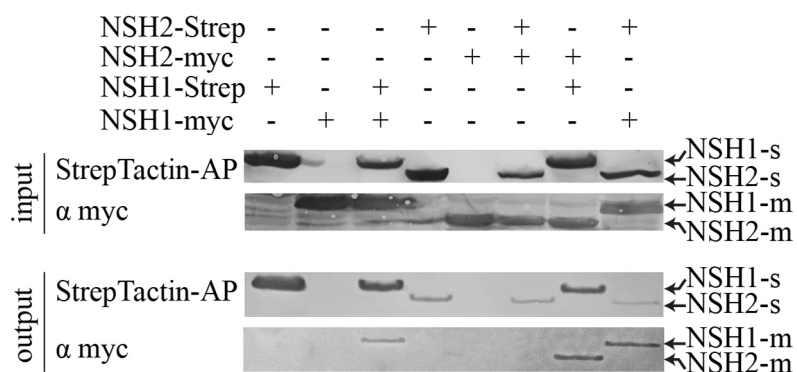


**Figure 21. Interaction of NSH1 and NSH2 *in planta*.**

*Nicotiana benthamiana* leaves were infiltrated with different combinations of NSH1 and NSH2 as Strep- or myc- tagged variants, as indicated. Proteins were purified via Strep tag affinity chromatography. Protein expression (input) and protein (co-) purification (output) were evaluated by immunoblot developed either with StrepTactin-AP conjugate or with anti-myc antibodies ( $\alpha$  myc). Per lane, 12  $\mu$ L of clarified leaf extracts or affinity purified proteins were loaded. Suffix s, Strep-tagged; suffix m, myc-tagged. The data are from Baccolini and Witte, 2019.

The activity of NSH1, NSH2 and the complex NSH1-NSH2 was measured with 250  $\mu$ M of xanthosine, inosine and uridine as substrates (Table 3-1, first three rows). NSH1 was mostly active with uridine, approximately nine fold less active with xanthosine, and active with inosine only when supplied at higher concentration (Figure 20 and Table 3-1, last two columns). NSH2 was not active with any of the substrates (Figure 20 and Table 3-1). The

complex NSH1-NSH2 showed activity with all the three substrate tested (Table 3-1). It was most active with xanthosine, showing a 25 fold higher activity than NSH1 alone. The heterocomplex was also active with inosine at 250  $\mu$ M, whereas NSH1 was active with inosine only at very high concentrations. There was also some activity with uridine, but it was approximately three fold lower than NSH1 uridine hydrolase activity (Table 3-1).

**Table 3-1 Specific activities of different nucleoside hydrolase species.**

NSH <sup>1</sup>	specific activity <sup>3,4</sup> ( $\mu$ mol min <sup>-1</sup> mg <sup>-1</sup> )			specific activity with higher concentration of substrate <sup>3,4</sup> ( $\mu$ mol min <sup>-1</sup> mg <sup>-1</sup> )	
	xanthosine (0.25 mM)	inosine (0.25 mM)	uridine (0.25 mM)	inosine (2 mM)	uridine (1 mM)
NSH1	0.61 $\pm$ 0.01	0 <sup>2</sup>	5.7 $\pm$ 0.2	3 $\pm$ 1	15.2 $\pm$ 0.7
NSH2	0	0	0	0	0
NSH1 NSH2	15.4 $\pm$ 0.4	3.9 $\pm$ 0.9	2.0 $\pm$ 0.5	19 $\pm$ 2	8 $\pm$ 1
$\Delta$ NSH1	0	0	0	0	0
$\Delta$ NSH1 NSH2	6 $\pm$ 2	0 <sup>2</sup>	0 <sup>2</sup>	1 $\pm$ 0.5	2 $\pm$ 1.5
$\Delta$ NSH2	0	0	0	0	0
NSH1 $\Delta$ NSH2	0.22 $\pm$ 0.02	0	0.4 $\pm$ 0.1	0	3 $\pm$ 1

<sup>1</sup> NSH1-NSH2 heterocomplexes were always purified via Strep-tagged NSH2 to avoid excess NSH1.

<sup>2</sup> The activity was detected at higher substrate concentrations (last two columns).

<sup>3</sup> Error are SD (n = 3).

<sup>4</sup> The tables in the current Section (Section 3.2.2) are from Baccolini and Witte, 2019.

The activity measurement showed that the NSH1-NSH2 complex has a higher xanthosine inosine hydrolase activity than NSH1. This suggests that either NSH2 is a positive regulator of NSH1 or NSH2 is a xanthosine inosine hydrolase activated by the presence of NSH1. To discriminate between the two possibilities, an inactive NSH1 mutant was generated ( $\Delta$ NSH1). The second aspartate of the N-terminal DTDPGIDD motif was exchanged to alanine by site directed mutagenesis creating a D29A variant. This Asp is involved in calcium binding and acts as catalytic base activating a water molecule for the hydrolysis of the glycosidic bond (Figure 22 and Section 1.3.1). The mutation of the corresponding aspartate in *Physcomitrella* NSH2 causes a reduction of the activity by 10<sup>4</sup> fold in comparison to the wild type protein (Kopečná et al., 2013). However the mutation does not strongly change the NSH structure as shown by circular dichroism analysis (Kopečná et al., 2013).

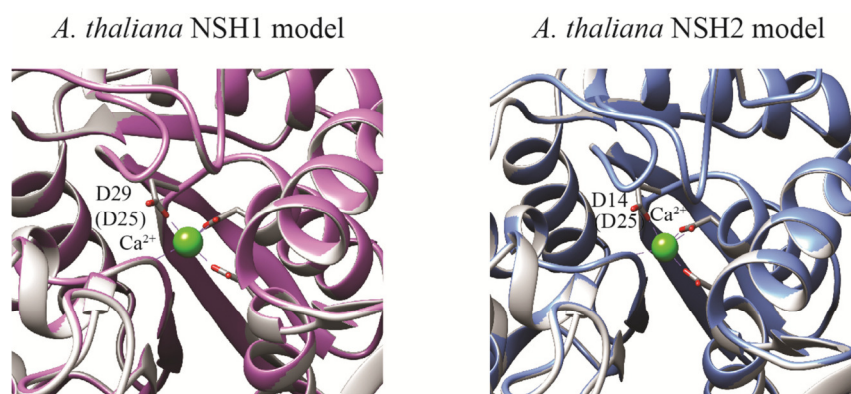


**Figure 22. Function of the aspartate mutated to alanine in NSH1 and NSH2.**

Models of *A. thaliana* NSH1 and NSH2 calcium binding sites. Proteins have been modelled by Phyre<sup>2</sup> with *P. patens* NSH2 as template. The two structures have been superimposed and visualized by Chimera. The aspartate residues (Asp29 for *A. thaliana* NSH1 and Asp14 for *A. thaliana* NSH2) which were mutated to alanine are shown. The numbers in brackets refer to the equivalent residues in the respective *Physcomitrella* proteins.

NSH2 and  $\Delta$ NSH1 were co-expressed in *N. benthamiana* leaves and could be co-purified, indicating that the mutation did not alter the dimerization capability of the two enzymes (Figure 23, second last lane).

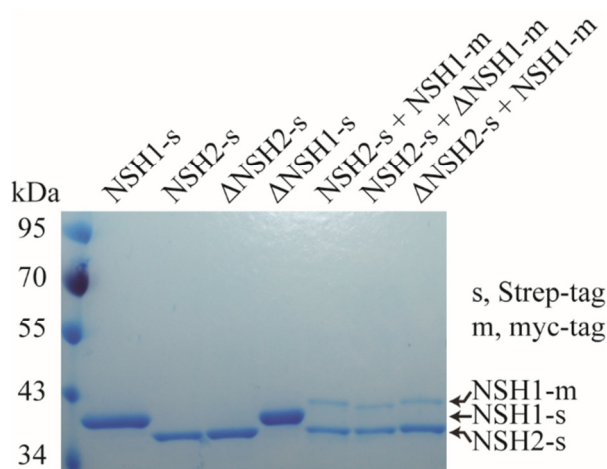


**Figure 23. Purity of affinity (co-) purified nucleoside hydrolases.**

Affinity purified NSHs were loaded on a SDS gel (12.5  $\mu$ L per sample). Strep-tagged enzymes had been expressed alone or in combination with myc-tagged ones.  $\Delta$ NSH1 and  $\Delta$ NSH2 are inactive point mutants of NSH1 and NSH2. The gel was stained with colloidal Coomassie Blue. The data are from Baccolini and Witte, 2019.

The mutant  $\Delta$ NSH1 was inactive but the complex  $\Delta$ NSH1-NSH2 was active for all the substrates tested (Table 3-1). Therefore, the hypothesis that NSH2 is merely a modulator of NSH1 and lost its catalytic function is wrong. NSH2 is a xanthosine inosine hydrolase that



becomes active only in presence of NSH1. To determine the contribution of the xanthosine hydrolase activity derived from NSH2 and the one derived from NSH1, the second aspartate of the N-terminal DTDPGIDD motif of NSH2 was mutated to alanine (D14A, Figure 22) and the activity of the complex NSH1- $\Delta$ NSH2 measured.  $\Delta$ NSH2-NSH1 was approximately 27 fold less active for xanthosine than the complex  $\Delta$ NSH1-NSH2 (Table 3-1, Figure 23), indicating that NSH2 is the main contributor to xanthosine hydrolysis *in vitro*. Uridine hydrolase activity was higher in  $\Delta$ NSH2-NSH1 than  $\Delta$ NSH1-NSH2; therefore, NSH1 was mainly responsible for uridine hydrolysis. Inosine hydrolase activity was detected only in  $\Delta$ NSH1-NSH2, indicating that it is mainly associated with NSH2.

To confirm that the NSH1-NSH2 complex was a more efficient xanthosine hydrolase than NSH1 alone, the kinetic constants were determined (Table 3-2). The NSH1-NSH2 complex had the highest catalytic efficiency for xanthosine, 5.5 fold higher than for inosine and 30 fold higher than for uridine. It was a more efficient xanthosine hydrolase in comparison to NSH1 because of an 8 fold smaller  $K_M$  and an 8 fold higher  $k_{cat}$ . It was not possible to determine the catalytic constants of NSH1 for inosine with the spectrophotometric assay, because the linear range of the spectrophotometer was exceeded by the high concentrations of inosine required – apparently the  $K_M$  for this nucleoside is rather high. However, Jung et al., 2009 reported a  $K_M$  of 1.4 mM and a  $k_{cat}$  of  $8.7 \text{ s}^{-1}$  of NSH1 for inosine, which indicates that the NSH1-NSH2 complex has an approximately 10 fold higher catalytic efficiency for inosine than NSH1.

In summary, the data show that the NSH1-NSH2 heterocomplex and the NSH1 homomeric complex have distinct enzymatic properties: NSH1-NSH2 is a more efficient xanthosine inosine hydrolase, whereas the NSH1 homomer is a more efficient uridine hydrolase.

**Table 3-2 Kinetic constants of the NSH1 homomer and the NSH1-NSH2 heteromer.**

Substrate	NSH1				NSH1-NSH2			
	$K_M$ (mM)	$k_{cat}$ ( $\text{s}^{-1}$ )	$k_{cat}/K_M$ ( $\text{s}^{-1} \text{ mM}^{-1}$ )	$R^2$	$K_M$ (mM)	$k_{cat}$ ( $\text{s}^{-1}$ )	$k_{cat}/K_M$ ( $\text{s}^{-1} \text{ mM}^{-1}$ )	$R^2$
xanthosine	0.52	2.65	5.10	0.96	0.06	23.3	389.2	0.99
inosine	-	-	-	-	0.60	42.3	70.5	0.90
uridine	0.73	33.5	45.9	0.98	4.30	55.3	12.9	0.95

One intriguing question about the biochemistry of NSH2 is still unresolved: why the enzyme is inactive on its own. The reason of this might reside in the inability of NSH2 to form a homodimer. *Physcomitrella* NSH2 has one lysine in the active site (Lys297) which protrudes from one subunit of the homodimer and completes the active site of the other subunit of the homodimer. This residue is conserved in all NSHs (Figure A2 Appendix). The monomeric NSH2 of *Arabidopsis* might therefore have an incomplete active site that is completed in the heterodimer by the lysine provided by NSH1 (Lys300, Figure 24).

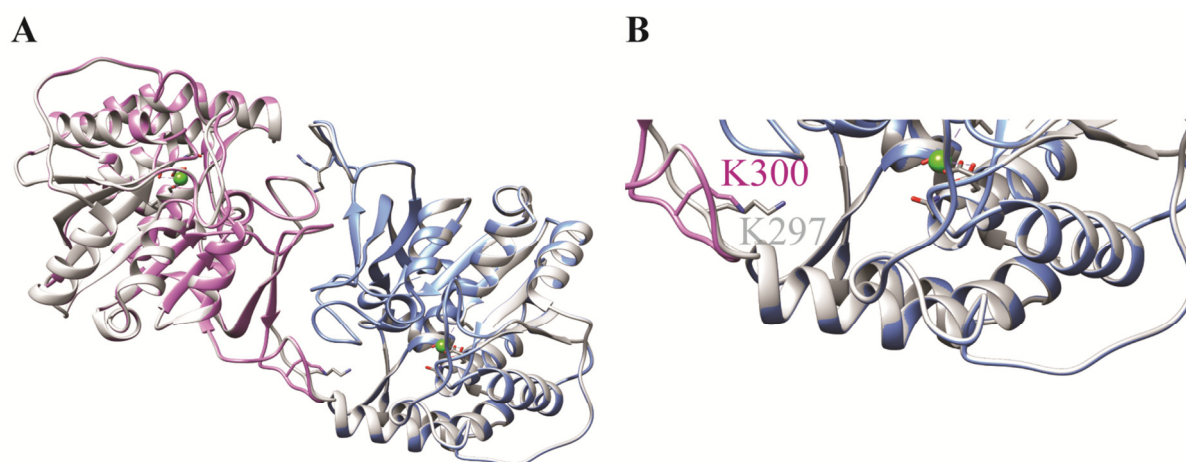


**Figure 24. Model of the heterodimer NSH1-NSH2.**

(A) Model of the heterodimer NSH1-NSH2. The model was generated by superimposing the AtNSH2 model (blue) with one subunit of PpNSH2 homodimer (white) and the AtNSH1 model (purple) with the other subunit. (B) Focus on the active site of AtNSH2. The lysine protruding from the AtNSH1 (K300) is shown; the corresponding lysine in *Physcomitrella* (K297) is also shown. In green is indicated the Ca<sup>2+</sup> ion present in the active site.

A lysine 300 to alanine mutant of NSH1 (K300A) was generated to test this hypothesis. In this work,  $\Delta$ NSH refers to the mutation of the aspartate in the aspartate motif, whereas K300A refers to the mutation of the lysine 300 in NSH1. The mutation of the lysine lowered the activity of NSH1, showing that it has a role in the active site (Figure 25). The complex (K300A) NSH1-NSH2 was active, showing that the mutation does not impair NSH2 activation by NSH1. The complex (K300A) NSH1- $\Delta$ NSH2 was also investigated, and its reduced activity for xanthosine in comparison to (K300A) NSH1-NSH2 confirms that xanthosine hydrolase activity is provided mainly by NSH2, whereas uridine hydrolase activity is generated by NSH1 (Figure 25).

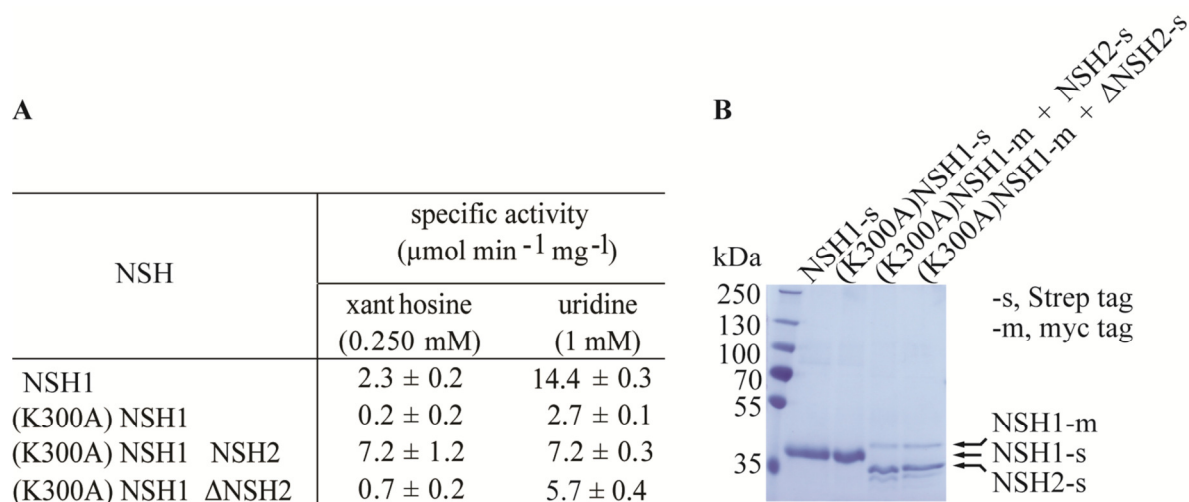


**Figure 25. Investigation of NSH2 inactivity.**

(A) Xanthosine and uridine hydrolase activity of NSH complexes with the mutant of NSH1 for Lys300, (K300A) NSH1. (B) Purity of the NSHs used in A for the activity measurement.

### 3.2.3 Analysis of NSH1 and NSH2 expression in Arabidopsis

To study the expression profile of NSH1 and NSH2 in different tissues of Arabidopsis, antibodies for the two NSHs were developed. The first batch of anti-NSH1 and anti-NSH2 antibodies showed cross reactivity: the anti-NSH2 antibody recognized NSH2 but also NSH1 and the anti-NSH1 antibody recognized NSH1 but also NSH2. The antibody purification strategy adopted to overcome this problem is described in Material and Methods (Section 2.2.4.1). Two types of antibodies were obtained in the end, an anti-NSH1 antibody which specifically detects NSH1 down to sub-nanomolar concentrations (Figure 26A), and a dual specific anti-NSH1/2 that recognizes both NSH1 and NSH2 with approximately the same affinity (Figure 27). Using these antibodies, the expression levels of NSH1 and NSH2 were determined in different tissues of *A. thaliana* by immunoblot (Figure 26). The anti-NSH1 specific antibody detected NSH1 in all the tissues of the wild type, the NSH1 signal in seeds was lower probably due to a higher buffer to sample ratio used in the extraction (Figure 26A). NSH2 was detected with the dual anti-NSH1/2 antibody (Figure 26B). NSH2 could be detected reliably only in roots and flowers, and weakly in seedlings and middle rosette leaves. Considering that transcriptomic data (Figure A3 Appendix) show that the *NSH2* transcript is present in almost all tissues, it is possible that the NSH2 protein is ubiquitously present, but could not be detected by the antibody. In those tissues where it was detected by the antibody (roots and flowers), the transcript abundance is also higher (Figure A3 Appendix).

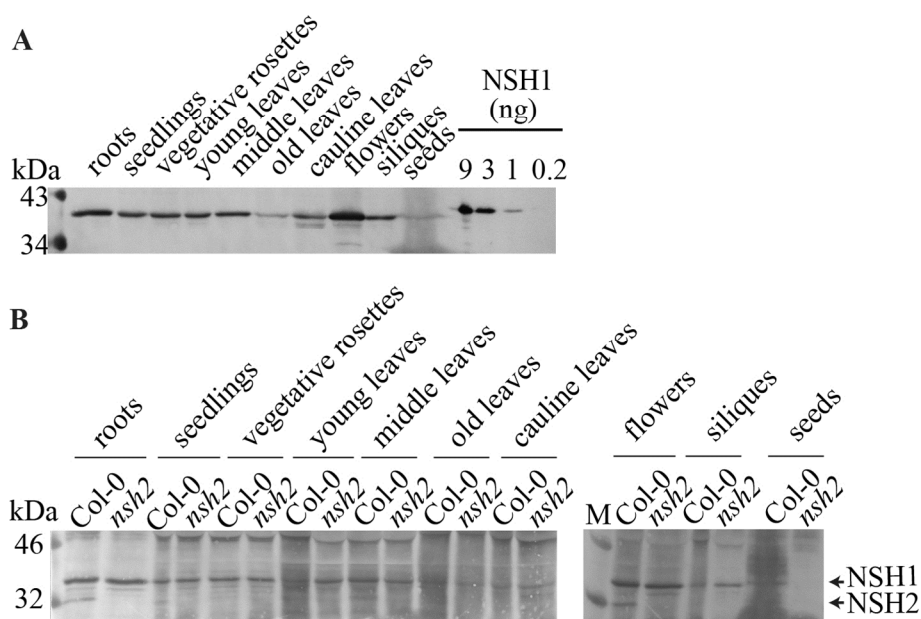


**Figure 26. NSH1 and NSH2 protein expression profiles in different tissues of *A. thaliana*.**

NSH1 and NSH2 expression levels were assessed by immunoblot. (A) Immunoblot developed with anti-NSH1 antibody. A 2 : 1 buffer to sample ratio was used for extraction, with the exception of seeds that were extracted with a 4 : 1 buffer to sample ratio. 12  $\mu$ L of sample were loaded per lane. Samples: 10-day-old seedlings grown on agar plates, roots and the rosettes of a 4-week-old plant before bolting grown in soil, young leaves (leaves up to position 14), middle leaves (13 to 7), old leaves (6 to 1), cauline leaves, flowers and siliques of a 6-week-old plant. NSH1 standard curve is loaded next to the samples. (B) As (A) but developed with the dual specific NSH1/2 antibody. The *NSH2* mutant was used as negative control for the NSH2 signal.

In roots, the NSH1 and NSH2 signals were quantified and NSH2 resulted to be less abundant than NSH1 (Figure 27). NSH1 was detected in all the tissues by the anti NSH1/2 antibody, whereas NSH2 could only be detected in root and flowers although the antibody had similar affinity for NSH1 and NSH2 (Figure 27). Therefore, it can be concluded that NSH2 was less abundant than NSH1 in all the tissues.

To note that NSH1 was still present in *nsh2* and NSH2 was still present in *nsh1* (Figure 27), indicating that the NSH protein abundance is independent from the presence of the respective partner.

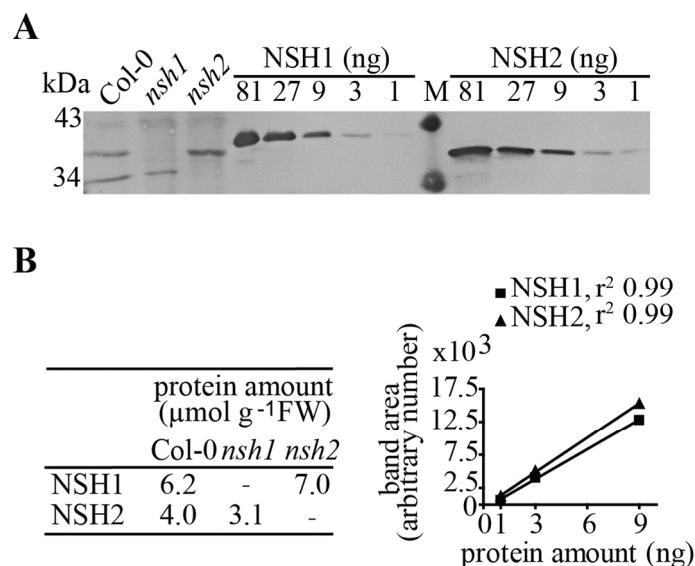


**Figure 27. Quantification of NSH1 and NSH2 in roots of *A. thaliana*.**

A) Cell lysates of roots from Col-0, *nsh1* and *nsh2* were analyzed by SDS page loaded on a constant fresh weight basis. Quantification standards for NSH1 and NSH2 were analyzed side by side. Protein quantification was achieved by immunoblot developed with the dual anti-NSH1/2 antibody coupled with StrepTactin-AP detection and band intensity measurements with ImageJ. B) Standard curves for NSH1 and NSH2. The data are from Baccolini and Witte, 2019.

### 3.2.4 Co-immunoprecipitation

The interaction between NSH1 and NSH2 needs to be confirmed with untagged proteins at native expression level to exclude artefacts due to heterologous overexpression of the nucleosidases as tagged variants. Therefore, an immunoprecipitation (IP) experiment was performed. The dual specific antibody reliably detected NSH2 in roots and flowers (Figure 26), and between these two tissues, roots were chosen for the IP. To easily access the root material, Col0, *nsh2*, and *nsh1* were grown hydroponically in short day conditions for six weeks. The IP was performed with the anti-NSH1 antibody which only recognizes NSH1 and not NSH2 *in vivo* (Figure 27 and Figure 28, input). The presence of NSH2 in the immune complex was assessed by immunoblot with the anti NSH1/NSH2 antibody. The experiment showed that NSH2 interacts with NSH1 (Figure 28, output), thus confirming that the NSH1-NSH2 complex is present under native conditions *in vivo*.

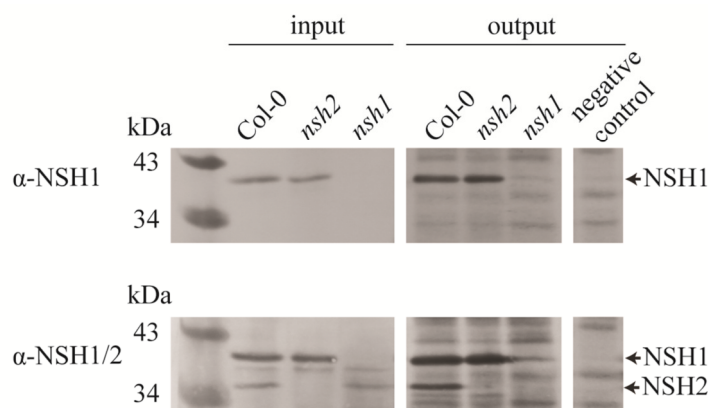


**Figure 28. Interaction of NSH1 and NSH2 in roots of *A. thaliana*.**

Clarified root cell lysates were immunoprecipitated with anti-NSH1 antibody. The presence of the nucleosidases in the tissue (input) and after IP (output) was assessed by immunoblot developed either with anti-NSH1 or anti-NSH1/2 antibody. The negative control lane refers to an IP with no addition of root extract. Data are from Baccolini and Witte, 2019.

The presence of the complex NSH1-NSH2 *in vivo* (Figure 28), the lower concentration of NSH2 in comparison to NSH1 in Arabidopsis tissues (Figure 26) and the consideration that plant NSHs are known to have a dimeric active form (Kopečná et al., 2013), indicate that NSH2 is present *in vivo* only in the NSH1-NSH2 heterodimer, whereas NSH1 is also present as homodimer.

### 3.2.5 Metabolite analysis of *NSH* mutants

#### 3.2.5.1 Metabolite analysis in roots

LC-MS analyses revealed that xanthosine accumulated in seeds and seedlings of the *NSH2* mutant, though to by far lower concentrations than in *nsh1* (Figure 12). The protein expression study (Figure 26) showed that NSH2 is more abundant in roots, maybe indicating a more important role of NSH2 in that tissue. The higher abundance of NSHs in roots might be related to a more efficient hydrolysis of nucleosides taken up from the soil (Riegler et al., 2011).

Metabolite analysis in roots of Col-0, *nsh1* and *nsh2* was conducted to assess the functional importance of NSH2 in particular, but as well the importance of NSH1 for xanthosine and inosine hydrolysis in root tissue (Figure 29). The data showed an accumulation of xanthosine in *nsh2*, whereas inosine and uridine did not accumulate. Similar to what was found in seeds and seedlings, the concentration of xanthosine in *nsh2* was more than two orders of

magnitude lower than in *nsh1*. Therefore, there is no evidence for a particularly prominent role of NSH2 in roots, even though the protein is more expressed here.

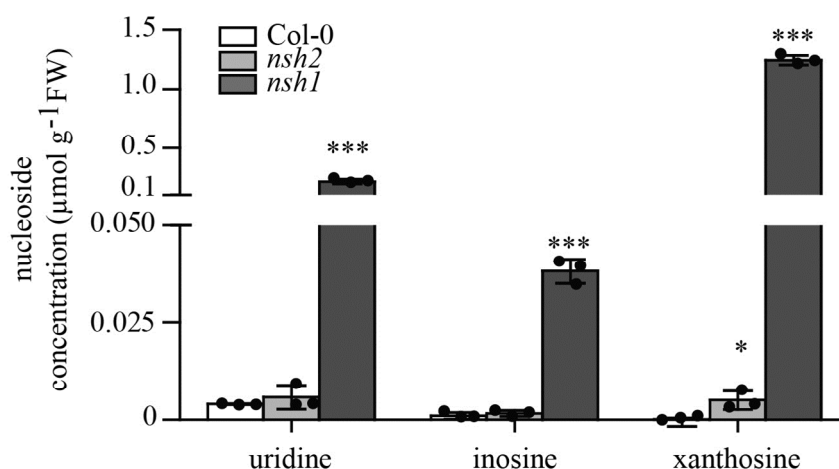


**Figure 29. Uridine, inosine and xanthosine content in root extracts of Col-0, *nsh1* and *nsh2*.**

The root material was harvested from 6-week-old hydroponically grown plants. The data are the mean (column) of three biological replicates, error bars are SD. Individual data points are indicated (dots). The \* indicate significant differences between the mutants and Col-0 as determined by unpaired two-tailed t-tests (\*,  $p < 0.05$ ; \*\*\*,  $p < 0.001$ ). FW, fresh weight.

The data in the current Section (Section 3.2.5) are from Baccolini and Witte, 2019.

### 3.2.5.2 Metabolite analysis in transgenic lines expressing nucleoside hydrolase variants

For the biochemical analysis (Section 3.2.2) N-terminal Strep- or myc- tagged NSH1 and NSH2 were used. To assess whether the tags interfered with the functionality of the proteins *in vivo*, transgenic lines overexpressing the tagged variants of NSH1 and NSH2 in the corresponding mutant backgrounds were created. A transgenic line overexpressing the mutated version of NSH1 ( $\Delta$ NSH1) in the *NSH1* mutant was generated as well. The expression of the transgene was shown in seedlings and roots (Figure 30).

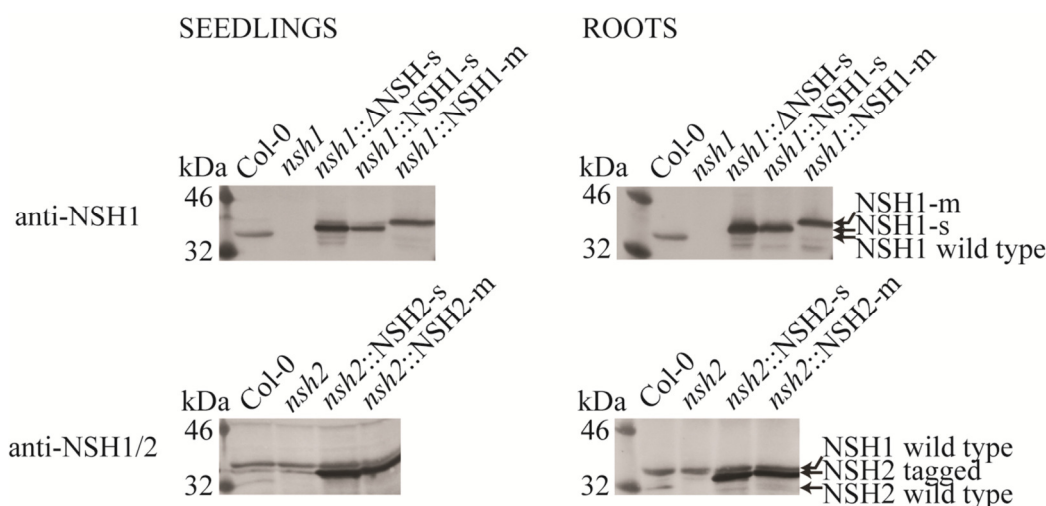


**Figure 30. Detection of tagged and mutant variants of NSH in Arabidopsis transgenic lines.**

Expression of Strep- and myc- tagged variants of NSH1 in seedlings and roots, and of the inactive point mutant of NSH1 ( $\Delta$ NSH1) as Strep-tagged variant in *nsh1* background. Detection by immunoblot developed with anti-NSH1 antibody (top panel). Expression of Strep- and myc- tagged variants of NSH2 in seedlings and roots in the *nsh2* background. Detection by immunoblot developed with anti-NSH1/NSH2 antibody (bottom panel). Seedlings were 7-day-old and the roots were from 4-week-old plants.

The metabolic profiles of seeds, seedlings and rosettes of the wild type, the *NSH1* mutant, the *NSH2* mutant, the *NSH1 NSH2* double mutant, and the transgenic lines were determined. As expected, an accumulation of xanthosine, inosine and uridine was detected in *nsh1* (Figure 31). The double mutant *nsh1 nsh2* accumulated these nucleosides to the same extent as *nsh1*. In *nsh1*, NSH2 is present but it is not active due to the absence of NSH1; therefore *nsh1* is a functional double mutant of *NSH1* and *NSH2*. The transgenic line *nsh1::ΔNSH1* expresses the inactive form of NSH1 and contains NSH2, thus assembling *in vivo* the  $\Delta$ NSH1-NSH2 complex, which had been biochemically characterized *in vitro* before (Table 3-1). In this line with *nsh1* background, xanthosine and inosine did not accumulate, demonstrating that NSH2 operates as xanthosine inosine hydrolase *in vivo*, requiring NSH1 protein but not activity to carry out its enzymatic function. In seedlings and rosettes, the level of uridine did not change in comparison to *nsh1*, supporting the hypothesis that NSH2 is primarily a xanthosine and inosine hydrolase. However in dried seeds, a significant reduction of the uridine level was detected. This may be explained by the combination of (i) high uridine concentration in *nsh1* seeds together with (ii) the low but detectable uridine hydrolase activity of the  $\Delta$ NSH1-NSH2 complex at high uridine concentrations (Table 3-1) and (iii) the long exposure time of the substrate to the enzyme in seeds.



The metabolic profiles of the complementation lines *nsh1::NSH1-Strep*, *nsh1::NSH1-myc*, *nsh2::Strep*, *nsh2::NSH2-myc* showed that the tagged protein variants complemented the molecular phenotypes. Therefore, the tags do not interfere with the activity of the NSHs (Figure 31).

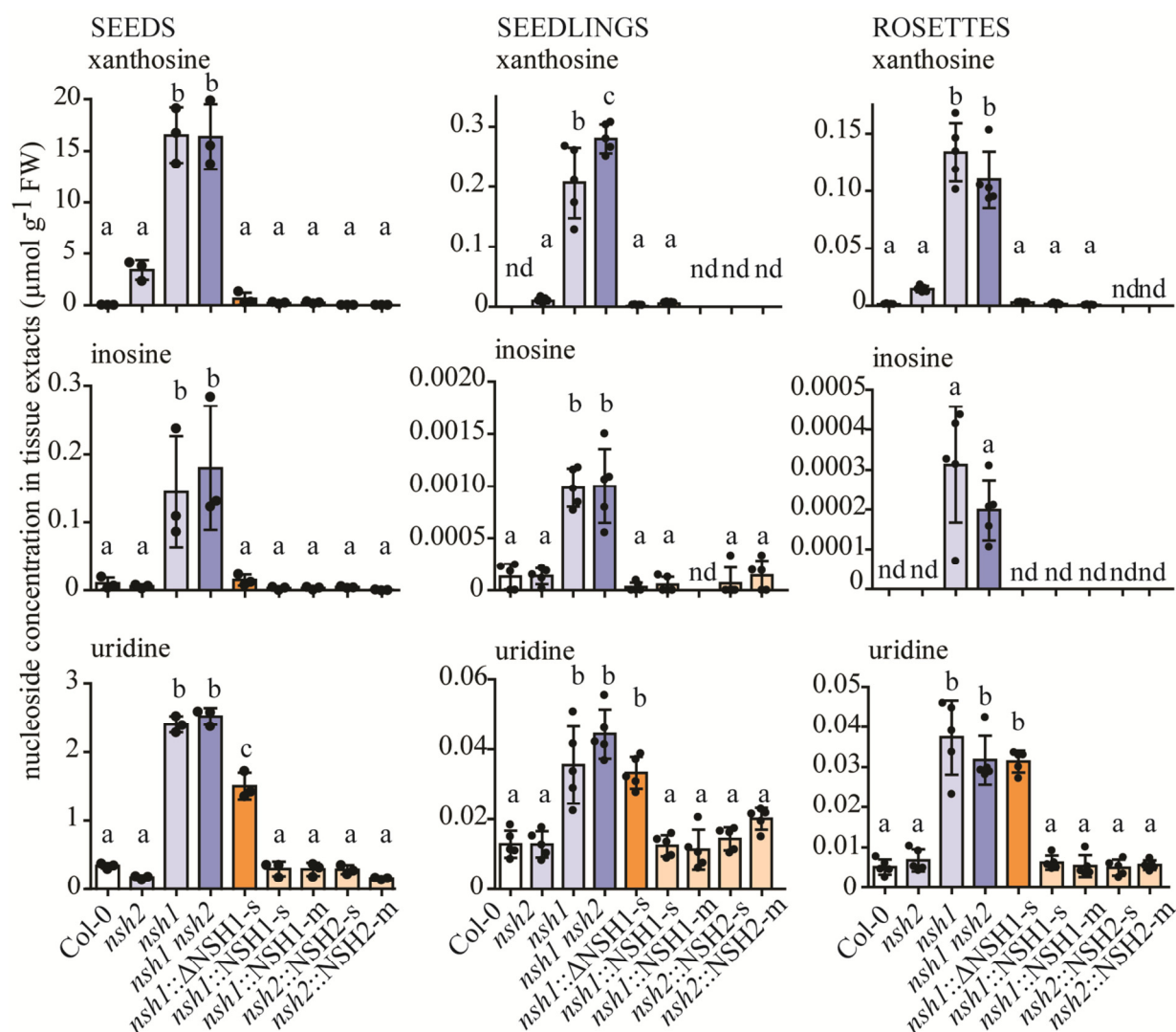


**Figure 31. Concentration of xanthosine, inosine and uridine in extracts of seeds, seedlings and rosettes of the wild type, *nsh1*, *nsh2*, *nsh1 nsh2*, and of the transgenic lines expressing mutant and tagged variants of the NSHs.**

The genotypes analyzed were: Col-0 (white), *NSH1* and *NSH2* single mutants (light blue), *NSH1 NSH2* double mutant (blue), a transgenic line overexpressing Strep-tagged  $\Delta NSH1$  in *nsh1* background (orange) and complementation lines overexpressing Strep- or myc- tagged NSH1 in *nsh1* background and Strep- or myc-tagged NSH2 in *nsh2* background (pale orange). Seeds, 7-day-old seedlings and rosettes from 4-week-old plants were analyzed. Columns indicate the mean of three (seeds) or five (seedlings and rosettes) biological replicates. Individual data points are shown (dots). Error bars are SD. Different letters indicate significant differences ( $p < 0.05$ ) as determined by One-Way ANOVA with Tukey's post-test analysis. nd, not detectable. FW, fresh weight.

### 3.2.5.3 Dark stress experiment with NSH mutants

NSH2 is an efficient xanthosine and inosine hydrolase upon activation by NSH1 *in vitro* (Table 3-1) and *in vivo* (Figure 31). Xanthosine accumulates in four different tissues of the *NSH2* mutant (Figure 12, Figure 29, and Figure 31). However, this accumulation is minor in comparison to the massive accumulation of xanthosine in *nsh1*.

The dark stress was employed to assess whether in a condition of enhanced purine nucleotide degradation, *NSH2* abrogation had a bigger impact on purine nucleoside catabolic capacity. An experiment similar to the one described in Section 3.1.4 was set up with Col-0, *nsh2*, *nsh1*, and *nsh1 nsh2*. The transgenic line *nsh1::ΔNSH1* was included as well to assess whether NSH2 was *in vivo* capable of hydrolyzing xanthosine and inosine even in condition of a high metabolic flux of purine nucleotide catabolism. The results (Figure 32) show that there was no increased accumulation of either xanthosine or inosine in *nsh2* with the progression of the dark stress, which suggests that NSH2 does not play a critical role in this process. The transgenic line *nsh1::ΔNSH1* showed no xanthosine and inosine accumulation, further confirming that *in vivo* NSH2 hydrolyzes xanthosine and inosine, and is sufficiently active to maintain wild-type concentrations of these metabolites without the aid of NSH1. Nevertheless, NSH1 alone is sufficient to hydrolyze most of the xanthosine and inosine in standard and dark stress conditions. As observed in seeds of *nsh1::ΔNSH1* (Figure 31), uridine was also significantly lower at day 3 of dark stress in the transgenic line in comparison to the single mutant. As explained before (Section 3.2.5.3), at a high concentration of uridine as in *nsh1* background during dark stress, the  $\Delta$ NSH1-NSH2 complex can hydrolyze some uridine.

It is interesting to note that in *nsh1* xanthosine accumulated at day 2 and 3 of darkness. Inosine accumulated as well, but only after 3 days. The inosine content was three orders of magnitude lower than the one of xanthosine, further supporting that xanthosine is the main intermediate of plant nucleotide catabolism (see Section 3.1.4).

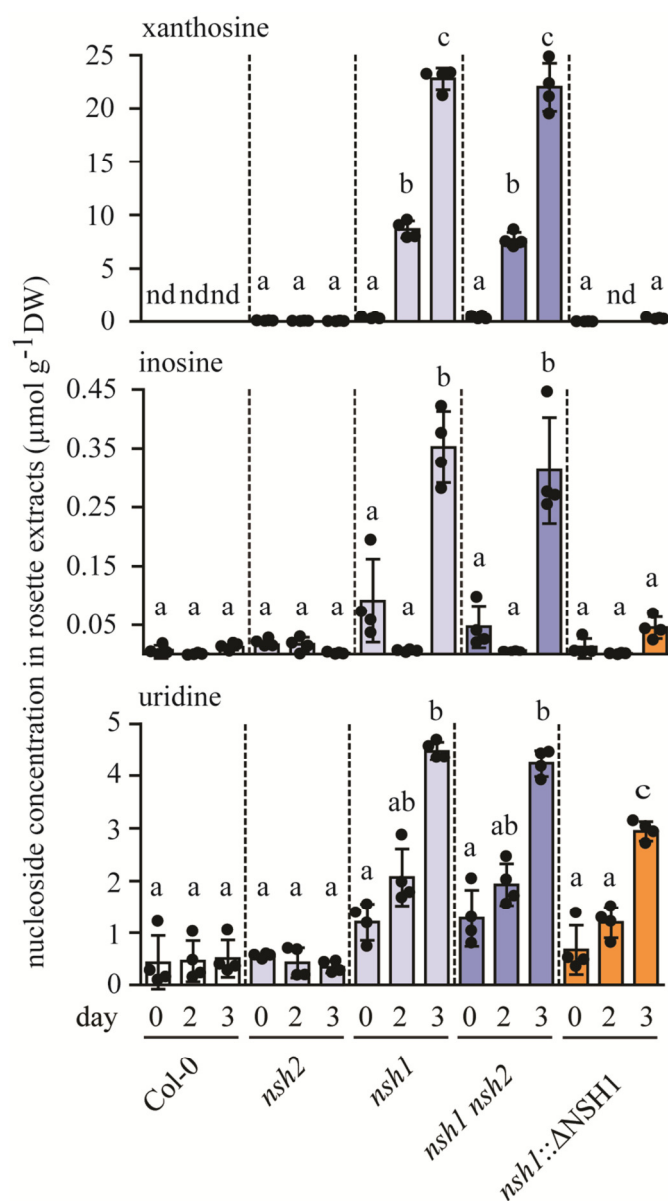


**Figure 32. Nucleoside content in rosettes exposed to dark stress.**

The genotypes analyzed were Col-0 (white), *NSH1* and *NSH2* single mutants (light blue), *NSH1 NSH2* double mutants (blue), and the transgenic line overexpressing Strept-tagged  $\Delta\text{NSH1}$  in *nsh1* background (orange). Samples were harvested at day 0 (before dark stress) and at day 2 and 3 of darkness. Columns indicate the mean of four biological replicates. Error bars are SD. Individual data points are shown (dots). Different letters indicate significant differences ( $p < 0.05$ ) as determined by One-Way ANOVA with Tukey's post-test analysis. nd, not detectable. DW, dried weight.



Physcomitrella nucleosidases (PpNSHs) show in part a different interaction pattern than the NSHs from Arabidopsis. PpNSH1 and PpNSH2 interacted as the Arabidopsis NSHs. In contrast to Arabidopsis NSHs, PpNSH1 could not form a homodimer, whereas PpNSH2 dimerized (Figure 33). In Arabidopsis NSH1 forms dimers and NSH2 does not. The dimerization of PpNSH2 has been shown before in the crystal structure and in size exclusion chromatography experiments (Kopečná et al., 2013). Considering that PpNSH1 is insoluble when it is expressed in *E. coli* (Kopečná et al., 2013), it might be that there is a causal linkage between the capacity to form homodimers and the solubility in *E. coli*. The interaction patterns of coffee nucleosidases resembled those from Arabidopsis: NSH2 did not form homodimers, whereas NSH1 did (data not shown), and the two nucleosidases interacted (Figure 33).

The interaction between NSH1 and NSH2 in three different and evolutionary distant plant species suggests that it is probably conserved in all plants.

## 4. Discussion

### 4.1 Arabidopsis *in vivo* purine nucleotide catabolism

#### 4.1.1 Functionality of *XDH*, *HGPRT*, *NSH1*, *NSH2* and *GSDA* upstream of *UOX* in purine nucleotide catabolism

The potential suppression of the *uox* mutant phenotype obtained by crossing a mutant allele of the gene of interest into the *uox* background was employed to assess the functionality of that gene in purine nucleotide catabolism (Figure 6, Figure 7, and Figure 8). A suppression of the mutant phenotype at least to some degree was expected for *uox xdh*, *uox nsh1* and *uox gsd-1* and *uox gsd-2*, since *XDH*, *NSH1*, and *GSDA* were known to operate upstream of *UOX* (Jung et al., 2009; Dahncke and Witte, 2013; Hauck et al., 2014). Figure 6 and Figure 7 of this work show that the wild type phenotype is restored in *uox xdh*. This finding is in accordance with Hauck et al., 2014, who already reported the suppression of the *UOX* mutant phenotype and the absence of uric acid in *uox xdh*, concluding that uric acid is deleterious for the plant and not the absence of the *UOX* gene in itself or the defective purine catabolism.

The uric acid content of *uox nsh1* and *uox gsd-1* as well as *uox gsd-2* (Figure 8) provides quantitative information about the suppression by *NSH1* and *GSDA*. *NSH1*, like *XDH*, is a strong suppressor: *uox nsh1* and *uox xdh* did not significantly differ as far as the phenotype and the uric acid concentrations are concerned (Figure 6, Figure 7, and Figure 8). This confirms that the abrogation of both gene functions completely block the flux of metabolites directed to *UOX*. The strong, but incomplete suppression of the *uox* phenotype in *uox gsd-1* and *uox gsd-2*, indicates that purine nucleotide catabolism is mostly dependent on *GSDA*, but some purine nucleotide degradation is managed by other enzymes.

The potential function in purine nucleotide catabolism of two more genes, *NSH2* and *HGPRT*, was studied by assessing the suppression of the *uox* mutant phenotype in the *UOX NSH2* and *UOX HGPRT* double mutants. Introducing an *NSH2* mutant allele into the *uox* background had a weak, but statistically significant effect on uric acid accumulation (Figure 8), suggesting the involvement of *NSH2* in the pathway. The mutation of *HGPRT* did not influence the uric acid content in the *uox* background, indicating a decoupling between *HGPRT* and purine nucleotide degradation and suggesting that guanine and hypoxanthine are not intermediates of this pathway in Arabidopsis. This has been reported for guanine (Dahncke and Witte, 2013), but not yet for hypoxanthine.

The decoupling between HGPRT and purine nucleotide degradation is a substantial difference between plants and humans. Humans with an *HGPRT* defect have a partially compromised purine salvage metabolism. The substrate of HGPRT, PRPP (Figure 2), accumulates, inducing *de novo* purine biosynthesis and causing a significant increase in the purine nucleotide pool and ultimately in more uric acid. Uric acid has a low solubility in the serum, and precipitates forming monosodium urate crystals in kidney and joints causing gout, arthritis, and renal diseases. The complete absence or the severe deficiency of HGPRT causes the Lesch-Nyhan syndrome, for which gout in young age, mental disorder, and self-mutilating behavior are main characteristics. The syndrome shows that a correct brain function is highly dependent on guanine and hypoxanthine salvage. By contrast, compromising hypoxanthine and guanine salvage does not affect plants in standard growth conditions. Accordingly, *hgprt* has no abnormal phenotype (Schroeder et al., 2017).

It is worth to note that the germination phenotype of *gsda-1* and *gsda-2* observed here (Figure 6) confirms results from Schroeder et al., 2017. These two mutant lines accumulate high amounts of guanosine that becomes toxic for the plants. As a consequence, the *GSDA* mutants show a dark stress phenotype and impaired seed germination (Schroeder et al., 2017). The cause for the toxicity of increased guanosine pool is still not known. It might interfere with GMP dephosphorylation by product inhibition. GMP dephosphorylation is important for GMP homeostasis because it is the only way to degrade this metabolite since no GMP reductase (catalyzing the conversion of GMP to IMP) has been found in plants (Ashihara et al., 2018; Stasolla et al., 2003). The germination delay was stronger in the double mutants *UOX GSDA-1* and *UOX GSDA-2* (Figure 6), probably because of the added effect of guanosine toxicity together with uric acid toxicity. The uric acid accumulation was in fact strongly, but not completely prevented in these two lines (Figure 8). The two double mutants *UOX NSH1* and *UOX XDH* showed also a slight germination delay at day 3 (Figure 6), probably due to traces of uric acid that were still present.

#### **4.1.2 Purine nucleotide catabolism proceeds mainly via guanosine deamination to xanthosine**

The *XDH* mutant was employed in analogy to *uox* as a tool to study the possible function of genes upstream of *XDH* in purine nucleotide catabolism. The suppression of xanthine content in *xdh hgprt*, *xdh gsda-2*, *xdh nsh2*, *xdh nsh1*, and *xdh nsh1 nsh2* (Section 3.1.2, Figure 9) confirms that (i) *HGPRT* is disconnected from purine nucleotide catabolism, (ii) *NSH2* is

functional and (iii) purine nucleotide catabolism proceeds mainly, but not completely, via guanosine deamination.

The purine nucleotide degradation route independent from the GSDA reaction might run via the inosine-hypoxanthine branch, as postulated in the current model of purine nucleotide catabolism. The comprehensive analysis of the nucleobase and nucleoside content of the set of mutants in Figure 9, Figure 10, and Figure 12 demonstrates that this is not the case because neither inosine nor hypoxanthine considerably accumulated in mutants that block this branch. Inosine is a substrate of NSH1 (Jung et al., 2011), but it could be detected in *nsh1* only by sensitive mass spectrometry analysis and its concentration was far below the one of xanthosine (Figure 13). Previously, HPLC analysis with UV detection never showed inosine accumulation in any genotype under standard conditions (Jung et al., 2011; Riegler et al., 2011). Hypoxanthine was not detected in the *XDH* mutant, although it is a substrate of XDH. A similar result was obtained by HPLC analysis of the same mutant (Brychkova et al., 2008b). Hypoxanthine only accumulated in the double mutant *XDH HGPRT* (Figure 10), where its salvage and degradation systems are blocked, and to a far lower extent in comparison to xanthine (Figure 9). This is a strong evidence that hypoxanthine oxidation is only a minor source of xanthine in comparison to xanthosine hydrolysis. One more evidence supports the hypothesis that purine nucleotide catabolism, precisely AMP and IMP catabolism, does not proceed via inosine-hypoxanthine: the concentration of inosine in *nsh1* was approximately 10 times lower than the concentration of hypoxanthine in *xdh hgprt* (Figure 10 and Figure 12). This suggests that hypoxanthine originates only partially from inosine hydrolysis. The main source of hypoxanthine might be base excision repair of the DNA. Hypoxanthine occurs in DNA because dITP is erroneously incorporated by DNA polymerases and because adenine spontaneously deaminates to hypoxanthine at a low rate (Alseth et al., 2014).

The current model of purine nucleotide catabolism includes the branch from IMP to xanthine via IMP dephosphorylation, inosine hydrolysis and hypoxanthine oxidation (Ashihara et al., 2018). This model is mainly derived from *in vitro* experiments in which labelled nucleosides and nucleobases were supplied to cell cultures, plant tissue preparations or tissues extracts and the metabolic fate of the label was investigated (Katahira and Ashihara 2006, Deng and Ashihara, 2010, Yin et al., 2014). The data presented in this work are derived from a genetic approach in which several mutants of genes involved in purine nucleotide catabolism and salvage have been analyzed. This approach allows determining the *in vivo* contribution of the enzymatic activities encoded by these genes to purine nucleotide catabolism. The results



(Section 3.1) clearly demonstrate that purine nucleotides are degraded *in vivo* via xanthosine hydrolysis and not via the inosine-hypoxanthine route.

#### **4.1.3 XMP dephosphorylation bypassed guanosine deamination in purine nucleotide catabolism**

AMP and GMP catabolism depends to a great extent, yet not completely, on GSDA (Figure 8 and Figure 9). The exclusion of the inosine branch as an *in vivo* route of AMP and IMP degradation (Figure 9, Figure 10, and Figure 12) and the absence of inosine dehydrogenase (Dahncke and Witte, 2013), highlights the dephosphorylation of XMP as the reaction by which purine nucleotide catabolism bypassed GSDA.

In *Vigna unguiculata*, the addition of XMP was shown to increase ureide production in cell-free extracts of nodules (Atkins, 1981). However, in *Arabidopsis* this step was excluded as source of xanthosine because HPLC analysis of *nsh1 gsd-2* showed that the mutation of *GSDA* was preventing xanthosine accumulation in the *nsh1* background (Dahncke and Witte, 2013). However, mass spectrometry analyses performed in this work suggest that this reaction is indeed a source of xanthosine (Figure 13 and Figure 14); though minor in comparison to the deamination of guanosine. Similar to xanthosine in *nsh2*, or inosine in *nsh1*, the amount of xanthosine in *nsh1 gsd-2* was below the detection limit of the HPLC-UV technique and was revealed only by the usage of a more sensitive method.

A xanthosine monophosphate phosphatase (XMPP) has not yet been identified, but a promising candidate enzyme is being characterized currently in our laboratory. The relevance of XMP dephosphorylation as a xanthosine source seems to be minor in comparison to guanosine deamination accounting for approximately 20% of xanthosine in seeds and seedlings (Figure 13) and making hardly any contribution in adult rosettes (Figure 14). It might be that this contribution is underestimated, because it is derived from studies in which mutants that accumulated high amounts of nucleobases and nucleosides were used. It is known that up to a certain extent the accumulation of nucleobases, for example xanthine, is inhibiting enzymes that are acting upstream of XDH in the pathway. Guanosine might have a similar effect and potentially inhibits XMPP leading to a wrong estimation of XMPP contribution to purine nucleotide catabolism. This hypothesis could be tested by checking whether guanosine is an inhibitor of XMPP *in vitro*.

#### 4.1.4 Inosine, hypoxanthine and guanine are not generated by cytosolic purine nucleotide catabolism

A link between purine catabolism and dark stress was reported in the literature (Jung et al., 2011; Brychkova et al., 2008a; Schroeder et al., 2017). It is thought that purine nucleotide catabolism is induced under dark stress to enhance the production of allantoin and allantoate which might help in withstanding the effects of prolonged periods of darkness due to their ability to function as scavengers of reactive oxygen species known to play a role in stress responses. Some mutants of the genes involved in purine catabolism are reported to undergo senescence earlier than wild type under dark stress conditions, such as *xdh* (Brychkova et al., 2008b), *nsh1* (Jung et al., 2011) and *gsda* (Schroeder et al., 2017). However the dark stress phenotype of *xdh* and *nsh1* could not be reproduced by Schröder et al., 2017 in an experiment where all mutants were grown side by side under standard growing conditions. These authors also found that the premature senescence of *gsda* in darkness was due to toxicity of guanosine and not due to the impairment of purine nucleotide catabolism. Only the molecular phenotype, meaning an increased accumulation of purine nucleotide catabolism intermediates, could be reproduced (Schroeder et al., 2017).

In this work, dark stress treatment was employed as a tool to induce purine nucleotide catabolism and to evaluate the relevance of hypoxanthine as xanthine source in a condition demanding higher levels of purine catabolites. Xanthine concentrations in *xdh* increased after two and three days of darkness, whereas the hypoxanthine content in *xdh hgp1* remained constant, suggesting that hypoxanthine and xanthine are disconnected (Figure 15). Guanine did not significantly increase in *hgp1* during dark stress and the accumulation of this metabolite at day three of darkness in *xdh hgp1* could not be reproduced. Considering that in *Arabidopsis* there is no guanine deaminase, and there is no evidence for an enzymatic degradation of guanosine to guanine (Dahncke and Witte, 2013; Schroeder et al., 2017), it can be concluded that guanine is not derived from purine nucleotide degradation and it is not a xanthine source. However, guanine occurs in plants and it is actively recycled (Yin et al., 2014; Ashihara et al., 2018). As hypoxanthine is not derived from AMP catabolism, guanine probably originates from other sources than GMP catabolism as well, such as spontaneous depurination of nucleic acids, which occurs at a constant rate in every cell (An et al., 2014). The decoupling of hypoxanthine and guanine from major xanthine generation and from purine nucleotide catabolism is also supported by the absence of an effect of *HGPRT* abrogation on purine nucleotide degradation (Figure 6, Figure 7, Figure 8, and Figure 9). Using this

metabolic hard-wiring, a futile cycle of constant purine nucleotide degradation and salvage is avoided. The enzymes for purine nucleotide catabolism (GSDA, NSH, and XDH) and salvage (HGPRT) are located in the cytosol (Figure 2), and are not spatially separated. If the major catabolic routes would flow from IMP via hypoxanthine and GMP via guanine, HGPRT could directly interfere by catalyzing the salvage back to the nucleotides. With a catabolic route via guanosine/XMP and xanthosine to xanthine, this is avoided. The physiological role of HGPRT is probably to salvage guanine and hypoxanthine deriving from DNA repair and not from nucleotide catabolism. In contrast to hypoxanthine and guanine, xanthosine and xanthine cannot be recycled (Ashihara et al., 2018) which further indicates their prominent role in catabolism. In human, the situation is reversed because xanthine is derived from hypoxanthine oxidation and guanine deamination and the recycling of guanine and hypoxanthine by HGPRT is fundamental to prevent toxic accumulation of uric acid (Harrison, 2002; Maiuolo et al., 2016).

One additional dark stress experiment was performed with the mutants of the nucleoside hydrolases and the changes in the nucleoside concentrations were monitored (Figure 32). This experiment further corroborated the hypothesis that inosine is not a central metabolite of purine nucleotide catabolism. Inosine accumulated in *nsh1* during dark stress, but its absolute concentration was by far lower than the one of xanthosine. A similar result was previously obtained also by Jung et al., 2011. Additionally, inosine accumulated not before day 3 of darkness, whereas xanthosine started to accumulate already at day 2, suggesting that the sources of xanthosine and inosine are different. As hypoxanthine, inosine is probably also not derived from AMP degradation, but its source might be autophagy-mediated tRNA turn over since inosine occurs in tRNA species as wobble base (Alseth et al., 2014). Vacuolar autophagy mediated RNA degradation (Frankel et al., 2016) releases nucleosides probably via the nucleoside transporter ENT1 (Girke et al., 2014) into the cytosol. Whereas tRNA degradation releases inosine, ribosomal RNA degradation releases adenosine and guanosine. It is possible that vacuolar tRNA degradation is not triggered before day 3 of darkness, whereas ribosomal RNA degradation is triggered earlier. The alternative origin of inosine suggests that cytosolic IMP derived from AMP deamination is oxidized to XMP rather than being dephosphorylated to inosine. This is supported by the results of labelled IMP feeding experiments from Shelp and Atkins, 1983 which showed that IMP dephosphorylation is not a source of ureides in extracts of cow pea nodules (Shelp and Atkins, 1983).

#### 4.1.5 Updated model of purine nucleotide catabolism

The allopurinol treatment enabled the blockage of purine catabolism by short-term inhibition of XDH. This was used as an alternative to the genetic approach of employing an *XDH* mutant, and avoids the high concentration of xanthine in *xdh* background, which arguably might create some artefacts. The low level of hypoxanthine in comparison to xanthine in allopurinol and dark treated *hgpri* samples further confirmed that hypoxanthine is not a relevant source of xanthine (Figure 16). The accumulation of hypoxanthine in Col-0 samples treated with allopurinol and adenosine showed that this branch might be used when the plants take up inosine and hypoxanthine from external sources, such as uptake from the soil. It was shown that inosine feeding promoted root growth in rice, tomato, onion and sunflower (Tokuhisa et al., 2010). Inosine and other nucleosides can be taken up from the rhizosphere in substantial amounts, but whether this significantly supports the growth of plants in natural ecosystems is not yet known.

In conclusion, inosine and hypoxanthine are not generated by IMP dephosphorylation (Figure 34). They are likely derived from other sources, such as uptake from the rhizosphere, vacuolar tRNA turn over and DNA repair mechanisms. Therefore, an updated model of purine nucleotide catabolism can be drawn where AMP is deaminated to IMP, which is then oxidized to XMP. This metabolite is either dephosphorylated to xanthosine by a specific XMP phosphatase, or it is deaminated to GMP. The latter reaction rather belongs to GMP biosynthesis and not purine nucleotide catabolism. Nonetheless, GMP can enter catabolism by dephosphorylation mediated by a so far unknown phosphatase. GMP catabolism then proceeds via guanosine and xanthosine, whereas guanine is not an intermediate. Guanine is likely derived mainly from depurination of nucleic acids and can only re-enter metabolism by salvage to GMP. Between the two routes, (i) GMP via guanosine to xanthosine and (ii) XMP to xanthosine, the first one is preferentially used to degrade purine nucleotides, according to the higher impact of *GSDA* mutation on purine nucleotide catabolism. Especially in rosette tissues, purine nucleotide degradation seems to proceed exclusively via guanosine. Maybe GMP synthetase and XMP phosphatase are regulated in a coordinated way to channel XMP towards xanthosine or GMP depending on the cells metabolic requirements.

## SAM metabolism

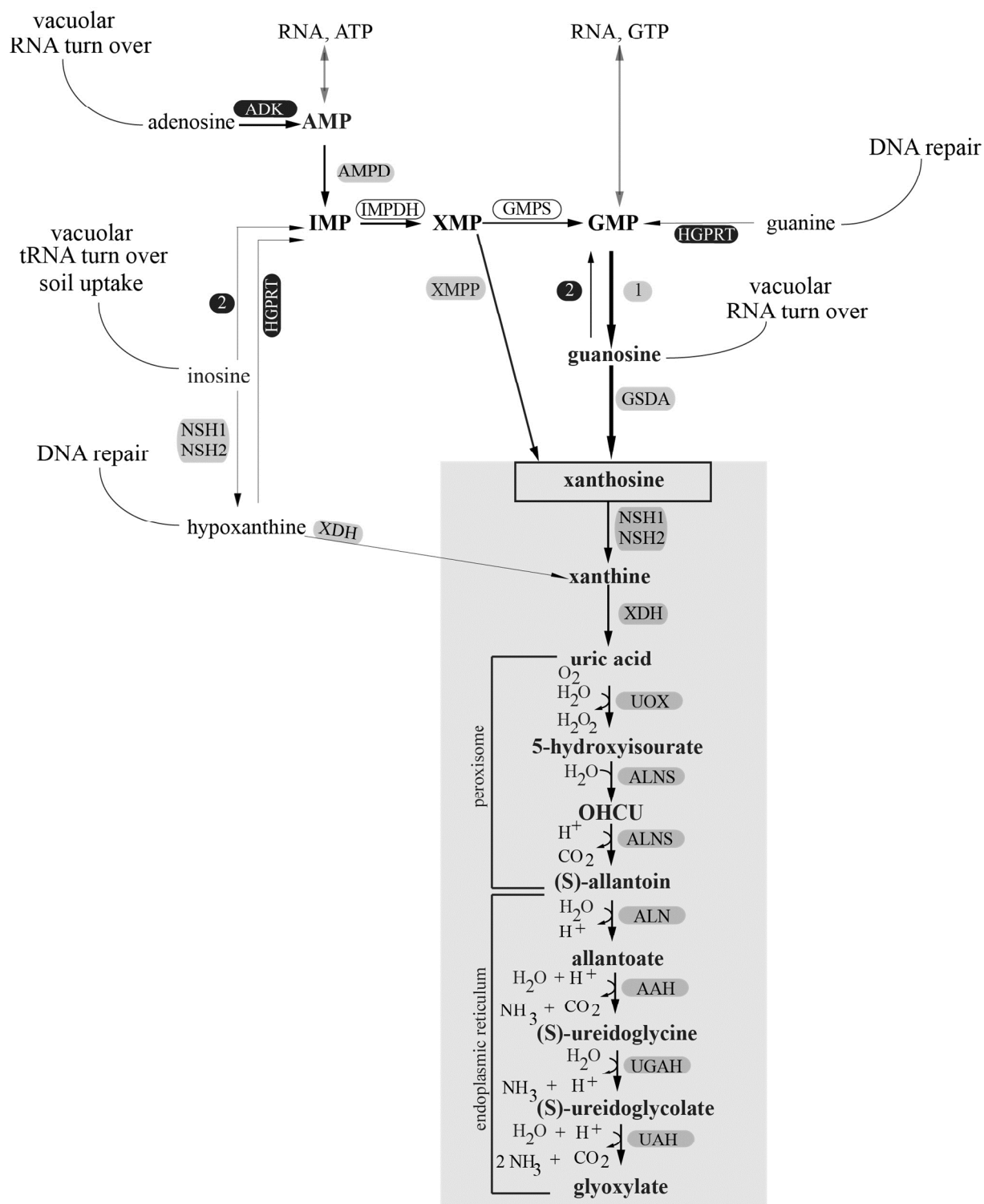


**Figure 34. Updated model of purine nucleotide catabolism.**

AMP and GMP derived from the cytosolic RNA decay pathway are degraded in Arabidopsis by two routes, one proceeding via a XMP specific phosphatase (XMPP) and one via a GMP phosphatase (1) and GSDA. The route via GSDA is predominant (thick black arrows). Both routes converge on xanthosine. Xanthosine is hydrolyzed to xanthine via the complex NSH1-NSH2. Starting from xanthosine, purine nucleotide catabolism intermediates are degraded and cannot be recycled (gray rectangle). The

subcellular localization of the reactions for purine ring catabolism is indicated. IMP is derived from AMP oxidation via AMPD, inosine salvage is mediated by an inosine guanosine kinase (2), and hypoxanthine salvage by HGPRT. GMP can also be derived from guanine salvage via HGPRT. The sources of inosine, hypoxanthine and guanine are indicated. Adenosine and guanosine are derived also from autophagy-mediated vacuolar RNA degradation and from the SAM (S-adenosyl methionine) metabolism (adenosine). Enzymes involved in salvage are indicated with black shading and the ones involved in catabolism with grey shading. The enzymes IMPDH and GMPS are shared between catabolism (AMP catabolism) and biosynthesis (GMP biosynthesis). Enzymes whose genetic identity is not clear are indicated with a number. Enzymes: AMP deaminase (AMPD), IMP dehydrogenase (IMPDH), GMP synthetase (GMPS), xanthosine monophosphate phosphatase (XMPP), putative GMP phosphatase (1), guanosine deaminase (GSDA), nucleoside hydrolase 1 (NSH1), nucleoside hydrolase 2 (NSH2), xanthine dehydrogenase (XDH), urate oxidase (UOX), allantoin synthase (ALNS) allantoin amidohydrolase or allantoinase (ALN), allantoate amidohydrolase (AAH), ureidoglycine aminohydrolase (UGAH), ureidoglycolate amidohydrolase (UAH), hypoxanthine guanine phosphoribosyltransferase (HGPRT), adenosine kinase (ADK), putative inosine guanosine kinase (2). OHCU, 2-oxo-4-hydroxy-4-carboxy-5-ureido-imidazoline.

## 4.2 Functional analysis of *NSH2*

### 4.2.1 NSH1 and NSH2 from plants cluster into two clades reflecting a difference in the substrate spectrum

The Arabidopsis genome encodes two annotated IU-NSH, NSH1 and NSH2. The function of NSH1 as a xanthosine, inosine and uridine hydrolase was shown *in vivo* and *in vitro* (Jung et al., 2009; Jung et al., 2011; Riegler et al., 2011), whereas the contribution of NSH2 to nucleotide catabolism was unclear. The molecular phylogenetic analysis (Figure 17, Figure A2 Appendix) included a wide number of species, from green algae to vascular plants. Algae only have one nucleoside hydrolase, whereas early divergent land plants (*Physcomitrella patens* and *Selaginella moellendorffii*) have two isoforms of NSHs, probably due to whole genome duplication (Kopečná et al., 2013; Rensing et al., 2007). These two isoforms were conserved during plant evolution leading to two phylogenetically distinct clades of NSHs in modern plants. The hypothesis of a possible correlation between the clustering of the NSH genes in different clades and distinct enzymatic properties (Kopečná et al., 2013) could be clearly confirmed in this work the first time for a vascular plant. NSH2 of Arabidopsis was shown to be a xanthosine, but not uridine hydrolase upon activation by NSH1 (Table 3-1), while the previously reported uridine hydrolase activity of NSH1 (Jung et al., 2009), which also has some xanthosine activity (Jung et al., 2011; Riegler et al., 2011), was confirmed

(Table 3-1). For *Physcomitrella patens*, Kopecná et al., 2013, had already shown that NSHs from these two clades have a different substrate spectrum. Furthermore, a link between NSH activity for xanthosine and the presence of Tyr-244 and Tyr-249 (PpNSH1 numbering) was postulated by Kopecná and colleges and could be confirmed here for *Arabidopsis* as the prime model species for vascular plants. This general concept regarding the substrate specificity of NSHs it is probably valid throughout the plant kingdom.

#### **4.2.2 Arabidopsis NSH1 and NSH2 interact forming a heterocomplex highly efficient for purine nucleosides hydrolysis**

The biochemical assessment of NSH2 function in vascular plants was impaired by the insolubility of the protein when expressed in *E. coli* (Jung et al., 2011; Riegler et al., 2011; Kopecná et al., 2013). The change in the expression system from *E. coli* to *N. benthamiana* enabled the successful purification of soluble NSH2 (Figure 19). However, the protein resulted to be inactive for the candidate substrates xanthosine, uridine and inosine (Figure 20 and Table 3-1). Interaction studies showed that the two proteins interact (Figure 21). Several nucleoside hydrolases from protists and plants have multimeric structures (Parkin, 1996a; Kopecná et al., 2013), but the existence of a heteromeric complex for nucleosidases has never been shown. An interaction between NSH1 and NSH2 was hypothesized by Riegler et al., 2011. In this study, the remaining xanthosine and inosine hydrolase activity in *nsh1* and *nsh2* root lysates did not sum up to the one of the wild type root lysate, suggesting that both proteins were somehow necessary for these activities. However, the absence of an efficient purification strategy for NSH2 limited further investigations of this matter. Riegler and colleges attempted an *in vitro* activity reconstruction with the two recombinant proteins, which was of limited success, in part due to the marked insolubility of NSH2 obtained from *E. coli*. The data presented here clearly demonstrate the existence of two nucleoside hydrolase complexes: a NSH1 homomer that has a higher catalytic efficiency for uridine hydrolysis and a NSH1-NSH2 heteromer that is a more efficient xanthosine and inosine hydrolase. It is interesting to note that the  $K_M$  of the NSH1-NSH2 complex for xanthosine (Table 3-2) is comparable to the *in vivo*  $K_M$  for the total xanthosine hydrolase activity in an *A. thaliana* leaf cell lysate determined by Riegler et al., 2011. This indicates that Riegler and colleges probably measured the activity of the native NSH1-NSH2 complex in their preparation. The higher xanthosine-inosine hydrolase activity of the NSH1-NSH2 complex is due to the activation of NSH2 by NSH1 and not due to NSH2 being a positive regulator of NSH1. This

was shown by biochemical and metabolic analyses employing a point mutant of NSH1 (Figure 18) that could still activate NSH2 *in vitro* (Table 3-1) and *in vivo* (Figure 31 and Figure 32). Therefore, NSH2 is primarily a xanthosine hydrolase, like its homologue in *Physcomitrella* (Kopečná et al., 2013), but the Arabidopsis enzyme is active only in the presence of NSH1. The inactivity of NSH2 might result from the inability to form homodimers (Figure 21), which distinguishes Arabidopsis NSH2 from its homologue in *Physcomitrella* whose active form in solution is dimeric, as shown by structural and gel filtration chromatography data (Kopečná et al., 2013).

The occurrence of homomeric and heteromeric complexes of different isoforms with different functions was shown in Arabidopsis also for aldehyde oxidases (Akaba et al., 1999). Two genes, AO-1 and AO-2, encode aldehyde oxidases that form homodimers with distinct substrate specificities and also a heterodimer with intermediate properties between the two homodimers. Not only the Arabidopsis NSH1-NSH2 complex is the first nucleoside hydrolase heteromeric complex described, but it also has the peculiarity that one of the partners can form homomers with different enzymatic characteristics whereas the other cannot.

#### 4.2.3 NSH2 exists *in vivo* in complex with NSH1

NSH1 and NSH2 interact *in vivo*, at native level, as determined by immunoprecipitation experiments using Arabidopsis root cell lysates (Figure 26). Protein quantification showed that NSH2 was generally less abundant than NSH1 (Figure 25 and Figure 26). Since NSH2 is not capable of forming homodimers, and is less abundant than NSH1, it can be concluded that it does not exist *in vivo* as a monomer, but is always associated with NSH1 in a complex. The reason for the NSH1-NSH2 association might be that the active sites contain residues donated from the adjacent subunit, as is the case of e.g. aspartate transcarbamoylase and chorismate mutase (Boulanger and Kantrowitz, 2003). According to Kopečná et al., 2013 there is only one residue in the active site of PpNSH2, Lys297, that protrudes from one subunit of the homodimer and completes the active site of the respective other subunit of the homodimer. However, the mutation of this residue in NSH1 of Arabidopsis did not impair NSH2 activation (Figure 25) showing that this lysine residue is not required to induce the activity of NSH2 in the NSH1-NSH2 complex. Either other residues are involved in completing the active site or the obliged interaction NSH1-NSH2 is due to other reasons. Maybe the monomer NSH2 cannot fold properly without contributions from the interaction with NSH1 or maybe, as in case of *E. coli* alkaline phosphatase, the dimeric structure allows cooperative



subunit interactions necessary for the activation of the enzyme (Hehir et al., 2000). Investigation of the models of the two proteins and the obtained biochemical data did not provide further hints to better understand the molecular mechanism underlying this activating interaction. A co-crystallization study might be required.

#### 4.2.4 *In vivo* function of *NSH2*

NSH2 function has remained obscure up to now also because none of the predicted candidate nucleosides accumulated in any tissue of the *NSH2* mutant (Jung et al., 2011; Riegler et al., 2011). The usage of a high sensitive LC-MS method enabled, for the first time, the detection of xanthosine accumulation in *nsh2* seeds, root, seedlings and rosette (Figure 12, 29, 31 and 32). Inosine and uridine did not accumulate. Therefore the *in vitro* function of NSH2 as a xanthosine hydrolase is confirmed *in vivo*.

NSH2 requires NSH1 to be active, thus the single mutant for *NSH1* is a functional mutant for both *NSH1* and *NSH2* because *NSH2* cannot be activated. This explains why *nsh1 nsh2* and *nsh1* accumulated metabolites, in particular xanthosine, to the same level (Figure 31). Also *uox nsh1 nsh2* and *xdh nsh1 nsh2* did not differ from *uox nsh1* and *xdh nsh1* in uric acid and xanthosine accumulation, respectively (Figure 8 and Figure 9).

The efficiency of NSH2 could be evaluated *in vivo* by the analysis of the transgenic line that expresses the NSH1 point mutant in the *nsh1* background (*nsh1::ΔNSH1*). In this line NSH2, activated by ΔNSH1, could suppress the accumulation of xanthosine and inosine normally seen in the *nsh1* background to the wild type level in standard condition (Figure 31) and after dark stress, when purine nucleotide catabolism is enhanced (Figure 32). Thus NSH2 is as efficient as NSH1 in hydrolyzing xanthosine and inosine, *in vivo*, especially considering that in this line NSH2 is not overexpressed, but it is at a native level. The unchanged content of uridine in *nsh1::ΔNSH1* confirmed that ΔNSH1, which was shown to be inactive *in vitro*, is also inactive *in vivo*.

In the *NSH2* mutant only a limited amount of xanthosine accumulated, indicating that the activity of NSH2 can be easily performed by NSH1 alone. It seems that NSH2, although it is as efficient as NSH1, does not have a prominent role in Arabidopsis. Dark stress was employed to enhance purine nucleotide catabolism and to test whether NSH2 was less dispensable in such a condition, but no further accumulation of xanthosine was observed in *nsh2* after three days of dark stress. It appears unclear why NSH2 is conserved and why the complex NSH1-NSH2 is useful for the plant taking into account that NSH1 is such an

efficient broad nucleoside hydrolase. The presence of NSH2 in all tissues (Figure A3 Appendix), the proof of the existence of the native complex in root (Figure 28), the slight accumulation of xanthosine *in vivo* when NSH2 is absent, and the considerably higher activity for xanthosine and inosine of the heterocomplex in comparison to the NSH1 homomer (Table 3-1), together suggest that NSH2 has a constitutive role in purine nucleotide catabolism, and that both, NSH1 and NSH2, are necessary at least for xanthosine and maybe also inosine homeostasis. This does not exclude the possibility that the homomeric and heteromeric complexes might be subject to dynamic regulation depending on certain stimuli. The NSH2 amount might be up-regulated to increase the catalytic capacity for purine nucleosides (more NSH1-NSH2 complex), probably leading to a concomitant decrease for pyrimidine nucleotides (less NSH1 homodimer). On one side, such a regulation mechanism could potentially maintain a balance between the pyrimidine and purine nucleoside pools; on the other side it could allow the plant to adjust the metabolic fluxes through purine versus pyrimidine nucleosides under certain stress conditions. Transcriptomic data shows that NSH1 and NSH2 are differentially regulated by the hormone jasmonate (JA), and by *Pseudomonas syringae* and *Botrytis cinerea* infection (Figure A4 Appendix). These conditions are related to each other. JA is involved in several processes such as flower development, leaf abscission, and responses against wounding and pathogen attack. Upon perception of pathogens, JA mediates a signaling cascade initiating various defense responses. *Pseudomonas syringae* produces coronatine, a toxin that mimics JA and manipulates plant hormone signaling, promoting the opening of stomata for bacterial entry and growth (Zheng et al., 2012). *Botrytis cinerea* belongs to the group of necrotrophic fungi, which are known to be the primary activators of JA-dependent defenses (Antico et al., 2012). Whereas NSH2 is upregulated upon these stimuli, NSH1 is not. Therefore, under environmental conditions invoking a JA response, NSH1 might be sequestered by increasing amounts of NSH2 favoring xanthosine over uridine hydrolysis. Ma et al., 2016 postulated that purine catabolism is upregulated as a differential part of the defense response. These authors propose that XDH has a dual role: production of ROS in the epidermal cells to prevent the spread of the pathogen infection and production of uric acid as a ROS scavenger in the mesophyll cells to constrain the hypersensitive response. Therefore, a higher xanthosine hydrolysis rate might be needed to increase the production of uric acid and ureides to counter balance the production of ROS during the local pathogen response. Interestingly, XMPP is also upregulated by JA and *P. syringae* infection (unpublished in house data). Maybe in unstressed conditions, the purine nucleotide catabolism operates in a mainly linear fashion via GSDA, but upon certain stress

stimuli, the flux of metabolites is directed through the route from XMP over xanthosine to xanthine with the combined contribution of XMPP and NSH2. The assessment of potential changes in the quantity of the NSH1 and NSH2 proteins upon JA treatment or pathogen infection would provide indication of an enhanced flux through the XMP-xanthosine-xanthine route in these conditions. Experiments with the *NSH2* mutant might also be performed to investigate if there is increased damage or inadequate ROS quenching in leaf tissues in the vicinity of a pathogen infection site.

It is interesting to note that one of the effector proteins of *Pseudomonas syringae* is a NSH type protein named HopQ1. HopQ1 has a nucleoside hydrolase structure, although it has a modified aspartate motif (Li et al., 2013). Upon pathogen infection purine metabolism is altered (Li et al., 2013); it would be interesting to know if HopQ1 interferes with the NSH1-NSH2 complex formation.

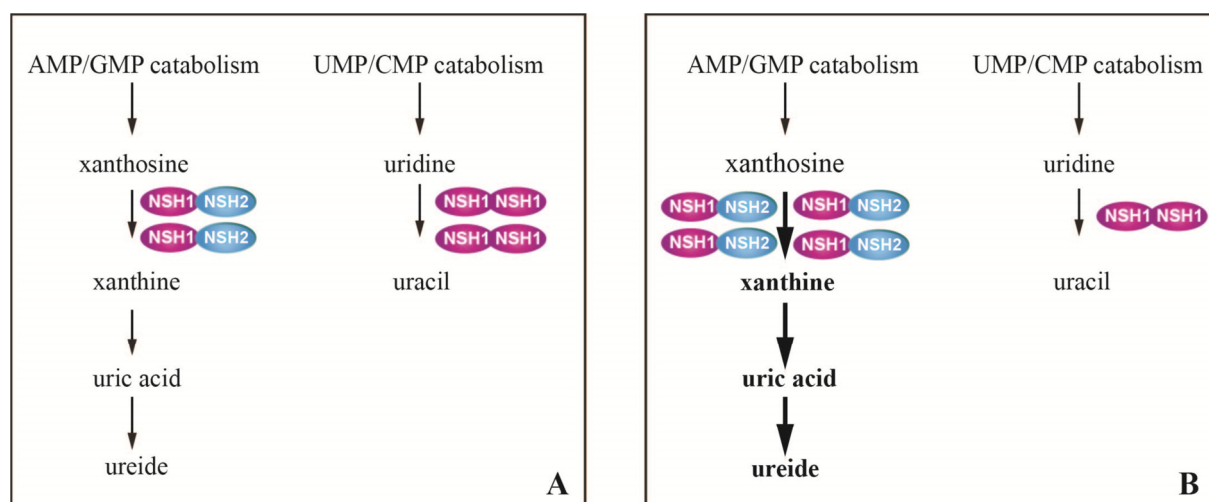


**Figure 35. Dynamic regulation of the NSH1 homomer and NSH-NSH2 heterocomplex.**

(A) NSH1 and NSH2 are required for a correct balance of purine and pyrimidine nucleosides in unstressed growth condition. By increasing NSH2 concentration (B) cell metabolism switches to a condition of higher xanthosine hydrolysis, increasing uric acid and ureide production. This dynamic regulation might be useful to face certain stress conditions, such as pathogen attack.

#### 4.2.5 Evolutionary considerations on NSHs activities and interactions in different plant species

In this work, the interaction between NSH1 and NSH2 was demonstrated for the enzymes of two other two species, *Coffea arabica* and *Physcomitrella patens* (Figure 33), which suggests that it is widely conserved in plants.

*Physcomitrella* and *Arabidopsis* nucleosidases have different biochemical characteristics. The insolubility in *E. coli*, the lack of activity, and the inability to form homodimers are three features that distinguish NSH2 of *Arabidopsis* from its homologue in *Physcomitrella*. PpNSH1 is also different from *Arabidopsis* NSH1: it is insoluble when expressed in *E. coli*, it cannot form a homodimer, and it is rather inactive, only weak activity for uridine could be detected (Doering, 2018, MSc thesis). The insolubility in *E. coli*, the inability to form homodimers, and the lack of activity seem to be three characteristics shared by PpNSH1 and *Arabidopsis* NSH2. It is not clear whether these aspects are based on common biochemical features as for example surface determinants which reduce the solubility (Figure 18) or suppress homomer formation. Finding such (common) determinants would increase the understanding of these enzymes.

The functional importance of the respective NSHs changed during evolution. In *Physcomitrella* it is the mutant of *NSH2*, and not of *NSH1*, that shows the greatest perturbation of nucleoside concentrations *in vivo* (Kopečná et al., 2013). It is possible that the *PpNSH2* mutant is actually a functional mutant of the *Physcomitrella* NSH1-NSH2 complex as is the *NSH1* mutant in *Arabidopsis*. It would be interesting to investigate the catalytic efficiency of the *Physcomitrella* NSH1-NSH2 complex and compare it with PpNSH2. In *Physcomitrella*, mutants of NSHs showed a far less pronounced accumulation of xanthosine, in comparison to *Arabidopsis nsh1* (Kopečná et al., 2013). On the other hand, there was a prominent accumulation of inosine. This indicates that inosine and not xanthosine is the major intermediate of purine nucleotide catabolism in this moss and maybe in bryophytes in general. It seems that bryophytes and seed plants differ as far as xanthosine and inosine homeostasis is concerned (Kopečná et al., 2013). This is reflected by the enzymes' activities, which are more active for inosine hydrolysis in *Physcomitrella* (Kopečná et al., 2013). The Gramineae have generally three isoforms of IU-NSHs: one NSH2 isoform, one canonical NSH1 isoform, and an additional non-canonical NSH1 isoform with higher specificity for xanthosine, like NSH2 (Figure 17 and Kopečná et al., 2013). It would be interesting to investigate whether the NSH2 isoform and the canonical NSH1 isoform interact and whether this complex is a more efficient

xanthosine hydrolase than the non-canonical NSH1. This would further indicate that both NSH1 and NSH2 are required for correct xanthosine homeostasis that is maybe more critical in the Gramineae. Preliminary data of the Coffee NSHs showed that their hydrolytic efficiency was lower compared to the Arabidopsis enzymes (data not shown), which is maybe required to make xanthosine available for caffeine production.

Based on these considerations and on these limited and in part preliminary data, it appears possible that the activities of the nucleosidases might be adjusted to the different variants of purine nucleotide catabolism found in plants.

### 4.3 Conclusions

The model of Arabidopsis purine nucleotide catabolism is derived mainly from experiments with labelled nucleosides and nucleobases applied to cell cultures or plant tissues and subsequent tracing of the metabolic distribution of the label. The availability of several mutants of the genes involved in purine nucleotide catabolism and salvage and of double order and triple order mutant of these genes enabled the investigation of purine nucleotide catabolism *in vivo* without external disturbances, by recording the changes of the purine nucleotide catabolism intermediates in these mutants by mass spectrometry analysis. Based on these results, an updated model of purine nucleotide catabolism is proposed (Figure 34).

An important change in the new model is the absence of an IMP dephosphorylation step. As a consequence, inosine and hypoxanthine catabolism are disconnected from AMP catabolism and become side activities of purine nucleotide degradation assigned to the catabolism of inosine and hypoxanthine derived from sources such as tRNA turnover, DNA repair mechanisms, and uptake from the rhizosphere.

Another important finding is that XMP dephosphorylation is part of the pathway. Consequently, AMP and IMP degradation can either be initiated via the dephosphorylation of XMP or via the dephosphorylation of GMP. The latter reaction seems to be predominant *in vivo*. Probably XMP phosphatase, GMP synthetase and GMP phosphatase are subject to regulatory controls which channel the purine nucleotide catabolism flux in one of the routes possibly depending on physiological needs. Both routes converge on xanthosine which is the starting point of a linear series of reactions that leads to the degradation of the purine ring.

A third important finding is the elucidation of the *in vitro* and *in vivo* function of NSH2 as xanthosine inosine hydrolase activated by interaction with NSH1. The NSH1-NSH2 complex has a higher catalytic efficiency for xanthosine and inosine than NSH1, which is in turn a

more efficient uridine hydrolase. By modulating NSH1 and NSH2 concentration, the plant cells might be able to fine-tune the flux through purine and pyrimidine catabolism. The dynamic regulation of the NSH complexes might be useful to react to certain stress conditions, such as pathogen attack. The interaction between the two NSH types is conserved in the plant kingdom and was probably fine-tuned by evolution to adjust to species-specific differences in purine nucleotide metabolism.

To summarize, this work elucidates the metabolic routes taken in the Arabidopsis purine nucleotide catabolic pathway *in vivo*, and proposes a revised model, in which xanthosine hydrolysis catalyzed by an NSH1-NSH2 heterocomplex is the main xanthine source.

## References

- Achar, B.S., and Vaidyanathan, C.S.** (1967). Purification and properties of uridine hydrolase from mung-bean (*Phaseolus radiatus*) seedlings. *Archives of Biochemistry and Biophysics* **119** (1): 356–362.
- Akaba, S., Seo, M., Dohmae, N., Takio, K., Sekimoto, H., Kamiya, Y., Furuya, N., Komano, T., and Koshiha, T.** (1999). Production of homo- and hetero-dimeric isozymes from two aldehyde oxidase genes of *Arabidopsis thaliana*. *Journal of Biochemistry* **126** (2): 395–401.
- Allen, M., Qin, W., Moreau, F., and Moffatt, B.** (2002). Adenine phosphoribosyltransferase isoforms of *Arabidopsis* and their potential contributions to adenine and cytokinin metabolism. *Physiologia Plantarum* **115** (1): 56–68.
- Alonso, J.M., Stepanova, A.N., Leisse, T.J., Kim, C.J., Chen, H., Shinn, P., Stevenson, D.K., Zimmerman, J., Barajas, P., Cheuk, R., Gadrinab, C., Heller, C., Jeske, A., Koesema, E., Meyers, C.C., Parker, H., Prednis, L., Ansari, Y., Choy, N., Deen, H., Geralt, M., Hazari, N., Hom, E., Karnes, M., Mulholland, C., Ndubaku, R., Schmidt, I., Guzman, P., Aguilar-Henonin, L., Schmid, M., Weigel, D., Carter, D.E., Marchand, T., Risseuw, E., Brogden, D., Zeko, A., Crosby, W.L., Berry, C.C., and Ecker, J.R.** (2003). Genome-wide insertional mutagenesis of *Arabidopsis thaliana*. *Science* (New York, N.Y.) **301** (5633): 653–657.
- Alseth, I., Dalhus, B., and Bjørås, M.** (2014). Inosine in DNA and RNA. *Current Opinion in Genetics & Development* **26**: 116–123.
- An, R., Jia, Y., Wan, B., Zhang, Y., Dong, P., Li, J., and Liang, X.** (2014). Non-enzymatic depurination of nucleic acids: factors and mechanisms. *PloS One* **9** (12): e115950.
- Antico, C.J., Colon, C., Banks, T., and Ramonell, K.M.** (2012). Insights into the role of jasmonic acid-mediated defenses against necrotrophic and biotrophic fungal pathogens. *Front. Biol.* **7** (1): 48–56.
- Ashihara, H., Sano, H., and Crozier, A.** (2008). Caffeine and related purine alkaloids: biosynthesis, catabolism, function and genetic engineering. *Phytochemistry* **69** (4): 841–856.
- Ashihara, H., Stasolla, C., Fujimura, T., and Crozier, A.** (2018). Purine salvage in plants. *Phytochemistry* **147**: 89–124.
- Atkins, C.A.** (1981). Metabolism of purine nucleotides to form ureides in nitrogen-fixing nodules of cowpea (*Vigna unguiculata* L. Walp.). *FEBS letters* **125** (1): 89–93.

- Atkins, C.A., Smith, P., and Storer, P.J.** (1997). Reexamination of the Intracellular Localization of de Novo Purine Synthesis in Cowpea Nodules. *Plant Physiology* **113** (1): 127–135.
- Baccolini, C., and Witte, C.-P.** (2019). AMP and GMP Catabolism in Arabidopsis Converge on Xanthosine which Is Degraded by a Nucleoside Hydrolase Heterocomplex. *The Plant Cell*.
- Boulanger, R.R., and Kantrowitz, E.R.** (2003). Characterization of a monomeric *Escherichia coli* alkaline phosphatase formed upon a single amino acid substitution. *J. Biol. Chem.* **278** (26): 23497–23501.
- Brychkova, G., Alikulov, Z., Fluhr, R., and Sagi, M.** (2008a). A critical role for ureides in dark and senescence-induced purine remobilization is unmasked in the *Atxdh1* Arabidopsis mutant. *The Plant Journal* **54** (3): 496–509.
- Brychkova, G., Fluhr, R., and Sagi, M.** (2008b). Formation of xanthine and the use of purine metabolites as a nitrogen source in Arabidopsis plants. *Plant Signaling & Behavior* **3** (11): 999–1001.
- Campos, A., Rijo-Johansen, M.J., Carneiro, M.F., and Fevereiro, P.** (2005). Purification and characterisation of adenosine nucleosidase from *Coffea arabica* young leaves. *Phytochemistry* **66** (2): 147–151.
- Cao, F.-Q., Werner, A.K., Dahncke, K., Romeis, T., Liu, L.-H., and Witte, C.-P.** (2010). Identification and characterization of proteins involved in rice urea and arginine catabolism. *Plant Physiology* **154** (1): 98–108.
- Chen, C.-M., and Kristopeit, S.M.** (1981). Metabolism of Cytokinin: Deribosylation of Cytokinin Ribonucleoside by Adenosine Nucleosidase from Wheat Germ Cells. *Plant Physiology* **68** (5): 1020–1023.
- Chen, M., Herde, M., and Witte, C.-P.** (2016). Of the Nine Cytidine Deaminase-Like Genes in Arabidopsis, Eight Are Pseudogenes and Only One Is Required to Maintain Pyrimidine Homeostasis in Vivo. *Plant Physiology* **171** (2): 799–809.
- Christensen, T.M.I.E., and Jochimsen, B.U.** (1983). Enzymes of Ureide Synthesis in Pea and Soybean. *Plant Physiology* **72** (1): 56–59.
- Clough, S.J., and Bent, A.F.** (1998). Floral dip: A simplified method for *Agrobacterium*-mediated transformation of *Arabidopsis thaliana*. *The Plant Journal* **16** (6): 735–743.
- Dahncke, K., and Witte, C.-P.** (2013). Plant purine nucleoside catabolism employs a guanosine deaminase required for the generation of xanthosine in Arabidopsis. *The Plant Cell* **25** (10): 4101–4109.



- Deng, W.W., and Ashihara, H.** (2010). Profiles of purine metabolism in leaves and roots of *Camelia sinesis* seedlings. *Plant and Cell Physiology* **51**: 2105-2118.
- Doering L.**, (2018). Stimulus-dependent Translocation of Nucleoside Hydrolase 1 (NSH1) in *Arabidopsis thaliana* and Dimerization of Nucleoside Hydrolase 1 (NSH1) and Nucleoside Hydrolase 2 (NSH2) in *Physcomitrella patens*. MSc Thesis.
- Estupiñán, B., and Schramm, V.L.** (1994). Guanosine-inosine-preferring nucleoside N-glycohydrolase from *Crithidia fasciculata*. *Journal of Biological Chemistry* **269** (37): 23068–23073.
- Fernández, J.R., Byrne, B., and Firestein, B.L.** (2009). Phylogenetic analysis and molecular evolution of guanine deaminases: From guanine to dendrites. *Journal of Molecular Evolution* **68** (3): 227–235.
- Frankel, L.B., Lubas, M., and Lund, A.H.** (2016). Emerging connections between RNA and autophagy. *Autophagy* **13** (1): 3–23.
- Giabbai, B., and Degano, M.** (2004). Crystal structure to 1.7 Å of the *Escherichia coli* pyrimidine nucleoside hydrolase YeiK, a novel candidate for cancer gene therapy. *Structure (London, England 1993)* **12** (5): 739–749.
- Girke, C., Daumann, M., Niopek-Witz, S., and Möhlmann, T.** (2014). Nucleobase and nucleoside transport and integration into plant metabolism. *Frontiers in Plant Science* **5**.
- Gopaul, D.N., Meyer, S.L., Degano, M., Sacchetti, J.C., and Schramm, V.L.** (1996). Inosine-uridine nucleoside hydrolase from *Crithidia fasciculata*. Genetic characterization, crystallization, and identification of histidine 241 as a catalytic site residue. *Biochemistry* **35** (19): 5963–5970.
- Guranowski, A.** (1982). Purine Catabolism in Plants: Purification and Some Properties of Inosine Nucleosidase from Yellow Lupin (*Lupinus Luteus* L.) Seeds. *Plant Physiology* **70** (2): 344–349.
- Guranowski, A., and Schneider, Z.** (1977). Purification and characterization of adenosine nucleosidase from barley leaves. *Biochimica et Biophysica Acta* **482** (1): 145–158.
- Harrison, R.** (2002). Structure and function of xanthine oxidoreductase: where are we now? *Free Radical Biology & Medicine* **33** (6): 774–797.
- Hauck, O., and Witte, C.-P.** (2015). Quantification of Uric Acid or Xanthine in Plant Samples. *Bio-Protocol* **5** (13).
- Hauck, O.K., Scharnberg, J., Escobar, N.M., Wanner, G., Giavalisco, P., and Witte, C.-P.** (2014). Uric acid accumulation in an *Arabidopsis* urate oxidase mutant impairs seedling establishment by blocking peroxisome maintenance. *The Plant Cell* **26** (7): 3090–3100.

- Hehir, M.J., Murphy, J.E., and Kantrowitz, E.R.** (2000). Characterization of heterodimeric alkaline phosphatases from *Escherichia coli*: an investigation of intragenic complementation. *Journal of Molecular Biology* **304** (4): 645–656.
- Hung, W.-F., Chen, L.-J., Boldt, R., Sun, C.-W., and Li, H.-M.** (2004). Characterization of *Arabidopsis* glutamine phosphoribosyl pyrophosphate amidotransferase-deficient mutants. *Plant Physiology* **135** (3): 1314–1323.
- Iovane, E., Giabbai, B., Muzzolini, L., Matafora, V., Fornili, A., Minici, C., Giannese, F., and Degano, M.** (2008). Structural basis for substrate specificity in group I nucleoside hydrolases. *Biochemistry* **47** (15): 4418–4426.
- Jung, B., Flörchinger, M., Kunz, H.-H., Traub, M., Wartenberg, R., Jeblick, W., Neuhaus, H.E., and Möhlmann, T.** (2009). Uridine-ribohydrolase is a key regulator in the uridine degradation pathway of *Arabidopsis*. *The Plant Cell* **21** (3): 876–891.
- Jung, B., Hoffmann, C., and Möhlmann, T.** (2011). *Arabidopsis* nucleoside hydrolases involved in intracellular and extracellular degradation of purines. *The Plant Journal for Cell and Molecular Biology* **65** (5): 703–711.
- Katahira, R., and Ashihara, H.** (2002). Profiles of pyrimidine biosynthesis, salvage and degradation in disks of potato (*Solanum tuberosum* L.) tubers. *Planta* **215** (5): 821–828.
- Katahira, R., and Ashihara, H.** (2006). Profiles of purine biosynthesis, salvage and degradation in disks of potato (*Solanum tuberosum* L.) tubers. *Planta* **225** (1): 115–126.
- Kleinboelting, N., Huel, G., Kloetgen, A., Viehoever, P., and Weisshaar, B.** (2012). GABI-Kat SimpleSearch: New features of the *Arabidopsis thaliana* T-DNA mutant database. *Nucleic Acids Research* **40** (Database issue): D1211-5.
- Koncz, C., and Schell, J.** (1986). The promoter of TL-DNA gene 5 controls the tissue-specific expression of chimaeric genes carried by a novel type of *Agrobacterium* binary vector. *Molecular and General Genetics* **204** (3): 383–396.
- Kopečná, M., Blaschke, H., Kopečný, D., Vigouroux, A., Koncítíková, R., Novák, O., Kotland, O., Strnad, M., Moréra, S., and Schwartzberg, K. von** (2013). Structure and function of nucleoside hydrolases from *Physcomitrella patens* and maize catalyzing the hydrolysis of purine, pyrimidine, and cytokinin ribosides. *Plant Physiology* **163** (4): 1568–1583.
- Lamberto, I., Percudani, R., Gatti, R., Folli, C., and Petrucco, S.** (2010). Conserved alternative splicing of *Arabidopsis* transthyretin-like determines protein localization and S-allantoin synthesis in peroxisomes. *The Plant Cell* **22** (5): 1564–1574.

- Leroch, M., Kirchberger, S., Haferkamp, I., Wahl, M., Neuhaus, H.E., and Tjaden, J.** (2005). Identification and characterization of a novel plastidic adenine nucleotide uniporter from *Solanum tuberosum*. *Journal of Biological Chemistry* **280** (18): 17992–18000.
- Li, W., Chiang, Y.-H., and Coaker, G.** (2013). The HopQ1 effector's nucleoside hydrolase-like domain is required for bacterial virulence in arabidopsis and tomato, but not host recognition in tobacco. *PloS One* **8** (3): e59684.
- Liu, X., Qian, W., Liu, X., Qin, H., and Wang, D.** (2007). Molecular and functional analysis of hypoxanthine-guanine phosphoribosyltransferase from *Arabidopsis thaliana*. *The New Phytologist* **175** (3): 448–461.
- Lohani, N.,** (2016). Cloning of genes & functional testing of the corresponding proteins involved in xanthosine and caffeine biosynthesis in Coffee. MSc. Thesis.
- Ma, X., Wang, W., Bittner, F., Schmidt, N., Berkey, R., Zhang, L., King, H., Zhang, Y., Feng, J., Wen, Y., Tan, L., Li, Y., Zhang, Q., Deng, Z., Xiong, X., and Xiao, S.** (2016). Dual and Opposing Roles of Xanthine Dehydrogenase in Defense-Associated Reactive Oxygen Species Metabolism in Arabidopsis. *The Plant Cell* **28** (5): 1108–1126.
- Manguet, S.E., Gakière, B., Majira, A., Pelletier, S., Bringel, F., Guérard, F., Caboche, M., Berthomé, R., and Renou, J.P.** (2009). Uracil salvage is necessary for early Arabidopsis development. *The Plant Journal for Cell and Molecular Biology* **60** (2): 280–291.
- Maiuolo, J., Oppedisano, F., Gratteri, S., Muscoli, C., and Mollace, V.** (2016). Regulation of uric acid metabolism and excretion. *International Journal of Cardiology* **213**: 8–14.
- Masclaux, C., Valadier, M.H., Brugière, N., Morot-Gaudry, J.F., and Hirel, B.** (2000). Characterization of the sink/source transition in tobacco (*Nicotiana tabacum* L.) shoots in relation to nitrogen management and leaf senescence. *Planta* **211** (4): 510–518.
- Masclaux-Daubresse, C., Daniel-Vedele, F., Dechorgnat, J., Chardon, F., Gaufichon, L., and Suzuki, A.** (2010). Nitrogen uptake, assimilation and remobilization in plants: challenges for sustainable and productive agriculture. *Annals of Botany* **105** (7): 1141–1157.
- Moffatt, B., and Somerville, C.** (1988). Positive Selection for Male-Sterile Mutants of Arabidopsis Lacking Adenine Phosphoribosyl Transferase Activity 1. *Plant Physiology* **86** (4): 1150–1154.

- Moffatt, B.A., and Ashihara, H.** (2002). Purine and pyrimidine nucleotide synthesis and metabolism. *The Arabidopsis Book 1*: e0018.
- Moffatt, B.A., Stevens, Y.Y., Allen, M.S., Snider, J.D., Pereira, L.A., Todorova, M.I., Summers, P.S., Weretilnyk, E.A., Martin-McCaffrey, L., and Wagner, C.** (2002). Adenosine kinase deficiency is associated with developmental abnormalities and reduced transmethylation. *Plant Physiology* **128** (3): 812–821.
- Moffatt, B.A., Wang, L., Allen, M.S., Stevens, Y.Y., Qin, W., Snider, J., and Schwartzberg, K.** (2000). Adenosine kinase of Arabidopsis. Kinetic properties and gene expression. *Plant Physiology* **124** (4): 1775–1785.
- Montalbini, P., and Della Torre, G.** (1995). Allopurinol Metabolites and Xanthine Accumulation in Allopurinol-Treated Tobacco. *Journal of Plant Physiology* **147** (3-4): 321–327.
- Myrach, T., Zhu, A., and Witte, C.-P.** (2017). The assembly of the plant urease activation complex and the essential role of the urease accessory protein G (UreG) in delivery of nickel to urease. *The Journal of Biological Chemistry* **292** (35): 14556–14565.
- Parkin, D.W.** (1996a). Purine-specific Nucleoside N<sup>6</sup>-Ribohydrolase from *Trypanosoma brucei brucei*. *The Journal of Biological Chemistry* **271** (36): 21713–21719.
- Parkin, D.W.** (1996b). Purine-specific nucleoside N-ribohydrolase from *Trypanosoma brucei brucei* purification, specificity, and kinetic mechanism. *The Journal of Biological Chemistry* **271** (36): 21713–21719.
- Parkin, D.W., Horenstein, B.A., Abdulah, D.R., Estupiñán, B., and Schramm, V.L.** (1991). Nucleoside hydrolase from *Crithidia fasciculata*. Metabolic role, purification, specificity, and kinetic mechanism. *The Journal of Biological Chemistry* **266** (31): 20658–20665.
- Pedley, A.M., and Benkovic, S.J.** (2017). A New View into the Regulation of Purine Metabolism: The Purinosome. *Trends in Biochemical Sciences* **42** (2): 141–154.
- Rensing, S.A., Ick, J., Fawcett, J.A., Lang, D., Zimmer, A., van de Peer, Y., and Reski, R.** (2007). An ancient genome duplication contributed to the abundance of metabolic genes in the moss *Physcomitrella patens*. *BMC Evolutionary Biology* **7**: 130.
- Ribeiro, J.M.C., and Valenzuela, J.G.** (2003). The salivary purine nucleosidase of the mosquito, *Aedes aegypti*. *Insect biochemistry and molecular biology* **33** (1): 13–22.

- Riegler, H., Geserick, C., and Zrenner, R.** (2011). *Arabidopsis thaliana* nucleosidase mutants provide new insights into nucleoside degradation. *The New Phytologist* **191** (2): 349–359.
- Roundtree, I.A., Evans, M.E., Pan, T., and He, C.** (2017). Dynamic RNA Modifications in Gene Expression Regulation. *Cell* **169** (7): 1187–1200.
- Rundles, R.W., and Wyngaarden, J.B.** (1969). Drugs and uric acid. *Annual Review of Pharmacology* **9**: 345–362.
- Schroeder, R.Y., Zhu, A., Eubel, H., Dahncke, K., and Witte, C.-P.** (2017). The ribokinases of *Arabidopsis thaliana* and *Saccharomyces cerevisiae* are required for ribose recycling from nucleotide catabolism, which in plants is not essential to survive prolonged dark stress. *The New Phytologist* **217** (1):233-244.
- Sessions, A., Burke, E., Presting, G., Aux, G., McElver, J., Patton, D., Dietrich, B., Ho, P., Bacwaden, J., Ko, C., Clarke, J.D., Cotton, D., Bullis, D., Snell, J., Miguel, T., Hutchison, D., Kimmerly, B., Mitzel, T., Katagiri, F., Glazebrook, J., Law, M., and Goff, S.A.** (2002). A high-throughput *Arabidopsis* reverse genetics system. *The Plant Cell* **14** (12): 2985–2994.
- Shelp, B.J., and Atkins, C.A.** (1983). Role of Inosine Monophosphate Oxidoreductase in the Formation of Ureides in Nitrogen-Fixing Nodules of Cowpea (*Vigna unguiculata* L. Walp.) 1. *Plant Physiology* **72** (4): 1029–1034.
- Shi, W., Schramm, V.L., and Almo, S.C.** (1999). Nucleoside Hydrolase from *Leishmania major*. *The Journal of Biological Chemistry* **274** (30): 21114–21120.
- Smith, P.M., and Atkins, C.A.** (2002). Purine Biosynthesis. Big in Cell Division, Even Bigger in Nitrogen Assimilation. *Plant Physiology* **128** (3): 793–802.
- Soltabayeva, A., Srivastava, S., Kurmanbayeva, A., Bekturova, A., Fluhr, R., and Sagi, M.** (2018). Early Senescence in Older Leaves of Low Nitrate-Grown *Atxdh1* Uncovers a Role for Purine Catabolism in N Supply. *Plant Physiology* **178** (3): 1027–1044.
- Stasolla, C., Katahira, R., Thorpe, T.A., and Ashihara, H.** (2003). Purine and pyrimidine nucleotide metabolism in higher plants. *Journal of Plant Physiology* **160** (11): 1271–1295.
- Szuwart, M., Starzyńska, E., Pietrowska-Borek, M., and Guranowski, A.** (2006). Calcium-stimulated guanosine—inosine nucleosidase from yellow lupin (*Lupinus luteus*). *Phytochemistry* **67** (14): 1476–1485.
- Todd, S.J., Moir, A.J.G., Johnson, M.J., and Moir, A.** (2003). Genes of *Bacillus cereus* and *Bacillus anthracis* Encoding Proteins of the Exosporium. *Journal of Bacteriology* **185** (11): 3373–3378.

- Tokuhisa, D., Shinano, T., Watanabe, T., Yamamura, T., and Osaki, M.** (2010). Promotion of root growth by the application of inosine. *Soil Science and Plant Nutrition* **56** (2): 272–280.
- Versées, W., Decanniere, K., Pellé, R., Depoorter, J., Brosens, E., Parkin, D.W., and Steyaert, J.** (2001). Structure and function of a novel purine specific nucleoside hydrolase from *Trypanosoma vivax*. *Journal of Molecular Biology* **307** (5): 1363–1379.
- Voinnet, O., Rivas, S., Mestre, P., and Baulcombe, D.** (2003). An enhanced transient expression system in plants based on suppression of gene silencing by the p19 protein of tomato bushy stunt virus. *The Plant Journal for Cell and Molecular Biology* **33** (5): 949–956.
- Werner, A.K., Medina-Escobar, N., Zulawski, M., Sparkes, I.A., Cao, F.-Q., and Witte, C.-P.** (2013). The ureide-degrading reactions of purine ring catabolism employ three amidohydrolases and one aminohydrolase in *Arabidopsis*, soybean, and rice. *Plant Physiology* **163** (2): 672–681.
- Werner, A.K., Romeis, T., and Witte, C.-P.** (2010). Ureide catabolism in *Arabidopsis thaliana* and *Escherichia coli*. *Nature Chemical Biology* **6** (1): 19–21.
- Werner, A.K., Sparkes, I.A., Romeis, T., and Witte, C.-P.** (2008). Identification, biochemical characterization, and subcellular localization of allantoate amidohydrolases from *Arabidopsis* and soybean. *Plant Physiology* **146** (2): 418–430.
- Werner, A.K., and Witte, C.-P.** (2011). The biochemistry of nitrogen mobilization: Purine ring catabolism. *Trends in Plant Science* **16** (7): 381–387.
- Witte, C.-P., Noël, L.D., Gielbert, J., Parker, J.E., and Romeis, T.** (2004). Rapid one-step protein purification from plant material using the eight-amino acid StrepII epitope. *Plant Molecular Biology* **55** (1): 135–147.
- Yanes, O., Tautenhahn, R., Patti, G.J., and Siuzdak, G.** (2011). Expanding coverage of the metabolome for global metabolite profiling. *Analytical Chemistry* **83** (6): 2152–2161.
- Yin, Y., Katahira, R., and Ashihara, H.** (2014). Metabolism of purine nucleosides and bases in suspension-cultured *arabidopsis thaliana* cells. *European Chemical Bulletin* **3**: 925-934.
- Zheng, X.-Y., Spivey, N.W., Zeng, W., Liu, P.-P., Fu, Z.Q., Klessig, D.F., He, S.Y., and Dong, X.** (2012). Coronatine promotes *Pseudomonas syringae* virulence in plants by activating a signaling cascade that inhibits salicylic acid accumulation. *Cell Host & Microbe* **11** (6): 587–596.

- Zrenner, R., and Ashihara, H.** (2011). Nucleotide Metabolism. In *Plant Metabolism and Biotechnology*, pp. 135–162.
- Zrenner, R., Stitt, M., Sonnewald, U., and Boldt, R.** (2006). Pyrimidine and purine biosynthesis and degradation in plants. *Annual Review of Plant Biology* **57**: 805–836.

## Acknowledgment

First of all I would like to thank Prof. Dr. Claus-Peter Witte, my PhD supervisor, for giving me the opportunity to join his group of research and pursue the PhD career. If I have matured as a scientist it was because of your constant guidance during these years.

My sincere thanks also go to Prof. Brüser and Dr. Offermann, my PhD supervisors in the framework of the Research Training Group GRK 1798, for giving me suggestions and ideas in the course of the GRK meetings. I would like to express my gratitude also to Prof. Küster for giving me the opportunity to join the GRK 1798 that significantly enriched my PhD experience.

I would like to thank the DAAD for the financial support of the first three years of the PhD.

Special thanks go to my colleagues for the nice working atmosphere here at the IPE. First of all I would like to thank the Postdoc team for the useful discussion during the lab meetings. Thank you Marco and Nieves for all your ideas, Marina for your useful advices and Mingjia because you are a wise man. I would also like to thank the technical staff: Andre that always helped me when there were bubbles appearing in the LC-MS, Hilde because it is a pleasure to talk to her in German and Iris because she takes care of us in a lovely way. I cannot omit to thank all the PhD students, Markus, mein liebligshupwagen, Kathy, meine Lieblingsdeutscherin, Rebekka, meine Sonnenblume, Linda because you introduce me to Natasha, Nabila, because you shared your food with me, Hendrik because you laugh at my jokes, and Jannis because you came to the Salsa class when nobody wanted. I would also like to thank Neeta and Lennart who helped me with this project.

A big thanks goes to Anting and Mouna, without you it would not have been the same. Anting you taught me a lot and I could not have done all the measurements at the LC-MS without you. Mouna, my Indian girl, I simply thank you for being who you are.

Finally I would like to express my profound gratitude to my family, my parents and my brother, for supporting and helping me despite the distance between us.



## Appendix of Figures

### Figure A-1. Current model of purine nucleotide catabolism.

The chemical formulas of the metabolites are shown. Oxo- and amino- substituents are highlighted in blue. The final products of purine nucleotide catabolism are highlighted in red. Enzymes: AMP deaminase (AMPD), IMP dehydrogenase (IMPDH), GMP synthetase (GMPS), putative IMP, XMP and GMP phosphatase (1), guanosine deaminase (GSDA), hypoxanthine guanine phosphoribosyltransferase (HGPRT), putative inosine guanosine kinase (2), nucleoside hydrolase 1 (NSH1), xanthine dehydrogenase (XDH), urate oxidase (UOX), allantoin synthase (ALNS) allantoin amidohydrolase or allantoinase (ALN), allantoate amidohydrolase (AAH), ureidoglycine aminohydrolase (UGAH), ureidoglycolate amidohydrolase (UAH). Enzymes involved in catabolism and salvage are indicated with grey and black shading respectively. The enzymes IMPDH and GMPS (white box) are shared between catabolism (AMP catabolism) and biosynthesis (GMP biosynthesis). Enzymes whose genetic identity is not clear are indicated with a number. OHCU, 2-oxo-4-hydroxy-4-carboxy-5-ureido-imidazoline.

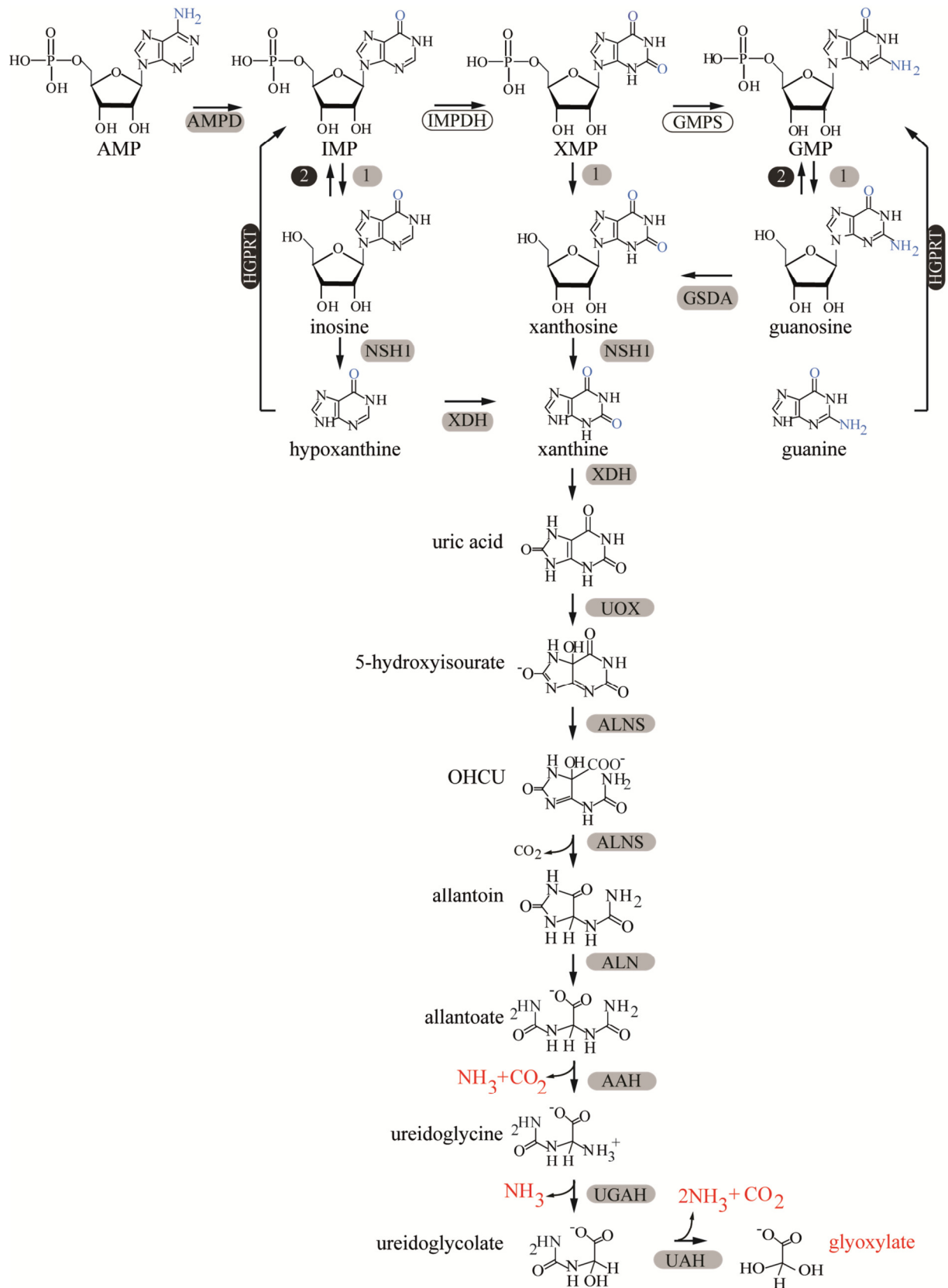
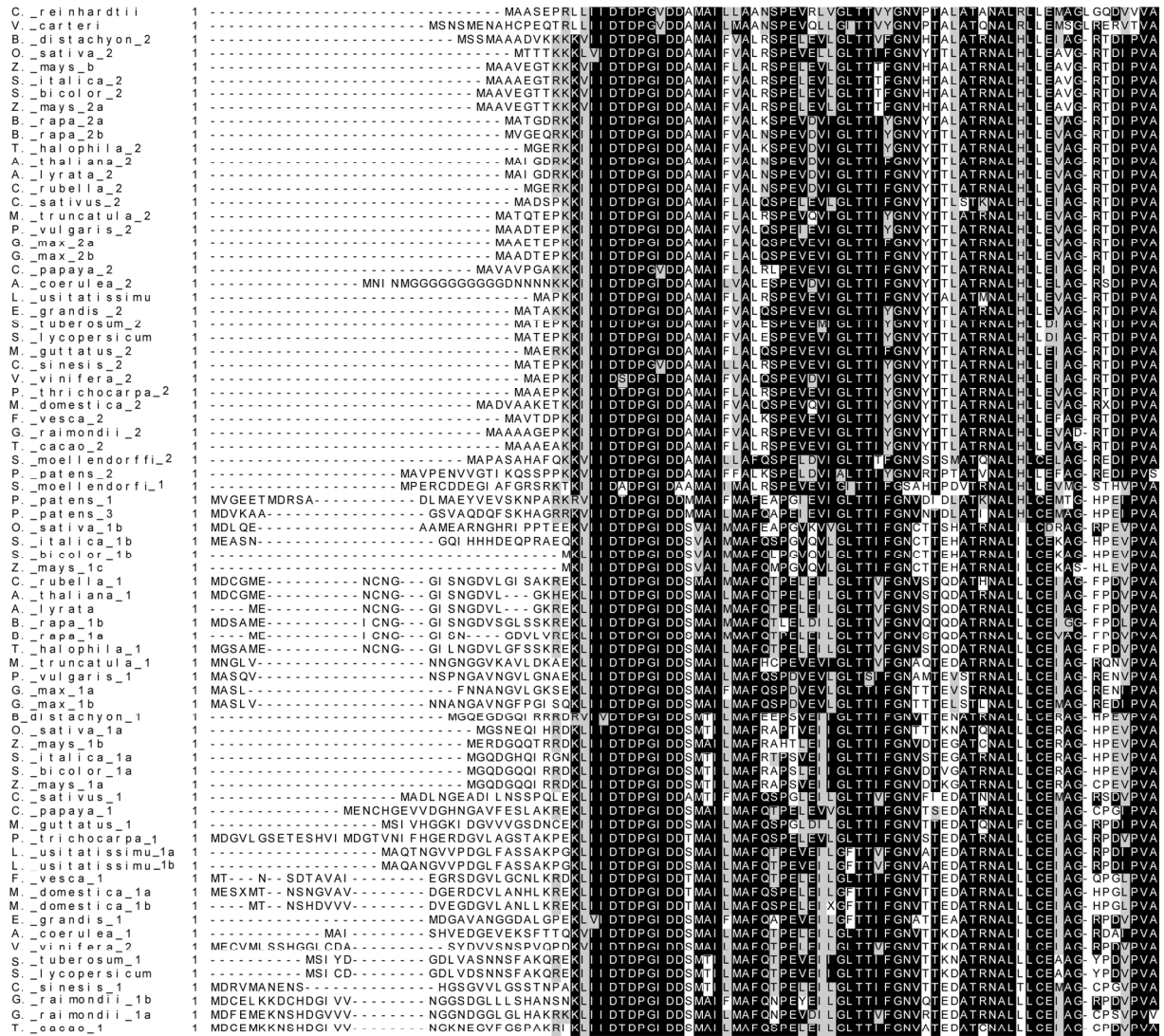


**Figure A-2. Multiple alignment of the amino acid sequences of plant and algae IU-NSHs.**

The alignment was generated with Clustal Omega (EBI) and shaded with Boxshade (Expasy). The black and grey shading indicates identical and similar amino acid respectively. The black triangles highlight the N terminal aspartate cluster hallmark of nucleosidases, and other conserved residues indicated with Physcomitrella numbering. Residues in position 244 and 249 determines substrate specificity and are a tyrosine in all NSH2 (specificity for xanthosine and inosine) and a tryptophan and aspartate in all NSH1 (specificity for uridine). Histidine 257 is involved in the protonation of the leaving base. Lysine 297 completes the active site of one subunit of IU-NSH dimer by protruding from the other subunit of the dimer. The arrow indicates a residue which might be involved in insolubility in *E. coli*. The star (\*) indicates the residue mutated in  $\Delta$ NSH1 and  $\Delta$ NSH2. Accession and gene locus numbers of the sequences are in Table B-1.



▲▲▲▲▲ NSH specific motif

\*Asp 25

C.\_reinhardtii 70 QGAARSLKAGMDVERIADVFHGDGDFEDI GLPPPK-GAA-ADGSAAEFLVIRTCRQHPRVITLALAPLITNIAGALMLDPQLGDVWESLVV LGGAFFVNGN  
V.\_carteri 74 QGAARSLKAGTDIERIADVFHGDGDFEDI GLPPPK-GQHLMDGSAAEFLVRSVNHHPGRVITLALAPLITNIAGALMLDPQLADWDELVV LGGAFFVNGN  
B.\_distachyon\_2 74 EGSFVTVKATK-LRIASVFHSGDGLGNQNFPPPA-GKPLD-GSAAEFLVQGANLYPGQVTVVVALGPLTNLALAVELDPSPFKKI GOV LGGAFFVNGN  
O.\_sativa\_2 68 EGSFVTVKATK-LRIASVFHSGDGLGNQNFPPPA-TKPLD-GSAAEFLVQGANLYPGQVTVVVALGPLTNLALAVELDPSPFKKI GOV LGGAFFVNGN  
Z.\_mays\_b 71 EGSFVTVKATK-LRIASVFHSGDGLGNQNFPPPA-TKPLD-GSAAEFLVQGANLYPGQVTVVVALGPLTNLALAVELDPSPFKKI GOV LGGAFFVNGN  
S.\_italica\_2 71 EGSFVTVKASK-LRIASVFHSGDGLGNQNFPPPA-TKPLD-GTAAAFVLEQANLYPGQVTVVVALGPLTNLALAVELDPSPFKKI GOV LGGAFFVNGN  
S.\_bicolor\_2 72 EGSFVTVKATK-LRIASVFHSGDGLGNQNFPPPA-TKPLD-GSAAEFLVQGANLYPGQVTVVVALGPLTNLALAVELDPSPFKKI GOV LGGAFFVNGN  
Z.\_mays\_2a 72 EGSFVTVKATK-LRIASVFHSGDGLGNQNFPPPA-TKPLD-GSAAEFLVQGANLYPGQVTVVVALGPLTNLALAVELDPSPFKKI GOV LGGAFFVNGN  
B.\_rapa\_2a 69 EGHHTKTLNNGK-LRIADVFHCKDGLGNQNFPPPK-GKPIE-KSAPFLVEQAKLHPGSEITVVALGPLTNLALAVQLDPEFSKNVGOV LGGAFFVNGN  
B.\_rapa\_2b 69 EGHHTKTLNNGK-LRIADVFHCKDGLGNQNFPPPK-GKPIE-KSAPFLVEQAKLHPGSEITVVALGPLTNLALAVQLDPEFSKNVGOV LGGAFFVNGN  
T.\_halophila\_2 67 EGHHTKTLNNGK-LRIADVFHCKDGLGNQNFPPPK-GKPIE-KSAPFLVEQAKLHPGSEITVVALGPLTNLALAVQLDPEFSKNVGOV LGGAFFVNGN  
A.\_thaliana\_2 69 EGHHTKTLNNDTK-LRIADVFHCKDGLGNQNFPPPK-GKPIE-KSAPFLVEQAKLHPGSEITVVALGPLTNLALAVQLDPEFSKNVGOV LGGAFFVNGN  
A.\_lyrata\_2 69 EGHHTKTLNNDTK-LRIADVFHCKDGLGNQNFPPPK-GKPIE-KSAPFLVEQAKLHPGSEITVVALGPLTNLALAVQLDPEFSKNVGOV LGGAFFVNGN  
C.\_rubella\_2 67 EGHHTKTLNNDTK-LRIADVFHCKDGLGNQNFPPPK-GKPIE-KSAPFLVEQAKLHPGSEITVVALGPLTNLALAVQLDPEFSKNVGOV LGGAFFVNGN  
S.\_sativus\_2 68 EGSFVTVKATK-LRIADVFHSGDGLGNQNFPPPA-TKPLD-GTAAAFVLEQANLYPGQVTVVVALGPLTNLALAVQLDPEFSKNVGOV LGGAFFVNGN  
M.\_truncatula\_2 70 EGSFVTVKATK-LRIADVFHSGDGLGNQNFPPPA-TKPLD-GSAAEFLVQGANLYPGQVTVVVALGPLTNLALAVQLDPEFSKNVGOV LGGAFFVNGN  
P.\_vulgaris\_2 70 EGHHTKTLNNGK-LRIADVFHCKDGLGNQNFPPPK-GKPIE-KSAPFLVEQAKLHPGSEITVVALGPLTNLALAVQLDPEFSKNVGOV LGGAFFVNGN  
G.\_max\_2a 70 EGSFVTVKATK-LRIADVFHSGDGLGNQNFPPPA-TKPLD-GSAAEFLVQGANLYPGQVTVVVALGPLTNLALAVQLDPEFSKNVGOV LGGAFFVNGN  
G.\_max\_2b 70 EGSFVTVKATK-LRIADVFHSGDGLGNQNFPPPA-TKPLD-GSAAEFLVQGANLYPGQVTVVVALGPLTNLALAVQLDPEFSKNVGOV LGGAFFVNGN  
C.\_papaya\_2 72 EGSFVTVKATK-LRIADVFHSGDGLGNQNFPPPA-TKPLD-GSAAEFLVQGANLYPGQVTVVVALGPLTNLALAVQLDPEFSKNVGOV LGGAFFVNGN  
A.\_coerulea\_2 84 EGSFVTVKATK-LRIADVFHSGDGLGNQNFPPPA-TKPLD-GSAAEFLVQGANLYPGQVTVVVALGPLTNLALAVQLDPEFSKNVGOV LGGAFFVNGN  
L.\_usitatissimu 66 EGSFVTVKATK-LRIADVFHSGDGLGNQNFPPPA-TKPLD-GSAAEFLVQGANLYPGQVTVVVALGPLTNLALAVQLDPEFSKNVGOV LGGAFFVNGN  
E.\_grandis\_2 68 EGSFVTVKATK-LRIADVFHSGDGLGNQNFPPPA-TKPLD-GSAAEFLVQGANLYPGQVTVVVALGPLTNLALAVQLDPEFSKNVGOV LGGAFFVNGN  
S.\_lycopersum\_2 68 EGSFVTVKATK-LRIADVFHSGDGLGNQNFPPPA-TKPLD-GSAAEFLVQGANLYPGQVTVVVALGPLTNLALAVQLDPEFSKNVGOV LGGAFFVNGN  
S.\_lycopersicum 68 EGSFVTVKATK-LRIADVFHSGDGLGNQNFPPPA-TKPLD-GSAAEFLVQGANLYPGQVTVVVALGPLTNLALAVQLDPEFSKNVGOV LGGAFFVNGN  
M.\_guttatus\_2 67 EGSFVTVKATK-LRIADVFHSGDGLGNQNFPPPA-TKPLD-GSAAEFLVQGANLYPGQVTVVVALGPLTNLALAVQLDPEFSKNVGOV LGGAFFVNGN  
C.\_sinensis\_2 68 EGSFVTVKATK-LRIADVFHSGDGLGNQNFPPPA-TKPLD-GSAAEFLVQGANLYPGQVTVVVALGPLTNLALAVQLDPEFSKNVGOV LGGAFFVNGN  
V.\_viniifera\_2 67 EGSFVTVKATK-LRIADVFHSGDGLGNQNFPPPA-TKPLD-GSAAEFLVQGANLYPGQVTVVVALGPLTNLALAVQLDPEFSKNVGOV LGGAFFVNGN  
P.\_thrichocarpa\_2 68 EGSFVTVKATK-LRIADVFHSGDGLGNQNFPPPA-TKPLD-GSAAEFLVQGANLYPGQVTVVVALGPLTNLALAVQLDPEFSKNVGOV LGGAFFVNGN  
M.\_domestica\_2 72 EGSFVTVKATK-LRIADVFHSGDGLGNQNFPPPA-TKPLD-GSAAEFLVQGANLYPGQVTVVVALGPLTNLALAVQLDPEFSKNVGOV LGGAFFVNGN  
F.\_vesca\_2 69 EGSFVTVKATK-LRIADVFHSGDGLGNQNFPPPA-TKPLD-GSAAEFLVQGANLYPGQVTVVVALGPLTNLALAVQLDPEFSKNVGOV LGGAFFVNGN  
G.\_raimondii\_2 71 EGSFVTVKATK-LRIADVFHSGDGLGNQNFPPPA-TKPLD-GSAAEFLVQGANLYPGQVTVVVALGPLTNLALAVQLDPEFSKNVGOV LGGAFFVNGN  
T.\_cacao\_2 69 EGSFVTVKATK-LRIADVFHSGDGLGNQNFPPPA-TKPLD-GSAAEFLVQGANLYPGQVTVVVALGPLTNLALAVQLDPEFSKNVGOV LGGAFFVNGN  
S.\_moellendorffi\_2 73 QGHKSLKGLGDK-EHAVDFIHKGDGLGNTNPPAPK-GKPIE-MTASFFPTSKVKEPFGVETITVVALGPLTNLALAVQLDPEFSKNVGOV LGGAFFVNGN  
P.\_patens\_2 80 EGRRTSLRGLK-LRIADVFHSGDGLGNQNFPPPA-TKPLD-GTAAAFVLEQANLYPGQVTVVVALGPLTNLALAVQLDPEFSKNVGOV LGGAFFVNGN  
S.\_moellendorffi\_1 89 EGNIKWAGS-VRIADVFHSGDGLGNQNFPPPA-TKPLD-GSAAEFLVQGANLYPGQVTVVVALGPLTNLALAVQLDPEFSKNVGOV LGGAFFVNGN  
P.\_patens\_1 89 EGSSEPLKGG-K-PRVADVFHCKDGLGNQNFPPPK-RKKEE-KSAAEFLVQGANLYPGQVTVVVALGPLTNLALAVQLDPEFSKNVGOV LGGAFFVNGN  
P.\_patens\_3 83 EGSSEPLKGG-K-PRVADVFHCKDGLGNQNFPPPK-RKKEE-KSAAEFLVQGANLYPGQVTVVVALGPLTNLALAVQLDPEFSKNVGOV LGGAFFVNGN  
O.\_sativa\_1b 83 EGSSEPLKGG-K-PRVADVFHCKDGLGNQNFPPPK-RKKEE-KSAAEFLVQGANLYPGQVTVVVALGPLTNLALAVQLDPEFSKNVGOV LGGAFFVNGN  
S.\_italica\_1b 81 EGSSEPLKGG-K-PRVADVFHCKDGLGNQNFPPPK-RKKEE-KSAAEFLVQGANLYPGQVTVVVALGPLTNLALAVQLDPEFSKNVGOV LGGAFFVNGN  
S.\_bicolor\_1b 63 EGSSEPLKGG-K-PRVADVFHCKDGLGNQNFPPPK-RKKEE-KSAAEFLVQGANLYPGQVTVVVALGPLTNLALAVQLDPEFSKNVGOV LGGAFFVNGN  
Z.\_mays\_1c 63 EGSSEPLKGG-K-PRVADVFHCKDGLGNQNFPPPK-RKKEE-KSAAEFLVQGANLYPGQVTVVVALGPLTNLALAVQLDPEFSKNVGOV LGGAFFVNGN  
C.\_rubella\_1 87 EGSSEPLKGG-K-PRVADVFHCKDGLGNQNFPPPK-RKKEE-KSAAEFLVQGANLYPGQVTVVVALGPLTNLALAVQLDPEFSKNVGOV LGGAFFVNGN  
A.\_thaliana\_1 84 EGSSEPLKGG-K-PRVADVFHCKDGLGNQNFPPPK-RKKEE-KSAAEFLVQGANLYPGQVTVVVALGPLTNLALAVQLDPEFSKNVGOV LGGAFFVNGN  
A.\_lyrata 80 EGSSEPLKGG-K-PRVADVFHCKDGLGNQNFPPPK-RKKEE-KSAAEFLVQGANLYPGQVTVVVALGPLTNLALAVQLDPEFSKNVGOV LGGAFFVNGN  
B.\_rapa\_1b 87 EGSSEPLKGG-K-PRVADVFHCKDGLGNQNFPPPK-RKKEE-KSAAEFLVQGANLYPGQVTVVVALGPLTNLALAVQLDPEFSKNVGOV LGGAFFVNGN  
B.\_rapa\_1a 79 EGSSEPLKGG-K-PRVADVFHCKDGLGNQNFPPPK-RKKEE-KSAAEFLVQGANLYPGQVTVVVALGPLTNLALAVQLDPEFSKNVGOV LGGAFFVNGN  
T.\_halophila\_1 87 EGSSEPLKGG-K-PRVADVFHCKDGLGNQNFPPPK-RKKEE-KSAAEFLVQGANLYPGQVTVVVALGPLTNLALAVQLDPEFSKNVGOV LGGAFFVNGN  
M.\_truncatula\_1 82 EGSSEPLKGG-K-PRVADVFHCKDGLGNQNFPPPK-RKKEE-KSAAEFLVQGANLYPGQVTVVVALGPLTNLALAVQLDPEFSKNVGOV LGGAFFVNGN  
P.\_vulgaris\_1 82 EGSSEPLKGG-K-PRVADVFHCKDGLGNQNFPPPK-RKKEE-KSAAEFLVQGANLYPGQVTVVVALGPLTNLALAVQLDPEFSKNVGOV LGGAFFVNGN  
G.\_max\_1a 78 EGSSEPLKGG-K-PRVADVFHCKDGLGNQNFPPPK-RKKEE-KSAAEFLVQGANLYPGQVTVVVALGPLTNLALAVQLDPEFSKNVGOV LGGAFFVNGN  
G.\_max\_1b 82 EGSSEPLKGG-K-PRVADVFHCKDGLGNQNFPPPK-RKKEE-KSAAEFLVQGANLYPGQVTVVVALGPLTNLALAVQLDPEFSKNVGOV LGGAFFVNGN  
B.\_distachyon\_1 75 EGSSEPLKGG-K-PRVADVFHCKDGLGNQNFPPPK-RKKEE-KSAAEFLVQGANLYPGQVTVVVALGPLTNLALAVQLDPEFSKNVGOV LGGAFFVNGN  
O.\_sativa\_1a 72 EGSSEPLKGG-K-PRVADVFHCKDGLGNQNFPPPK-RKKEE-KSAAEFLVQGANLYPGQVTVVVALGPLTNLALAVQLDPEFSKNVGOV LGGAFFVNGN  
Z.\_mays\_1b 73 EGSSEPLKGG-K-PRVADVFHCKDGLGNQNFPPPK-RKKEE-KSAAEFLVQGANLYPGQVTVVVALGPLTNLALAVQLDPEFSKNVGOV LGGAFFVNGN  
S.\_italica\_1a 73 EGSSEPLKGG-K-PRVADVFHCKDGLGNQNFPPPK-RKKEE-KSAAEFLVQGANLYPGQVTVVVALGPLTNLALAVQLDPEFSKNVGOV LGGAFFVNGN  
S.\_bicolor\_1a 73 EGSSEPLKGG-K-PRVADVFHCKDGLGNQNFPPPK-RKKEE-KSAAEFLVQGANLYPGQVTVVVALGPLTNLALAVQLDPEFSKNVGOV LGGAFFVNGN  
Z.\_mays\_1a 73 EGSSEPLKGG-K-PRVADVFHCKDGLGNQNFPPPK-RKKEE-KSAAEFLVQGANLYPGQVTVVVALGPLTNLALAVQLDPEFSKNVGOV LGGAFFVNGN  
C.\_sativus\_1 80 EGSSEPLKGG-K-PRVADVFHCKDGLGNQNFPPPK-RKKEE-KSAAEFLVQGANLYPGQVTVVVALGPLTNLALAVQLDPEFSKNVGOV LGGAFFVNGN  
C.\_papaya\_1 86 EGSSEPLKGG-K-PRVADVFHCKDGLGNQNFPPPK-RKKEE-KSAAEFLVQGANLYPGQVTVVVALGPLTNLALAVQLDPEFSKNVGOV LGGAFFVNGN  
M.\_guttatus\_1 82 EGSSEPLKGG-K-PRVADVFHCKDGLGNQNFPPPK-RKKEE-KSAAEFLVQGANLYPGQVTVVVALGPLTNLALAVQLDPEFSKNVGOV LGGAFFVNGN  
P.\_thrichocarpa\_1 100 EGSSEPLKGG-K-PRVADVFHCKDGLGNQNFPPPK-RKKEE-KSAAEFLVQGANLYPGQVTVVVALGPLTNLALAVQLDPEFSKNVGOV LGGAFFVNGN  
L.\_usitatissimu\_1a 82 EGSSEPLKGG-K-PRVADVFHCKDGLGNQNFPPPK-RKKEE-KSAAEFLVQGANLYPGQVTVVVALGPLTNLALAVQLDPEFSKNVGOV LGGAFFVNGN  
L.\_usitatissimu\_1b 82 EGSSEPLKGG-K-PRVADVFHCKDGLGNQNFPPPK-RKKEE-KSAAEFLVQGANLYPGQVTVVVALGPLTNLALAVQLDPEFSKNVGOV LGGAFFVNGN  
F.\_vesca\_1 87 EGSSEPLKGG-K-PRVADVFHCKDGLGNQNFPPPK-RKKEE-KSAAEFLVQGANLYPGQVTVVVALGPLTNLALAVQLDPEFSKNVGOV LGGAFFVNGN  
M.\_domestica\_1a 90 EGSSEPLKGG-K-PRVADVFHCKDGLGNQNFPPPK-RKKEE-KSAAEFLVQGANLYPGQVTVVVALGPLTNLALAVQLDPEFSKNVGOV LGGAFFVNGN  
M.\_domestica\_1b 86 EGSSEPLKGG-K-PRVADVFHCKDGLGNQNFPPPK-RKKEE-KSAAEFLVQGANLYPGQVTVVVALGPLTNLALAVQLDPEFSKNVGOV LGGAFFVNGN  
E.\_grandis\_1 77 EGSSEPLKGG-K-PRVADVFHCKDGLGNQNFPPPK-RKKEE-KSAAEFLVQGANLYPGQVTVVVALGPLTNLALAVQLDPEFSKNVGOV LGGAFFVNGN  
A.\_coerulea\_1 80 EGSSEPLKGG-K-PRVADVFHCKDGLGNQNFPPPK-RKKEE-KSAAEFLVQGANLYPGQVTVVVALGPLTNLALAVQLDPEFSKNVGOV LGGAFFVNGN  
V.\_viniifera\_2 90 EGSSEPLKGG-K-PRVADVFHCKDGLGNQNFPPPK-RKKEE-KSAAEFLVQGANLYPGQVTVVVALGPLTNLALAVQLDPEFSKNVGOV LGGAFFVNGN  
S.\_lycopersum\_1 82 EGSSEPLKGG-K-PRVADVFHCKDGLGNQNFPPPK-RKKEE-KSAAEFLVQGANLYPGQVTVVVALGPLTNLALAVQLDPEFSKNVGOV LGGAFFVNGN  
S.\_lycopersicum 82 EGSSEPLKGG-K-PRVADVFHCKDGLGNQNFPPPK-RKKEE-KSAAEFLVQGANLYPGQVTVVVALGPLTNLALAVQLDPEFSKNVGOV LGGAFFVNGN  
C.\_sinensis\_1 86 EGSSEPLKGG-K-PRVADVFHCKDGLGNQNFPPPK-RKKEE-KSAAEFLVQGANLYPGQVTVVVALGPLTNLALAVQLDPEFSKNVGOV LGGAFFVNGN  
G.\_raimondii\_1b 92 EGSSEPLKGG-K-PRVADVFHCKDGLGNQNFPPPK-RKKEE-KSAAEFLVQGANLYPGQVTVVVALGPLTNLALAVQLDPEFSKNVGOV LGGAFFVNGN  
G.\_raimondii\_1a 92 EGSSEPLKGG-K-PRVADVFHCKDGLGNQNFPPPK-RKKEE-KSAAEFLVQGANLYPGQVTVVVALGPLTNLALAVQLDPEFSKNVGOV LGGAFFVNGN  
T.\_cacao\_1 92 EGSSEPLKGG-K-PRVADVFHCKDGLGNQNFPPPK-RKKEE-KSAAEFLVQGANLYPGQVTVVVALGPLTNLALAVQLDPEFSKNVGOV LGGAFFVNGN



C._reinhardtii	267	AVRWATDCVTRGOTVMDASPKGFHGEHGWAAPRRVVEALGINSDAVALIRDRITAA-----
V._carteri	276	AVRWACEGVTKGGTVMDBASVKGFHGHGWADRRPRVVALGVQHEAVRLIHDRITATA-----
B._distachyon_2	272	VVRVOTDGIKGLTVFQNTKKRYGEITAWTGGKPTTVKVAIVTDAPAVVELIMQRLTMD-----
O._sativa_2	265	VVRVOTDGIKGLTVFQNTKKRYGEITAWTGGKPTTVKVAIVTDAPAVVEMIMQRLTDD-----
Z._mays_b	268	VVRVOTVGIKGLTVFQNTKKRYGEITAWTGGKPTTVKVAIVTDAPAVVELIQRLTDD-----
S._italica_2	268	VVRVOTVGIKGLTVFQNTKKRYGEITAWTGGKPTTVKVAIVTDAPAVVELMMQRLTDD-----
S._bicolor_2	269	VVRVOTVGIKGLTVFQNTKKRYGEITAWTGGKPTTVKVAIVTDAPAVVELMMQRLTDD-----
Z._mays_2a	269	VVRVOTVGIKGLTVFQNTKKRYGEITAWTGGKPTTVKVAIVTDAPAVVELMMQRLTDD-----
B._rapa_2a	266	VVRVOTDGIKGLTVLNNQKRFEEETEWSDKPSVVKVAIVTDAPAVLKLIMDRIMES-----
B._rapa_2b	266	VVRVOTDGIKGLTVLNNQKRFEEETEWSDKPSVVKVAIVTDAPAVLKLIMDRIMES-----
T._halophila_2	264	VVRVOTNGITRGLTLLYNNRKRFEELNEWSDKPSVVKVAIVTDAPAVLNLIMDRIMES-----
A._thaliana_2	266	VVRVOTSGITRGLTLLYNNLKRFEELNEWSDKPSVVKVAIVTDAPAVLKLIMDRIMES-----
A._lyrata_2	266	VVRVOTSGITRGLTLLYNNPKRFEELNEWSDKPSVVKVAIVTDAPAVLKLIMDRIMES-----
C._rubella_2	264	VVRVOTSGITRGLTLLYNNQKRFEEVNEWSNKPSVVKVAIVTDAPAVLKLIMDRIMES-----
C._sativus_2	265	VVRVOTVGIKGLTVLNNQKRFEEVNEWSDKPSVVKVAIVTDAPAVLKLIMDRIMES-----
M._truncatula_2	267	VVRVOTSGITRGLTLLYNNQKRFEEVNEWSDKPSVVKVAIVTDAPAVLKLIMDRIMES-----
P._vulgaris_2	267	VVRVOTSGITRGLTLLYNNQKRFEEVNEWSDKPSVVKVAIVTDAPAVLKLIMDRIMES-----
G._max_2a	267	VVRVOTSGITRGLTLLYNNQKRFEEVNEWSDKPSVVKVAIVTDAPAVLKLIMDRIMES-----
G._max_2b	267	VVRVOTSGITRGLTLLYNNQKRFEEVNEWSDKPSVVKVAIVTDAPAVLKLIMDRIMES-----
C._papaya_2	269	VVRVOTNGITRGLTLLYNNRKRFEELNEWSDKPSVVKVAIVTDAPAVLKLIMDRIMES-----
A._coerulea_2	281	VVRVOTNGITRGLTLLYNNRKRFEELNEWSDKPSVVKVAIVTDAPAVLKLIMDRIMES-----
L._usitatissimu	263	VVRVOTSGITRGLTLLYNNLKRFEELNEWSDKPSVVKVAIVTDAPAVLKLIMDRIMES-----
E._grandis_2	265	VVRVOTVGIKGLTVLNNQKRFEEVNEWSDKPSVVKVAIVTDAPAVLKLIMDRIMES-----
S._tuberosum_2	265	VVRVOTNGITRGLTLLYNNQKRFEEVNEWSDKPSVVKVAIVTDAPAVLKLIMDRIMES-----
S._lycopersicum	265	VVRVOTNGITRGLTLLYNNQKRFEEVNEWSDKPSVVKVAIVTDAPAVLKLIMDRIMES-----
M._guttatus_2	264	VVRVOTSGITRGLTLLYNNQKRFEEVNEWSDKPSVVKVAIVTDAPAVLKLIMDRIMES-----
C._sinesis_2	265	VVRVOTSGITRGLTLLYNNQKRFEEVNEWSDKPSVVKVAIVTDAPAVLKLIMDRIMES-----
V._viniifera_2	264	VVRVOTSGITRGLTLLYNNQKRFEEVNEWSDKPSVVKVAIVTDAPAVLKLIMDRIMES-----
P._trichocarpa_2	265	VVRVOTVGIKGLTVLNNQKRFEEVNEWSDKPSVVKVAIVTDAPAVLKLIMDRIMES-----
M._domestica_2	269	VVRVOTNGITRGLTLLYNNRKRFEELNEWSDKPSVVKVAIVTDAPAVLKLIMDRIMES-----
F._vesca_2	266	VVRVOTNGITRGLTLLYNNRKRFEELNEWSDKPSVVKVAIVTDAPAVLKLIMDRIMES-----
G._raimondii_2	268	VVRVOTNGITRGLTLLYNNQKRFEEVNEWSDKPSVVKVAIVTDAPAVLKLIMDRIMES-----
T._cacao_2	266	VVRVOTNGITRGLTLLYNNRKRFEELNEWSDKPSVVKVAIVTDAPAVLKLIMDRIMES-----
S._moellendorffi_2	270	VVRVOTVGIKGLTVLNNQKRFEEVNEWSDKPSVVKVAIVTDAPAVLKLIMDRIMES-----
P._patens_2	277	VVRVOTVGIKGLTVLNNQKRFEEVNEWSDKPSVVKVAIVTDAPAVLKLIMDRIMES-----
S._moellendorffi_1	276	ALRVETLQVGRVTLFDVGLKKNWGLNPNVWGRPHVVDVAVTVDASKVLELVLERLHTDT-----
P._patens_1	285	AVRVETEGVCGVTLDMGLKKNWGLNPNVWGRPHVVDVAVTVDADGVRSLVKKLTCSSP-----
P._patens_3	279	AVRVETEGVCGVTLDMGLKKNWGLNPNVWGRPHVVDVAVTVDADGVRSLVKKLTCSSP-----
O._sativa_1b	280	VVRVETGQICGHTLMDQGLKKNWNSNPWTGYSPPVAVTVDVDPKVLAYAKELFNQA-----
S._italica_1b	277	VVRVETGQICGHTLMDQGLKKNWNSNPWTGYSPPVAVTVDVDPKVLAYAKELFNQA-----
S._bicolor_1b	259	VVRVETGQICGHTLMDQGLKKNWNSNPWTGYSPPVAVTVDVDPKVLAYAKELFNQA-----
Z._mays_1c	259	VVRVETGQICGHTLMDQGLKKNWNSNPWTGYSPPVAVTVDVDPKVLAYAKELFNQA-----
C._rubella_1	282	VVRVETGQICGHTLMDQGLKKNWNSNPWTGYSPPVAVTVDVDPKVLAYAKELFNQA-----
A._thaliana_1	280	VVRVETGQICGHTLMDQGLKKNWNSNPWTGYSPPVAVTVDVDPKVLAYAKELFNQA-----
A._lyrata	276	VVRVETGQICGHTLMDQGLKKNWNSNPWTGYSPPVAVTVDVDPKVLAYAKELFNQA-----
B._rapa_1b	283	VVRVETGQICGHTLMDQGLKKNWNSNPWTGYSPPVAVTVDVDPKVLAYAKELFNQA-----
B._rapa_1a	275	VVRVETGQICGHTLMDQGLKKNWNSNPWTGYSPPVAVTVDVDPKVLAYAKELFNQA-----
T._halophila_1	283	VVRVETGQICGHTLMDQGLKKNWNSNPWTGYSPPVAVTVDVDPKVLAYAKELFNQA-----
M._truncatula_1	278	VVRVETGQICGHTLMDQGLKKNWNSNPWTGYSPPVAVTVDVDPKVLAYAKELFNQA-----
P._vulgaris_1	278	VVRVETGQICGHTLMDQGLKKNWNSNPWTGYSPPVAVTVDVDPKVLAYAKELFNQA-----
G._max_1a	274	VVRVETGQICGHTLMDQGLKKNWNSNPWTGYSPPVAVTVDVDPKVLAYAKELFNQA-----
G._max_1b	278	VVRVETGQICGHTLMDQGLKKNWNSNPWTGYSPPVAVTVDVDPKVLAYAKELFNQA-----
B._distachyon_1	271	VVRVETGQICGHTLMDQGLKKNWNSNPWTGYSPPVAVTVDVDPKVLAYAKELFNQA-----
O._sativa_1a	268	VVRVETGQICGHTLMDQGLKKNWNSNPWTGYSPPVAVTVDVDPKVLAYAKELFNQA-----
Z._mays_1b	269	VVRVETGQICGHTLMDQGLKKNWNSNPWTGYSPPVAVTVDVDPKVLAYAKELFNQA-----
S._italica_1a	269	VVRVETGQICGHTLMDQGLKKNWNSNPWTGYSPPVAVTVDVDPKVLAYAKELFNQA-----
S._bicolor_1a	269	VVRVETGQICGHTLMDQGLKKNWNSNPWTGYSPPVAVTVDVDPKVLAYAKELFNQA-----
Z._mays_1a	269	VVRVETGQICGHTLMDQGLKKNWNSNPWTGYSPPVAVTVDVDPKVLAYAKELFNQA-----
C._sativus_1	276	VVRVETGQICGHTLMDQGLKKNWNSNPWTGYSPPVAVTVDVDPKVLAYAKELFNQA-----
C._papaya_1	282	VVRVETGQICGHTLMDQGLKKNWNSNPWTGYSPPVAVTVDVDPKVLAYAKELFNQA-----
M._guttatus_1	278	VVRVETGQICGHTLMDQGLKKNWNSNPWTGYSPPVAVTVDVDPKVLAYAKELFNQA-----
P._trichocarpa_1	296	VVRVETGQICGHTLMDQGLKKNWNSNPWTGYSPPVAVTVDVDPKVLAYAKELFNQA-----
L._usitatissimu_1a	278	VVRVETGQICGHTLMDQGLKKNWNSNPWTGYSPPVAVTVDVDPKVLAYAKELFNQA-----
L._usitatissimu_1b	278	VVRVETGQICGHTLMDQGLKKNWNSNPWTGYSPPVAVTVDVDPKVLAYAKELFNQA-----
F._vesca_1	283	VVRVETGQICGHTLMDQGLKKNWNSNPWTGYSPPVAVTVDVDPKVLAYAKELFNQA-----
M._domestica_1a	286	VVRVETGQICGHTLMDQGLKKNWNSNPWTGYSPPVAVTVDVDPKVLAYAKELFNQA-----
M._domestica_1b	282	VVRVETGQICGHTLMDQGLKKNWNSNPWTGYSPPVAVTVDVDPKVLAYAKELFNQA-----
E._grandis_1	273	VVRVETGQICGHTLMDQGLKKNWNSNPWTGYSPPVAVTVDVDPKVLAYAKELFNQA-----
A._coerulea_1	276	VVRVETGQICGHTLMDQGLKKNWNSNPWTGYSPPVAVTVDVDPKVLAYAKELFNQA-----
V._viniifera_1	286	VVRVETGQICGHTLMDQGLKKNWNSNPWTGYSPPVAVTVDVDPKVLAYAKELFNQA-----
S._tuberosum_1	278	VVRVETGQICGHTLMDQGLKKNWNSNPWTGYSPPVAVTVDVDPKVLAYAKELFNQA-----
S._lycopersicum	278	VVRVETGQICGHTLMDQGLKKNWNSNPWTGYSPPVAVTVDVDPKVLAYAKELFNQA-----
C._sinesis_1	282	VVRVETGQICGHTLMDQGLKKNWNSNPWTGYSPPVAVTVDVDPKVLAYAKELFNQA-----
G._raimondii_1b	288	VVRVETGQICGHTLMDQGLKKNWNSNPWTGYSPPVAVTVDVDPKVLAYAKELFNQA-----
G._raimondii_1a	288	VVRVETGQICGHTLMDQGLKKNWNSNPWTGYSPPVAVTVDVDPKVLAYAKELFNQA-----
T._cacao_1	288	VVRVETGQICGHTLMDQGLKKNWNSNPWTGYSPPVAVTVDVDPKVLAYAKELFNQA-----

▲Lys 297

**Figure A-3. Expression profile of *NSH2* in Arabidopsis.**

Expression profile of *NSH2* according to the Arabidopsis eFP browser (<http://bar.utoronto.ca/efp/cgi-bin/efpWeb.cgi>). The coloring scale is from yellow (low expression) to red (high expression), as indicated in the figure.

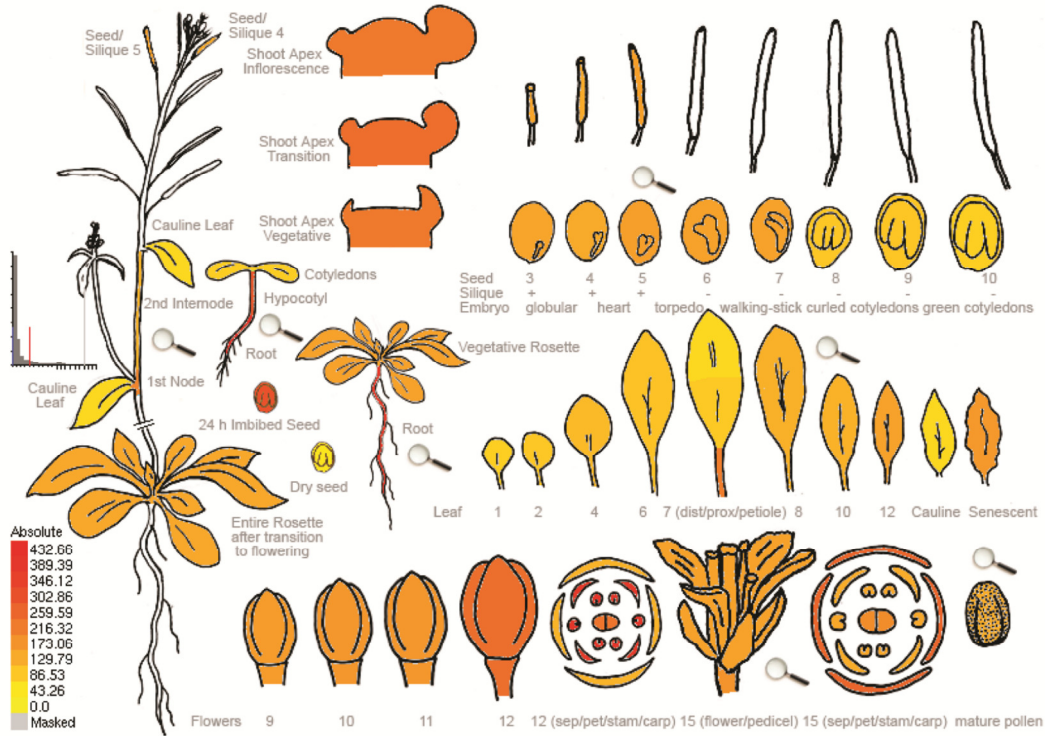
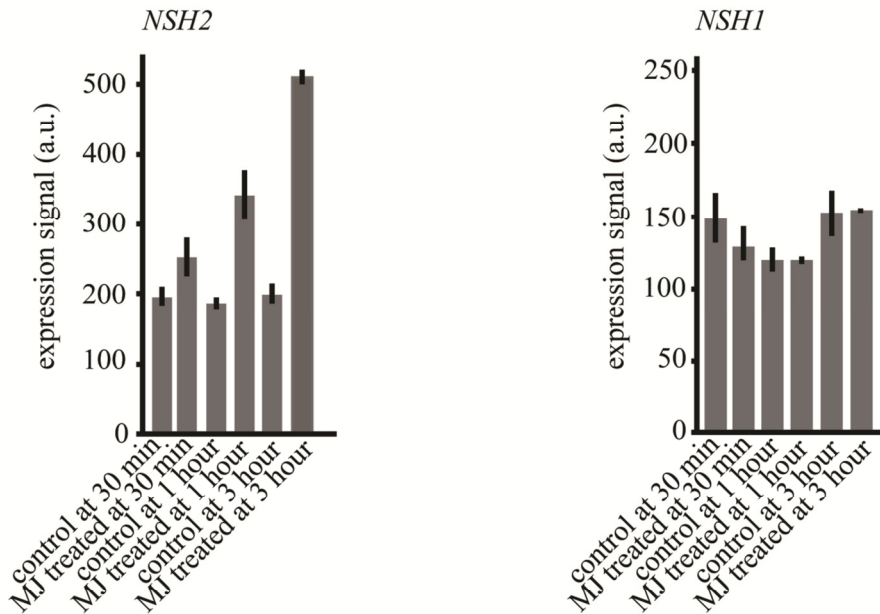


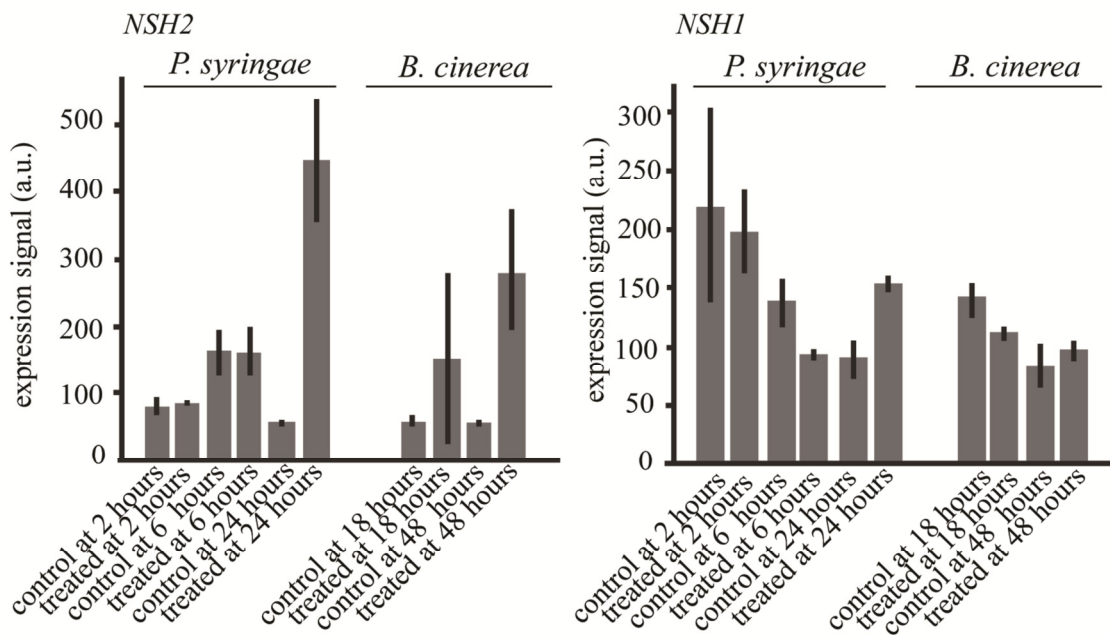
**Figure A-4. Expression profile of *NSH1* and *NSH2* after hormone and biotic stress treatments.**

A) Changes of *NSH2* and *NSH1* expression level after methyl jasmonate (MJ) treatment.  
 B) Changes of *NSH2* and *NSH1* expression level after *Pseudomonas syringae* and *Botrytis cinerea* infection. Data are from the Arabidopsis eFP browser.

**A Hormone treatment (MJ)**



**B Biotic stress**





## Appendix of Tables

**Table B-1. Gene locus numbers and accession number.**  
Protein sequences were retrieved from NCBI and Phytosome.

Species	Accession number
<i>Linum usitatissimum 1a</i>	Lus10003251
<i>Linum usitatissimum 1b</i>	Lus10035601
<i>Populus trichocarpa 1</i>	Potri.006G083400.1
<i>Medicago truncatula 1</i>	Medtr7g104270.1
<i>Phaseolus vulgaris 1</i>	Phvul.001G188700.1
<i>Glycine max 1a</i>	Glyma19g37830.3
<i>Glycine max 1b</i>	XP_006577068.1
<i>Cucumis sativus 1</i>	Cucsa.083290.1
<i>Malus domestica 1a</i>	MDP0000132583
<i>Malus domestica 1b</i>	MDP0000232956
<i>Fragraria vesca 1</i>	mrna30260.1-v1.0-hybrid
<i>Arabidopsis lyrata 1</i>	482605
<i>Capsella rubella 1</i>	Carubv10023574m
<i>Brassica rapa 1a</i>	Bra023060
<i>Brassica rapa 1b</i>	Bra005283
<i>Thellungiella halophila 1</i>	Thhalv10016893m
<i>Carica papaya 1</i>	evm.model.supercontig_5.45
<i>Gossypium raimondii 1a</i>	Gorai.006G156300.1
<i>Gossypium raimondii 1b</i>	Gorai.009G404900.1
<i>Theobroma cacao 1</i>	Thecc1EG022528t1
<i>Citrus sinensis 1</i>	orange1.1g019632m
<i>Eucaliptus grandis 1</i>	Eucgr.A01518.1
<i>Vitis vinifera 1</i>	GSVIVT01033806001
<i>Solanum tuberosum 1</i>	PGSC0003DMP400015775
<i>Solanum lycopersicum 1</i>	Solyc09g009690.2.1
<i>Mimulus guttatus 1</i>	mgv1a009694m
<i>Aquilegia coerulea 1</i>	Aquca_072_00170.1
<i>Sorghum bicolor 1a</i>	Sb07g024220.1
<i>Sorghum bicolor 1b</i>	Sb02g011950.1
<i>Zea mays 1a</i>	GRMZM2G015344_T01
<i>Zea mays 1b</i>	GRMZM2G085960_T02
<i>Zea mays 1c</i>	GRMZM2G104999_T05
<i>Setaria italica 1a</i>	Si014086m
<i>Setaria italica 1b</i>	Si030460m
<i>Oryza sativa 1a</i>	LOC_Os08g44370.1
<i>Oryza sativa 1b</i>	LOC_Os09g39440.2
<i>Brachiopodium distachyon 1</i>	Bradi3g42790.1
<i>Selaginella moellendorffii 1</i>	97048
<i>Physcomitrella patens 1</i>	JX861385
<i>P.patens 3</i>	JX861386
<i>Linum usitatissimum 2</i>	Lus10042608
<i>Populus trichocarpa 2</i>	Potri.007G144600.2

---

<i>Medicago truncatula</i> 2	BT052412.1
<i>Phaseolus vulgaris</i> 2	Phvul.003G000600.1
<i>Glycine max</i> 2a	Glyma0048s00280.2
<i>Glycine max</i> 2b	Glyma20g00200.1
<i>Cucumis sativus</i> 2	Cucsa.266250.1
<i>Malus domestica</i> 2	XP_008383867
<i>Fragraria vesca</i> 2	mrna10152.1-v1.0-hybrid
<i>Arabidopsis lyrata</i> 2	470564
<i>Capsella rubella</i> 2	Carubv10009769m
<i>Brassica rapa</i> 2a	Bra030616
<i>Brassica rapa</i> 2b	Bra032458
<i>Thellungiella halophila</i> 2	Thhalv10008223m
<i>Carica papaya</i> 2	evm.model.supercontig_151.9
<i>Gossypium raimondii</i> 2	Gorai.012G120100.2
<i>Theobroma cacao</i> 2	Thecc1EG021538t1
<i>Citrus sinensis</i> 2	XP_006493127.1
<i>Eucalyptus grandis</i> 2	Eucgr.A00423.1
<i>Vitis vinifera</i> 2	GSVIVT01038253001
<i>Solanum tuberosum</i> 2	XP_006353123.1
<i>Solanum lycopersicum</i> 2	Solyc12g018990.1.1
<i>Mimulus guttatus</i> 2	mgv1a010172m
<i>Aquilegia coerulea</i> 2	Aquca_058_00004.1
<i>Sorghum bicolor</i> 2	Sb03g009290.1
<i>Zea mays</i> 2a	GRMZM2G029845_T01
<i>Zea mays</i> 2b	GRMZM2G134149_T02
<i>Setaria italica</i> 2	Si002233m
<i>Oryza sativa</i> 2	LOC_Os03g31170.1
<i>Brachiopodium distachyon</i> 2	Bradi1g57470.1
<i>Selaginella moellendorffii</i> 2	80581
<i>Physcomitrella patens</i> 2	JQ649322
<i>Clamidomonas reinhardtii</i>	Cre06.g271050.t1.3
<i>Volvox carteri</i>	Vocar20002469m

---

# Curriculum Vitae

## Personal Data

---

Name	Chiara Baccolini
Nationality	Italian
Date of birth	15 <sup>th</sup> November, 1989
Place of birth	Bologna, Italy

---

## Education

---

10.2014 – present	PhD study in the Department of Molecular Nutrition and Biochemistry of Plants Gottfried Wilhelm Leibniz Universität Hannover Supervisor: Prof. Dr. Claus-Peter Witte Financed by a fellowship from the German Academic Exchange Service (DAAD)
05.2013 – 08.2013	Internship at the Freie Universität Berlin Supervisor: Prof. Dr. Claus-Peter Witte
10.2011 – 03.2014	Master study at the Alma Mater Studiorum, University of Bologna
10.2008 – 10.2011	Bachelor study at the Alma Mater Studiorum, University of Bologna

---

## Publications

---

Baccolini C., and Witte C.P. (2019). AMP and GMP Catabolism in Arabidopsis Converge on Xanthosine which Is Degraded by a Nucleoside Hydrolase Heterocomplex. *Plant Cell*, in press.

Borghese R., Baccolini C., Francia F., Sabatino P., Turner R.J., Zannoni D. (2014). Reduction of chalcogen oxyanions and generation of nanoprecipitates by the photosynthetic bacterium *Rhodobacter capsulatus*. *J Hazard Mater.* 269: 24-30.

---